UNIVERSITY OF OKLAHOMA

GRADUATE COLLEGE

HIGGS PHENOMENOLOGY WITH TAU LEPTONS IN THE STANDARD MODEL AND BEYOND AT LHC

A DISSERTATION

SUBMITTED TO THE GRADUATE FACULTY

in partial fulfillment of the requirements for the

Degree of

DOCTOR OF PHILOSOPHY

By

KESHENG YANG
Norman, Oklahoma
2013

HIGGS PHENOMENOLOGY WITH TAU LEPTONS
IN THE STANDARD MODEL AND BEYOND AT LHC

A DISSERTATION APPROVED FOR THE
HOMER L. DODGE DEPARTMENT OF PHYSICS AND ASTRONOMY

BY

Dr. Chung Kao, Chair

Dr. Nikola Petrov

Dr. Phillip Gutierrez

Dr. Ron Kantowski

Dr. Kieran Mullen

DEDICATION

to

My parents

Daifu Yang and Yaya Wang

For

Encouraging me to follow my dreams

Acknowledgements

At first, I would like to express my gratitude to my research advisor, Professor Chung Kao, for teaching me a great deal of physics, for encouraging me to explore and work in High Energy physics, for his guidance and unconditional support during all these years of graduate school, and for being an excellent mentor. I am grateful for having had the opportunity to work with him.

And I have to thank the members of my Ph.D. committee, Professors Phil Gutierrez, Ron Kantowski, Kieran Mullen and Nikola Petrov for their helpful career advice and suggestions in general.

I also wish to thank Dr. Baris Altunkaynak and Mrs. Priyangi Wickramarachchi. They are good coworkers and always helpful.

Contents

Abstract

In this dissertation, the discovery potential of neutral Higgs bosons has been discussed respectively in the Standard Model (SM), minimal supersymmetric standard model (MSSM), and unified supersymmetric models. In the SM, we consider the Higgs boson being produced together with one jet, i.e., $pp \to jh^0 + X$ where $j = g, q$ or $\bar{q}$ ($q = u, d, c, s$); in supersymmetric theories, we focused on such channel as $bg \to b\phi$ ($\phi = h^0, H^0$ or A^0). The interesting decay mode is Higgs to tau pair followed with one tau decaying to $e^{\pm}$ or $\mu^{\pm}$ and the other to mesons (π, a_1 or ρ). By comparing with the relevant background processes, we found that the discovery of the SM Higgs boson is pessimistic at $\sqrt{s} = 8$ TeV, but it is very promising to search for neutral Higgs bosons in supersymmetric models owing to a large $\tan\beta$. In addition, we considered the experimental constraints from $Br(b \to s\gamma)$, $Br(B_s^0 \to \mu^+\mu^-)$, Δa_μ and $m_{h^0} = 125$ GeV. In the MSSM, the constraint from light Higgs mass favors the parameter space which has an intermediate $\tan\beta$ and is explorable at the next run of LHC. The minimal supergravity unified model (mSUGRA) has large space allowed by $m_{h^0} \approx 125$ GeV, but it seems difficult to reconcile the flavor problems. In the model with minimal gauge mediated supersymmetry breaking (mGMSB), the situation is totally opposite.

Chapter 1

Introduction

Following the great successes of Quantum Electrodynamics (QED), physicists' endeavor to unify the electromagnetic interaction with the weak interation spread through 1960's and the first half of 1970's, and finally led to the establishment of the Standard Model. This nice model got a unified picture of the eletromagnetic interaction, the weak interaction and even the strong interaction under the concept of gauge invariance. Since then it has been experimentally proven to be correct over and over again. For example, the consecutive discoveries of $W^{\pm}$ and Z^0 bosons in 1983 were the direct proof of this renormalizable description about the weak interaction. Since this model put all fermions in doublets of weak isospin, the discovery of tau lepton in 1974 implied the existence to tau neutrino. Therefore the discvoery of tau neutrino in 2000 was another proof. The discovery of top quark in 1995 not only gave the SM more positive support, but also proved the Cabbibo-Kobayash-Maskawa (CKM) theory which predicted the third generation of quarks and proposed the unique origin of CP violation in the SM. In 2012, both ATLAS and CMS independently claimed the discovery of a new boson with mass about 125 GeV . If this signal is truly the trace of the Higgs boson, it

would be the most important discovery in this century, because, as the building block of the SM, Higgs boson is the last particle to be detected, and because the Higgs boson is related to the most elementary problem of physics, i.e., mass. In the next chapter, I will give a brief explanation of the Higgs mechanism and its simplest extension, i.e., the Two-Higgs-Doublet Model (THDM).

However the SM seems incomplete. Nowadays many experiments favored the existence of massive neutrinos but they are massless in the SM. And dark matter and dark energy both are puzzles to the SM. Cosmological observations have shown that there is a large fraction of the uninverse which is non-observable through optical methods, but can be detected through gravitational effects, i.e., dark matter. It's commonly believed that this fraction is composed of weakly interacting massive particles (WIMPs). As the only candidate for dark matter in the SM, neutrinos are too light to account for all the dark matter in the universe. In supersymmetric models, there are some other candidates. For example, the Minimal Supersymmetric Standard Model predicts that the lightest neutralino is stable, massive and weakly interacting with other matters if we assume the conservation of the R-parity. Moreover baryogenesis requires that CP be violated. Otherwise we couldn't have our current universe which is made up dominantly of matters. As mentioned in last paragraph, the SM has one and only one source of CP violation, the CKM phase. But experimental measurements put many constraints on the phase, so it's not enough to explain baryogenesis under the framework of the SM. The general THDM has two terms responsible for CP violation to be discussed in Chapter 2. In supersymmetric theories, the soft supersymmetry breaking (SSB) terms could introduce large CP-violating phases. We will discuss supersymmetry in Chaper 3, especially the MSSM. Since our goal of this thesis is the analysis of Higgs phenomenology, we will focus on the Higgs

sector of the MSSM. After the spontaneous breaking of eletroweak symmetry, five Higgs bosons survive among the eight degrees of freedom of the THDM, i.e., two CP-even neutral Higgs bosons (H^0 and h^0), one CP-odd neutral pseudoscalar (A^0) and two charged Higgs bosons ($H^{\pm}$). In addition to the SM parameters, the Higgs sector of MSSM has only two free parameters which are often chosen as the mass of the psudeo scalar (m_{A^0}) and the ratio of the vacuum expection values ($\tan\beta = \frac{v_2}{v_1}$). Therefore the masses of other Higgs bosons and their couplings to the SM particles can be expressed in term of m_{A^0} and $\tan\beta$ together with other SM parameters.

In the SM with $m_{h^0} \approx 125$ GeV, Higgs boson dominantly decays to $b\bar{b}$ with $\mathrm{Br}(h^0 \to b\bar{b}) \sim 60\%$, to WW^* with $\mathrm{Br}(h^0 \to WW^*) \sim 22\%$, to $\tau^+\tau^-$ with $\mathrm{Br}(h^0 \to \tau^+\tau^-) \sim 6\%$ and to gg with $\mathrm{Br}(h^0 \to gg) \sim 6\%$. In the decoupling limit of MSSM, the light Higgs boson behaves like the SM Higgs boson while the pseudoscalar and the heavy Higgs dominantly decay to $b\bar{b}$ and $\tau^+\tau^-$. Compared with other decay modes, Higgs to tau pairs has a much cleaner background and tau tagging can help us remove a lot of background events. That is the reason we are interested in the decay channel of Higgs to tau pair. To simulate the production of Higgs bosons and the decay to tau pairs, we use Madgraph to generate the transition matrices, and then do the full calculation, or just apply the narrow width approximation (NWA). Since the masses of Higgs bosons are much heavier than the mass of the tau lepton, the two tau leptons are very energetic. So the final particles from tau decay are almost along the diretions of their parent particles. This is the so-called "collinear approximation". In our calculation, we consider the decays of the two tau leptons respectively to lighter leptons ($e^{\pm}$ or $\mu^{\pm}$) and to mesons ($\pi/a_1/\rho$). By measuring the momenta of detectable particles, we can reconstruct the mass of the original Higgs bosons.

Chapter 4 will be dedicated to the details of the mathematical methods and two important selection cuts, i.e., the cuts on the energy fractions (x_l and x_h) and the reconstructed mass ($m_{\tau\tau}$).

In Chapter 5, the production of the SM Higgs associated with one jet will be discussed, especially the selection cuts. After a complete analysis of the basic cuts, we found that the cuts on the energy fractions and the reconstructed mass are so stringent that there is not much space left for other selection cuts to significantly enhance the discovery potential. And we found that this channel is pessimistic to search the SM Higgs boson in the near future, but could be promising for $\sqrt{s} = 14$ TeV.

According to the methods given in Chapter 4 and based on the information in Chapter 5, we discuss the discovery potential of MSSM Higgs bosons through the fusion of b quark and gluon in Chapter 6. It's found that this channel is very promising to search for the MSSM Higgs bosons because the couplings of Higgs bosons to down flavors can be greatly enhanced by $\tan\beta$. It's even possible to find MSSM Higgs bosons with the mass of pseudoscalar up to 1000 GeV and $\tan\beta$ around 50 at LHC with $\sqrt{s} = 14$ TeV. And, to compare the mass of light Higgs with the SM Higgs ($\sim$ 125 GeV), we scan through the parameter space 100 GeV $\leq m_{A^0} \leq$ 1000 GeV and $1 \leq \tan\beta \leq 50$, and then find that the experimental constraint of $m_{h^0} \approx 125$ GeV favors the region with an intermediate value of $\tan\beta$ ($3 \leq \tan\beta \leq 10$). This region of $\tan\beta$ together with 100 GeV $\leq m_{A^0} \leq 400$ GeV will be reachable to the next run of LHC.

In MSSM, soft terms are introduced to break supersymmetry. Meanwhile huge free parameters are brought in. These parameters are very difficult to deal with for a general discuss in MSSM. To reduce the number of free parameters, we investigate two popular SUSY grand unified theories, i.e., mSUGRA and

mGMSB, in Chapter 7. It's commonly believed that MSSM is just an effective theory at EW scale of some supersymmetric theories which have higher symmetry at high energy scale. Under these theories, the supersymmetry is broken in the hidden sector, and then the effect of SUSY breaking is mediated to the visible sector through certain interactions. Due to the higher symmetry, many parameters are correlated. Therefore we have fewer free parameters. In both mSUGRA and mGMSB, we consider the production of Higgs bosons through the fusion of b quark and gluon. Scanning through the parameter spaces of these two models, we plot the 5-σ discovery contours and four experimental constraints which are the branching ratio of b to $s\gamma$, the branching ratio of B_s^0 to $\mu^+\mu^-$, the anomalous magnetic moment of muon (Δa_μ) and the mass of light Higgs.

The conclusions are given in Chapter 8.

Chapter 2

Higgs Mechanism and Standard Model

2.1 Local Gauge Invariance

The idea of gauge invariance originated from classical Maxwell equations [1]. Looking at the following equations

$$\begin{cases} \vec{B} &= \nabla \times \vec{A}, \\ \vec{E} &= -\nabla\phi - \dfrac{\partial \vec{A}}{\partial t} \end{cases} . \tag{2.1}$$

It's easy to see that the electric and magnetic fields stay the same if the vector potential ($\vec{A}$) and scalar potential (ϕ) simultaneously take a local transformation as $\vec{A} \to \vec{A} + \nabla\Lambda$ and $\phi \to \phi - \dfrac{\partial\Lambda}{\partial t}$. Here Λ is a scalar function of $x = (x^0, \vec{x})$. In what follows, all vectors are 4-vectors unless explicitly stated.

Moving to the quantum theory of Electrodynamics (QED), such invariance is

also true, as shown in the following Lagrangian.

$$\mathcal{L}^{QED} = -\frac{1}{4}F^{\mu\nu}F_{\mu\nu} + \bar{\psi}(i\gamma^{\mu}D_{\mu} - m)\psi. \tag{2.2}$$

Here, the field strength tensor of the photon is $F^{\mu\nu} = \partial^{\mu}A^{\nu} - \partial^{\nu}A^{\mu}$; and its covariant derivative has the form of $D^{\mu} = \partial^{\mu} + ieQA^{\mu}$. In this thesis, e stands for the positive electron charge with $\frac{e^2}{4\pi} = \frac{1}{128.8}$ at weak scale. Under an infinitesimal local transformation as $\psi(x) \to (1 - ieQ\Lambda(x))\psi(x)$ and $A_{\mu} \to A_{\mu} + \partial_{\mu}\Lambda(x)$, the Lagrangian is gauge invariant.

In 1954, this gauge symmetry was extended first by Yang and Mills in the context of the strong interaction [2], and then was applied to describe the weak interaction. Finally all the fundamental interactions but gravity are unified in the so called $SU(2)_L \otimes U(1)_Y \otimes SU(3)_C$ theory. Not losing generality, $SU(2)_L$ of leptons would be good enough for the elucidation of such extension. In this case, the fermionic field is generalized to be a doublet $\Psi_l^L = \begin{pmatrix} \psi_{\nu_l} \\ \psi_l \end{pmatrix}_L$, and the wave-function of the photon is replaced by three gauge bosons, e.g. $\vec{W} = (W_1, W_2, W_3)$. Therefore the Lagrangian becomes

$$\mathcal{L} = -\frac{1}{4}W_{a\mu\nu}W_a^{\mu\nu} + i\bar{\Psi}_l\gamma^{\mu}D_{\mu}\Psi_l, a = 1, 2, 3 \tag{2.3}$$

with

$$\begin{cases} W_{\mu\nu}^a &= \partial_{\mu}W_{\nu}^a - \partial_{\nu}W_{\mu}^a - g(\vec{W}_{\mu} \times \vec{W}_{\nu})^a, \\ D_{\mu} &= \partial_{\mu} + igW_{\mu}^a t^a, a = 1, 2, 3. \end{cases} \tag{2.4}$$

Eq. 2.3 is invariant under transformation such as

$$\begin{cases} \Psi_L & \rightarrow & \exp(-igt^a\alpha^a)\Psi_L, \\ W_\mu^a & \rightarrow & W_\mu^a + \partial_\mu\alpha^a + g(\vec{\alpha}\times\vec{W})^a, \end{cases} \tag{2.5}$$

where $\alpha = (\alpha_1(x), \alpha_2(x), \alpha_3(x))$, and $t = (t_1, t_2, t_3) = \frac{1}{2}(\sigma_1, \sigma_2, \sigma_3)$. The σ's are the Pauli matrices, i.e.,

$$\sigma_1 = \begin{pmatrix} 0 & 1 \\ 1 & 0 \end{pmatrix}, \ \sigma_2 = \begin{pmatrix} 0 & -i \\ i & 0 \end{pmatrix} \text{ and } \sigma_3 = \begin{pmatrix} 1 & 0 \\ 0 & -1 \end{pmatrix}. \tag{2.6}$$

2.2 Higgs Mechanism and Spontaneous Symmetry Breaking

In Eq. 2.3, the fermionic particle and gauge bosons are all set to be massless because the mass terms violate the $SU(2)_L$ symmetry, even the $U(1)_Y$ symmetry. In order to construct a realistic and renormalizable model, it's necessary to introduce one mass generation mechanism, the *Higgs Mechanism*. The revolutionary works about Higgs mechanism can be found in such papers [3, 4, 5, 6]. In this thesis, only one simple description and its application to $SU(2)_L \otimes U(1)_Y$ will be given. Since the $SU(3)_C$ symmetry of strong interaction isn't broken by this mechanism, it won't be discussed in this section.

The Higgs potential is given as

$$V(\Phi) = -\mu^2\Phi^\dagger\Phi + \lambda(\Phi^\dagger\Phi)^2, \tag{2.7}$$

where $\Phi = \begin{pmatrix} \phi^+ \\ \phi^0 \end{pmatrix}$, and μ^2 and λ are positive real numbers. Fig. 2.1 shows that the origin is an unstable extremum, so the system tends to prefer one point in the valley, i.e. *Spontaneous Symmetry Breaking*.

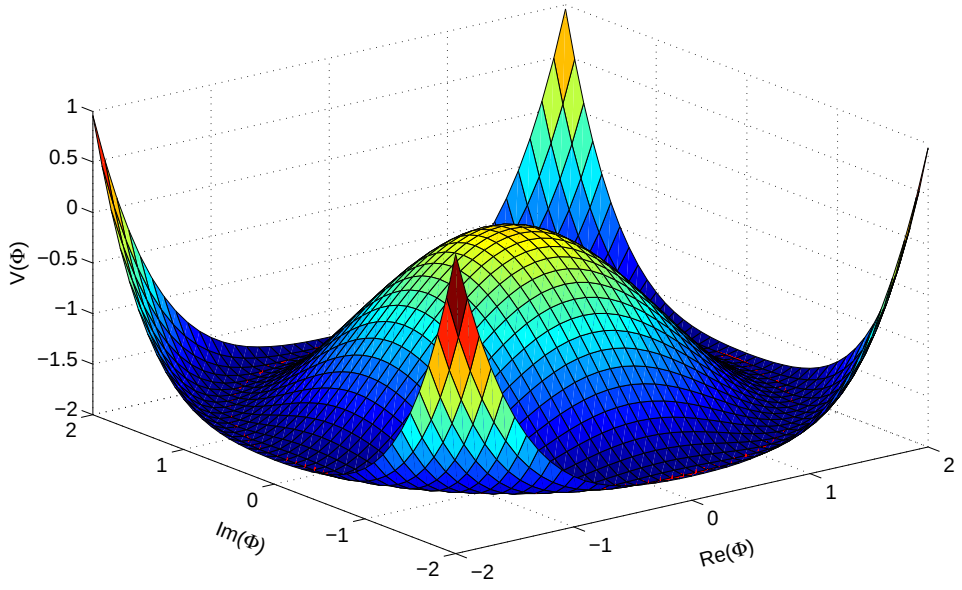

Figure 2.1: Higgs Potential. Here ϕ is a complex nuber with one axis be the real part and the other be the imaginary part. The red dotted curve denotes the minimal value of Higgs potential.

In the Standard Model, the Lagrangian of the Higgs sector can be written as

$$\begin{cases} \mathcal{L}^H &= \left(D^\nu \Phi\right)^\dagger \left(D_\nu \Phi\right) + \mu^2 - \lambda \left(\Phi^\dagger \Phi\right)^2, \\ D^\nu &= \partial^\nu + igt_j W_j^\nu + ig' Y B^\nu \end{cases}, \tag{2.8}$$

where Y denotes the weak hyper-charge $+1$, or in the form of a matrix such as $Y = \frac{1}{2}\begin{pmatrix} 1 & 0 \\ 0 & 1 \end{pmatrix}$, and $B(x)$ is the gauge boson corresponding to $U(1)_Y$ group. As discussed in the previous section, this Lagrangian is invariant under $SU(2)_L \otimes$

$U(1)_Y$ gauge transformation. Once the symmetry is broken, for example,

$$\Phi = \begin{pmatrix} \Phi_a \\ \Phi_b \end{pmatrix} = \frac{1}{\sqrt{2}} \begin{pmatrix} 0 \\ v + H(x) \end{pmatrix} \text{ with } v = \sqrt{\frac{\mu^2}{\lambda}}, \tag{2.9}$$

the Lagrangian changes to

$$\begin{aligned} \mathcal{L}^H &= \frac{1}{2}\partial_\mu H \partial^\mu H + \frac{g^2 v^2}{4} W^+_\mu W^{-\mu} + \frac{g^2}{4} W^+_\mu W^{-\mu} H^2 + \frac{g^2 v}{2} W^-_\mu W^{+\mu} H \\ &+ \frac{g^2 v^2}{8\cos^2\theta_w} Z_\mu Z^\mu + \frac{g^2}{8\cos^2\theta_w} Z_\mu Z^\mu H^2 + \frac{g^2 v}{4\cos^2\theta_w} Z_\mu Z^\mu H \\ &+ \frac{\lambda}{4} v^4 - \lambda v^2 H^2 - \lambda v H^3 - \frac{\lambda}{4} H^4. \end{aligned} \tag{2.10}$$

In Eq. 2.9, only the real part of Φ_b survives while three other degrees of Φ are rotated away. Put in another way, these three degrees are eaten by $W^\pm$ and Z, therefore the gauge bosons get masses, $M_W = \frac{gv}{2}$ and $M_Z = \frac{gv}{2\cos\theta_w}$. Here v is the *Vacuum Expectation Value* (VEV), $v \approx 246$ GeV. The mass of Higgs boson is $M_H = \sqrt{2\lambda v^2}$, which is a free parameter in the SM.

The fermions get their masses through the same mechanism with *Yukawa coupling*,

$$\begin{aligned} \mathcal{L}^{fH} &= -\lambda_l (\bar{\Psi}^L_l \Phi \psi^R_l + \bar{\psi}^R_l \Phi^\dagger \Psi^L_l) \\ &\quad -\lambda_{\nu_l} (\bar{\Psi}^L_l \tilde{\Phi} \psi^R_{\nu_l} + \bar{\psi}^R_{\nu_l} \tilde{\Phi}^\dagger \Psi^L_l). \end{aligned} \tag{2.11}$$

Here $\tilde{\Phi}$ is the charge conjugate, $\tilde{\Phi} = i\sigma_2 \Phi^*$. In the SM, neutrinos are usually treated as massless, so λ_{ν_l} is set to be "0". After symmetry breaking, down flavor leptons get a mass $m_l = \frac{\lambda_l v}{\sqrt{2}}$.

In conclusion, the free parameter space of SM can be constructed as $\{\lambda^i_l, \lambda^i_u, \lambda^i_d,$

$\lambda, v, g, \cos\theta_w\}$. If we include strong interaction, one more parameter should be considered for the the strong coupling g_s; if we include quark mass mixing, there are four more parameters $\{c_{12}, c_{13}, c_{23}, \delta\}$ [7].

2.3 Two-Higgs-Doublet Model without CP Violation

The simplest extension of the scalar sector is a *Two-Higgs-Doublet Model* (2HDM). The reason to do so is multifold. First, in theories with supersymmetry between bosons and fermions we need one more doublet of left chiral superfields to give mass to the upper type fermions, and this doublet must carry weak hyper-charge -1 [8, 9, 10, 11]. The charge conjugate $\tilde{\Phi}$ cannot build such a doublet from the existing doublet. Moreover this new doublet is also required to restore the cancellation of chiral anomaly. When promoting the Higgs doublet to doublet of superfields, we have introduced one new fermion, i.e., higgsino. Secondly, the extended scalar sector has more interesting properties related to CP violation [12, 13, 14], where C is charge conjugation and P is parity. Sakharov conditions show that CP symmetry must be violated to explain baryongenesis [15]. However, in the SM there is only one parameter responsible for CP violation, i.e., the CKM phase, which cannot account for the current experimental results [16].

Now there are two Higgs doublets such as

$$H_1 = \begin{pmatrix} H_1^+ \\ H_1^0 \end{pmatrix} = \begin{pmatrix} \phi_1^+ \\ \dfrac{v_1 + \phi_1^0}{\sqrt{2}} \end{pmatrix}, \quad H_2 = \begin{pmatrix} H_2^- \\ H_2^0 \end{pmatrix} = \begin{pmatrix} \phi_2^- \\ \dfrac{v_2 + \phi_2^0}{\sqrt{2}} \end{pmatrix}, \tag{2.12}$$

where, H_1 carries weak hyper-charge $Y = 1$ and transforms as a doublet 2 under

$SU(2)_L$, while H_2 transforms as a doublet 2^* with $Y = -1$. And the general Higgs potential can be written as

$$\begin{aligned} V =& m_{11}^2 \Phi_1^\dagger \Phi_1 + m_{22}^2 \Phi_2^\dagger \Phi_2 - (m_{12}^2 \Phi_1^\dagger \Phi_2 + h.c.) \\ &+ \frac{1}{2}\lambda_1 (\Phi_1^\dagger \Phi_1)^2 + \frac{1}{2}\lambda_2 (\Phi_2^\dagger \Phi_2)^2 + \lambda_3 (\Phi_1^\dagger \Phi_1)(\Phi_2^\dagger \Phi_2) + \lambda_4 (\Phi_1^\dagger \Phi_2)(\Phi_2^\dagger \Phi_1) \\ &+ \{\frac{1}{2}\lambda_5 (\Phi_1^\dagger \Phi_2)^2 + [\lambda_6 (\Phi_1^\dagger \Phi_1) + \lambda_7 (\Phi_2^\dagger \Phi_2)] \Phi_1^\dagger \Phi_2 + h.c.\} \end{aligned} \tag{2.13}$$

In Eq. 2.13, m_{12}^2, λ_5, λ_6 and λ_7 are complex while other factors are real. Including the two vacuum expectation values, v_1 and v_2, there are 16 free parameters.

In this article, CP conservation is assumed, so all factors are real. Therefore the number of free parameters reduces to 12. Sin,ce flavor-changing neutral currents (FCNC) are highly suppressed by experimental measurements, we can apply one discrete symmetry ($\Phi_1 \to -\Phi_1$). This symmetry requires $\lambda_6 = \lambda_7 = 0$, and then exclude all tree-level Higgs-mediated FCNC's. In fact m_{12}^2 should be zero too under this symmetry, but we can relax this constraint because this cross term only mediates FCNC's at one loop. Therefore we have 10 free parameters, i.e., $\{m_{11}^2, m_{22}^2, m_{12}^2, \lambda 1, \lambda_2, \lambda_3, \lambda_4, \lambda_5, v_1, v_2\}$.

Applying the extreme condition, i.e.,

$$\frac{\partial V}{\partial \Phi_1} = \frac{\partial V}{\partial \Phi_2} = 0, \tag{2.14}$$

we have two more conditions such as

$$\begin{cases} m_{11}^2 &= m_{12}^2 \tan\beta - v^2 \dfrac{\lambda_1 \cos^2\beta + (\lambda_3 + \lambda_4 + \lambda_5)\sin^2\beta}{2} \\ m_{22}^2 &= m_{12}^2 \tan\beta - v^2 \dfrac{\lambda_2 \sin^2\beta + (\lambda_3 + \lambda_4 + \lambda_5)\cos^2\beta}{2} \end{cases}, \tag{2.15}$$

where $\tan\beta = \dfrac{v_2}{v_1}$ and $v = \sqrt{v_1^2 + v_2^2}$. Now the free parameter space becomes $\{m_{12}^2, \lambda_1, \lambda_2, \lambda_3, \lambda_4, \lambda_5, v_1, v_2\}$.

Diagonalizing the mass matrix leads to 3 Goldstone bosons ($G^{\pm}, G^0$), 2 CP-even scalars (H^0, h^0), one CP-odd scalar (A^0) and 2 charged bosons ($H^{\pm}$). After electroweak symmetry breaking, 3 degrees of freedom of Goldstons bosons are eaten by $W^{\pm}$ and Z bosons, therefore the gauge bosons get masses. All these scalars are the so-called mass eigenstates, and are related to the weak eigenstates as follows.

$$\begin{cases} H_1^{\pm} = G^{\pm}\cos\beta - H^{\pm}\sin\beta & H_2^{\pm} = G^{\pm}\sin\beta + H^{\pm}\cos\beta \\ \Im(H_1^0) = G^0\cos\beta - A^0\sin\beta & \Im(H_2^0) = G^0\sin\beta + A^0\cos\beta \\ \Re(H_1^0) = H^0\cos\alpha - h^0\sin\alpha + v_1 & \Re(H_2^0) = H^0\sin\alpha + h^0\cos\alpha + v_2 \end{cases} \tag{2.16}$$

In the above equation, α is the Higgs mixing angle between Higgs scalars which equals to

$$\tan 2\alpha = \frac{-2m_{12}^2 + 2(\lambda_3 + \lambda_4 + \lambda_5)v^2 \sin\beta\cos\beta}{(\lambda_1\cos^2\beta - \lambda_2\sin^2\beta)v^2 + m_{12}^2(\tan\beta - \cot\beta)} \tag{2.17}$$

And the eigenvalues, i.e. masses, have such solutions as

$$\begin{cases} m_A^2 &= \dfrac{m_{12}^2 - \lambda_5 v^2 \sin\beta\cos\beta}{\sin\beta\cos\beta}, \\ m_{H^{\pm}}^2 &= \dfrac{2m_{12}^2 - (\lambda_4 + \lambda_5)v^2\sin\beta\cos\beta}{2\sin\beta\cos\beta}, \\ m_{H,h}^2 &= \dfrac{\mathrm{Tr} \pm \sqrt{\mathrm{Tr}^2 - 4\mathrm{Det}}}{2}, \end{cases} \tag{2.18}$$

where, Tr and Det respectively represent the trace and determinant of the mass

matrix.

$$\begin{cases} \text{Tr} &= m_{12}^2(\cot\beta+\tan\beta)+v^2(\lambda_1\cos^2\beta+\lambda_2\sin^2\beta) \\ \text{Det} &= m_{12}^2v^2(\lambda_1\dfrac{\cos^3\beta}{\sin\beta}+\lambda_2\dfrac{\sin^3\beta}{\cos\beta}+2(\lambda_3+\lambda_4+\lambda_5)\sin\beta\cos\beta) \\ &\quad +v^4\sin^2\beta\cos^2\beta(\lambda_1\lambda_2-(\lambda_3+\lambda_4+\lambda_5)^2) \end{cases} \tag{2.19}$$

For the discussion of Higgs phenomena, it's more convenient to express our formula in terms of physical parameters, so the free parameter space can be reset as $\{m_{12}^2, m_{h^0}, m_{H^0},\ m_{A^0}, m_{H^\pm}, \alpha, v, \tan\beta\}$. In such space the trilinear couplings between neutral Higgs bosons are as follows.

$$\begin{aligned} \lambda_{hhh} =& \frac{1}{4v\sin^2(2\beta)}\{8m_{12}^2\cos(\alpha+\beta)\cos^2(\alpha-\beta) \\ & -m_{h^0}^2\left[3\cos(\alpha+\beta)+\cos(3\alpha-\beta)\right]\sin(2\beta)\} \end{aligned} \tag{2.20}$$

$$\begin{aligned} \lambda_{HHH} =& \frac{1}{4v\sin^2(2\beta)}\{8m_{12}^2\sin(\alpha+\beta)\sin^2(\alpha-\beta) \\ & -m_{H^0}^2\left[3\sin(\alpha+\beta)-\sin(3\alpha-\beta)\right]\sin(2\beta)\} \end{aligned} \tag{2.21}$$

$$\begin{aligned} \lambda_{HHh} =& \frac{1}{2v\sin^2(2\beta)}\{\sin(\alpha-\beta)\left[2m_{12}^2(\sin(2\beta)+3\sin(2\alpha))\right. \\ & \left.-(2m_{H^0}^2+m_{h^0}^2)\sin(2\alpha)\sin(2\beta)\right]\} \end{aligned} \tag{2.22}$$

$$\begin{aligned} \lambda_{hhH} =& \frac{1}{2v\sin^2(2\beta)}\{-\cos(\alpha-\beta)\left[2m_{12}^2(\sin(2\beta)-3\sin(2\alpha))\right. \\ & \left.+(m_{H^0}^2+2m_{h^0}^2)\sin(2\alpha)\sin(2\beta)\right]\} \end{aligned} \tag{2.23}$$

$$\begin{aligned} \lambda_{hAA} =& \frac{1}{4v\sin^2(2\beta)}\{4m_{A^0}^2\sin^2(2\beta)\sin(\alpha-\beta) \\ & -m_{h^0}^2\sin(2\beta)\left[\cos(\alpha-3\beta)+3\cos(\alpha+\beta)\right]+8m_{12}^2\cos(\alpha+\beta)\} \end{aligned} \tag{2.24}$$

$$\begin{aligned} \lambda_{HAA} =& \frac{1}{4v\sin^2(2\beta)}\{-4m_{A^0}^2\sin^2(2\beta)\cos(\alpha-\beta) \\ & -m_{H^0}^2\sin(2\beta)\left[\sin(\alpha-3\beta)+3\sin(\alpha+\beta)\right]+8m_{12}^2\sin(\alpha+\beta)\} \end{aligned} \tag{2.25}$$

Similar to the SM, fermions get masses from Yukawa coupling, but the situation in THDM is much more complicated since there are two Higgs doublets and both may give masses to up flavor and down flavor fermions. Based on the different structures, 3 classes of Yukawa couplings are most popularly discussed. Type I corresponds to one doublet coupling to both up- and down-type femions whereas the other does not couple to any fermions [17], type II corresponds to one doublet coupling to down flavor whereas the other couples to up flavor [18, 19], and type III to two doublets both coupling to two flavors [20]. In minimal supersymmetric standard model (MSSM), type-II is taken to be

$$\mathcal{L}^{fH} = \sum_{i,j=1}^{3} \left(G_u^{ij} \epsilon^{ab} \bar{\Psi}_L^{ia} H_1^b u_R^j + G_d^{ij} \bar{\Psi}_L^{ia} H_2^a d_R^j + h.c. \right), \tag{2.26}$$

where, ϵ is an anti-symmetric tensor, $\epsilon_{12} = 1$. Once $SU(2)_L$ is spontaneously broken, fermions get masses. The couplings between the Higgs and fermions are proportional to the mass of corresponding fermions. And these couplings depends on α and β as listed in 2.1.

g_{H^0tt}	$\dfrac{\sin\alpha}{\sin\beta}$	g_{H^0bb}	$\dfrac{\cos\alpha}{\cos\beta}$
g_{h^0tt}	$\dfrac{\cos\alpha}{\sin\beta}$	g_{h^0bb}	$-\dfrac{\sin\alpha}{\cos\beta}$
g_{A^0tt}	$\cot\beta$	g_{A^0bb}	$\tan\beta$

Table 2.1: Yukawa couplings between quarks and neutral Higgs bosons

The phenomenology of the Higgs also depends on the couplings of Higgs bosons to gauge bosons. These couplings can be derived from the kinetic part of

the Lagrangian as

$$\mathcal{L}^H = (D^\mu H_1)^\dagger (D_\mu H_1) + (1 \to 2) - V. \tag{2.27}$$

From Eq. 9.1 in the appendix, we have Table 2.2. If $\cos(\beta - \alpha) \to 0$, then the

g_{H^0WW}	$\cos(\beta - \alpha)$	g_{H^0ZZ}	$\cos(\beta - \alpha)$
g_{h^0WW}	$\sin(\beta - \alpha)$	g_{h^0ZZ}	$\sin(\beta - \alpha)$

Table 2.2: couplings between Higgs and gauge bosons

couplings of heavy Higgs to W and Z both approaches to 0 while h^0 becomes SM-like. It is the so-called decoupling limit.

Chapter 3

Minimal Supersymmetric Standard Model (MSSM)

3.1 Motivations for Supersymmetry

The fine-tuning problem shows that the SM is not complete. In the high-order correction, the physical mass is the bare mass plus the radiative corrections,

$$m_H^2 = (m_H^0)^2 + \delta m_H^2. \tag{3.1}$$

At the one-loop level, the possible corrections to the SM Higgs are listed in See Fig. 3.1. For simplicity, let's consider the first diagram, which comes from the

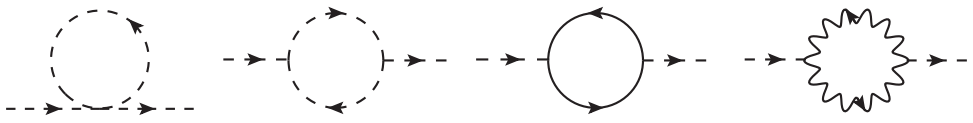

Figure 3.1: Radiative Correction to the Mass of Scalar Higgs. The first two loops come from the contributions of Higgs boson resptively through the interaction of four Higgs bosons and the interaction of three Higgs bosons. The third denotes the contribution from fermion while the fourth is for the gauge bosons.

coupling of four Higgs bosons, i.e,

$$\mathcal{L}_H = -\frac{g^2(m_H^0)^2}{32M_W^2} H_{SM}^4. \tag{3.2}$$

Therefore, the correction can be expressed as

$$\begin{aligned}
\delta m_H^2 &= \langle H_{SM} \left| \frac{g^2(m_H^0)^2}{32M_W^2} H_{SM}^4 \right| H_{SM} \rangle \\
&= 12 \frac{g^2(m_H^0)^2}{32M_W^2} \int \frac{d^4k}{(2\pi)^4} \frac{i}{k^2 - m_H^2} \\
&= 12 \frac{g^2(m_H^0)^2}{32M_W^2} \frac{1}{16\pi^2} \left(\Lambda^2 - m_H^2 \ln \left(\frac{\Lambda^2}{m_H^2} \right) + \mathcal{O}(\frac{1}{\Lambda^2}) \right),
\end{aligned} \tag{3.3}$$

where, Λ is the energy scale below which the SM is effective. From the above calculation, we find that the correction is quadratically divergent. However, theoretical consideration of unitarity shows that the physical mass of the SM Higgs should be at the weak scale, $m_H < (8\pi\sqrt{2}/3G_F)^{1/2}$ [21], and other calculations set both upper and lower limits [22, 23]. Moreover, the newest reports from CMS and Atlas both claim a scalar boson with mass about 125 GeV [24, 25]. If Λ is effective up to the GUT scale, $\Lambda \sim M_{GUT} \sim 10^{16}$GeV, then the squared bare mass of Higgs boson, $(m_H^0)^2$, should be fine tuned to 1 part in 10^{26} to maintain the physical mass at the predicted scale, so small and so weird. The SUSY model not only provides a new dark matter candidate, but also can solve the fine-tuning problem.

In the minimal supersymmetric standard model, we will introduce supermultiplets, each of which is composed of one fermionic field, one bosonic field and another to-be-canceled auxiliary field. The contributions to the loop correction will be cancelled between the ferimion loop and boson loop, which just leaves the logarithmically divergent term. For simplicity, let's demonstrate this in the

Wess-Zumino model,

$$\begin{aligned}\mathcal{L}_{int} = &-\frac{g}{\sqrt{2}}A\bar{\psi}\psi + \frac{ig}{\sqrt{2}}B\bar{\psi}\gamma_5\psi - gm\sqrt{2}AB^2 \\ &-\frac{gm}{\sqrt{2}}A(A^2-B^2) - g^2A^2B^2 - \frac{1}{4}g^2(A^2-B^2)^2. \end{aligned} \tag{3.4}$$

Now we consider the propagator of A to one-loop level as shown in Fig. 3.2.

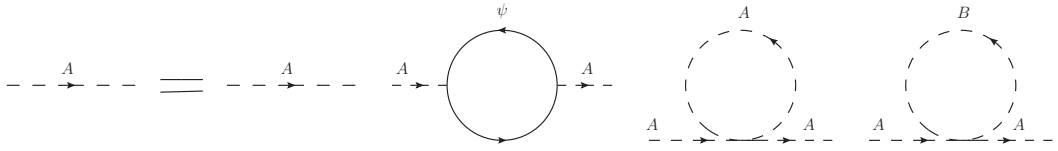

Figure 3.2: One-Loop Corrections to the Propagator of Boson A. The three loop diagrams respectively stand for the contributions of fermion, scalar and the auxiliary field.

The propagator should be modified to be

$$\frac{i}{p^2-m^2} \longrightarrow \frac{i}{p^2-m^2} + \frac{i}{p^2-m^2}\left(-i\Pi(p)\right)\frac{i}{p^2-m^2}, \tag{3.5}$$

and

$$\begin{aligned} i\Pi(p) &= g^2\int\frac{d^4q}{(2\pi)^4}\left[\frac{4q^2-4p.q+4m^2}{(q^2-m^2)\left((q-p)^2-m^2\right)} - \frac{1}{q^2-m^2} - 3\frac{1}{q^2-m^2}\right] \\ &= g^2\int\frac{d^4q}{(2\pi)^4}\frac{4p.q-4p^2+8m^2}{(q^2-m^2)\left((q-p)^2-m^2\right)} \end{aligned} \tag{3.6}$$

The loop correction from the boson has a different sign from the fermionic loops. Therefore, the cancellation between them leaves the integration logarithmically divergent.

Moreover, many experiments have proved that neutrinos are very light [26, 27, 28]. Experiments on tritium β decay set a upper limit for electron neutrino mass

which is $m(\nu_e) < 2eV$ [29], while a neutrino oscillation experiment measured the mass differences between 3 flavors of neutrinos: $\Delta m^2_{12} \approx 10^{-4} eV^2$ and $\Delta m^2_{23} \approx 10^{-3} eV^2$ [30]. So, as a dark matter candidate, the relic density from neutrinos could just account for a tiny fraction,

$$\Omega_\nu h^2 = \sum_{i=1}^{3} \frac{m_i}{93eV} < 0.07. \tag{3.7}$$

However, MSSM with R-parity conservation has an ideal candidate, the lightest neutralino, which is massive, neutral and stable.

And supersymmetry leads to a nice picture of gauge-coupling unification at large scale. Fig. 3.3 shows that, in SM, the discrepancy among three couplings is always there. However, in MSSM, the three couplings converge to one value at some large scale, i.e, *grand unified scale*, as shown in Fig. 3.4. It is commonly conjectured that there exists only one coupling beyond that scale. However, the physical picture beyond that scale is out of the discription of MSSM, or equivallently MSSM is just an effective theory at low energy scale. Maybe this unification of MSSM is just a coincidence, but it implies that we are on the right road.

3.2 Particle Spectrum of MSSM

In SUSY, each SM particle is extended to a supermultiplet, or superfields, which has a bosonic field and a fermionic field. They change to each other under SUSY transformation, so a SUSY theory should at least double the particle spectrum of the SM. The Minimal SUSY Model contains the smallest number of new particle states.

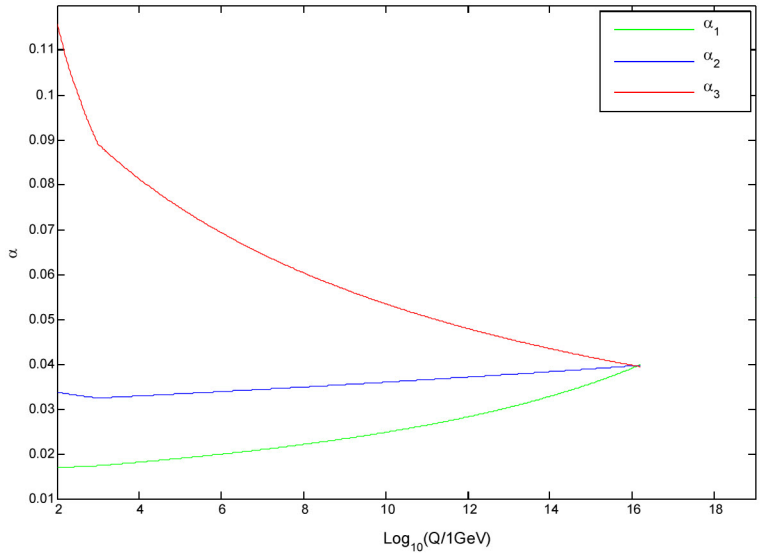

Figure 3.3: The evolution of gauge couplings generated by Isajet 7.8.1 in MSSM. The green curve stands for the evovtion of the gauge coupling of $SU(2)_L$, the blue one is for the gauge coupling of $U(1)_Y$, and the red is for the strong interaction.

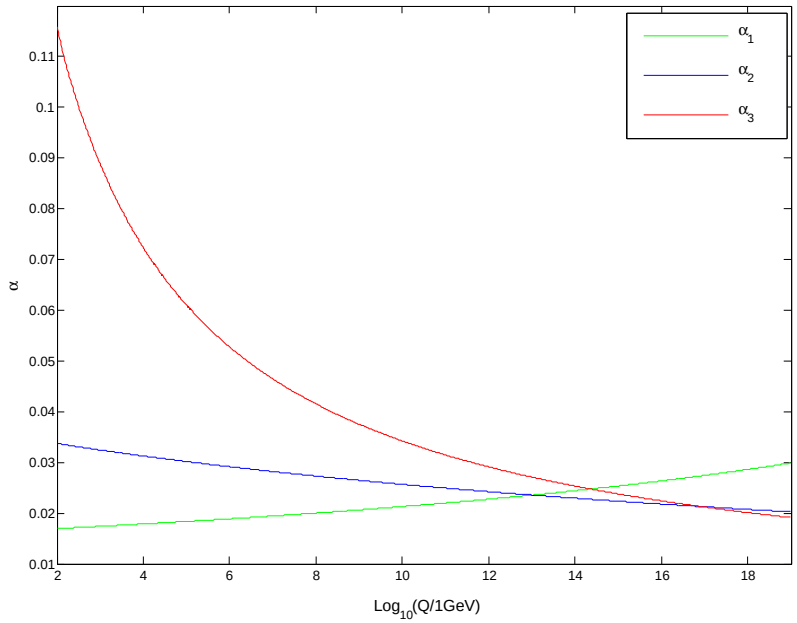

Figure 3.4: The evolution of gauge couplings generated by Isajet 7.8.1 in SM. The three curves have the same meanings as in Fig. 3.3

(1) Gauge Superfields of $SU(3)_C \otimes SU(2)_L \otimes U(1)_Y$

$$\begin{cases} B^{\nu} & \rightarrow & \hat{B} \ni (\lambda_0, B_{\nu}, D_B) \\ W_A^{\nu} & \rightarrow & \hat{W} \ni (\lambda_A, W_{A\nu}, D_{WA}), A = 1, 2, 3 \\ g_A^{\nu} & \rightarrow & \hat{g}_A \ni (\tilde{g}_A, G_{A\nu}, D_{gA}, A = 1, \cdots, 8 \end{cases} \tag{3.8}$$

Where, λ's stand for the gauginos, left-handed spinors, which are the corresponding superpartners of gauge bosons; D's are the auxiliary fields.

(2) Matter Superfields—Left Chiral Superfields

$$\begin{pmatrix} \nu_{iL} \\ e_{iL} \end{pmatrix} \rightarrow \hat{L}_i \equiv \begin{pmatrix} \hat{\nu}_i \\ \hat{e}_i \end{pmatrix} \tag{3.9}$$

Where, $\hat{e}_i \ni (\tilde{e}, \psi_{iL}, \mathcal{F}_i)$. The $\tilde{e}_i$ is the superpartner of the corresponding lepton; $\mathcal{F}_i$ denotes the auxiliary field. And $\hat{\nu}_i$ has the same components as $\hat{e}_i$

$$(e_{iR})^C \rightarrow \hat{E}_i^C \tag{3.10}$$

where, $(e_{iR})^C$ is the charge conjugate of right-handed electron since we need to construct the left chiral superfield.

$$\begin{pmatrix} u_{iL} \\ d_{iL} \end{pmatrix} \rightarrow \hat{Q}_i \equiv \begin{pmatrix} \hat{U}_i \\ \hat{D}_i \end{pmatrix} \tag{3.11}$$

$$\begin{cases} (u_{iR})^C & \rightarrow & \hat{U}_i^C \\ (d_{iR})^C & \rightarrow & \hat{D}_i^C \end{cases} \tag{3.12}$$

(3) Higgs Superfields

$$\begin{cases} H_1 = \begin{pmatrix} H_1^+ \\ H_1^0 \end{pmatrix} \rightarrow \hat{H}_1 = \begin{pmatrix} \hat{H}_1^+ \\ \hat{H}_1^0 \end{pmatrix} \\ H_2 = \begin{pmatrix} H_2^- \\ H_2^0 \end{pmatrix} \rightarrow \hat{H}_2 = \begin{pmatrix} \hat{H}_2^- \\ \hat{H}_2^0 \end{pmatrix} \end{cases} \tag{3.13}$$

As explained in last chapter, two Higgs doublets are needed to generate masses for all the elementary particles. Now there are two electrially charged fields, ϕ_1^+ and ϕ_2^-, and two electrically neutral fields, ϕ_1^0 and ϕ_2^0. Similarly any Higgs superfield is composed of one Higgs scalar, one left-handed spinor, i.e., higgsino, and one auxiliary field. The superpartners of ϕ_1^+ and ϕ_2^- are charged higgsinos, $\tilde{H}^{\pm}$. While the superpartners of ϕ_1^0 and ϕ_2^0 are two Majorana fermions, $\tilde{\psi}_{\phi_1^0}$ and $\tilde{\psi}_{\phi_2^0}$ respectively.

In Table 3.1 we list all the particles of MSSM.

Now we can define the charged winos as $\lambda^{\pm}$ in Eq. 3.14.

$$\lambda^{\pm} = \frac{\lambda_1 \mp i\lambda_2}{\sqrt{2}} \tag{3.14}$$

$\lambda^{\pm}$ mixes with $\tilde{H}^{\pm}$. By diagonalizing their mass matrix, we can get two fermionic mass eigenstates, $\chi_1^{\pm}$ and $\chi_2^{\pm}$, which are called charginos. Similarly the other four Majorana, λ_0, λ_3, $\tilde{\psi}_{\phi_1^0}$ and $\tilde{\psi}_{\phi_2^0}$, will mix with each other and lead to neutralinos, χ_1, χ_2, χ_3 and χ_4.

Boson Fields	Fermionic Partners	$SU(3)_C$	$SU(2)_L$	$U(1)_Y$
$G_{A\mu}$	$\tilde{g}_A$	8	0	0
$W_{A\mu}$	λ_A	1	3	0
B_μ	λ_0	1	1	0
$(\tilde{\nu}_{iL}, \tilde{e}_{iL})$	(ν_{iL}, e_{iL})	1	2	-1
$\tilde{e}^C_{iR}$	e^C_{iR}	1	1	2
$(\tilde{u}_{iL}, \tilde{d}_{iL})$	(u_{iL}, d_{iL})	3	2	1/3
$\tilde{u}^C_{iR}$	u^C_{iR}	3^*	1	$-4/3$
$\tilde{d}^C_{iR}$	d^C_{iR}	3^*	1	2/3
H^i_1	$(\tilde{H}^0_1, \tilde{H}^-_1)_L$	1	2	1
H^i_2	$(\tilde{H}^\dagger_2, \tilde{H}^0_2)_L$	1	2^*	-1

Table 3.1: Particle Spectrum of MSSM. The symbols with ˜ over them are SUSY partners of the SM particles. And the star symbols stand for the conjugate transformation.

3.3 Higgs Bosons in the MSSM

Satisfying supersymmetry and gauge symmetry of $SU(3)_C \otimes SU(2)_L \otimes U(1)_Y$, the master Lagrangian can be written as

$$\begin{aligned}
\mathcal{L} =& \sum_i (D_\mu S_i)^\dagger (D^\mu S_i) + \frac{i}{2}\sum_i \bar{\Psi}_i \not{D} \Psi_i + \sum_{\alpha,A}\left(\frac{i}{2}\bar{\lambda}_{\alpha A}\not{D}\lambda_{\alpha A} - \frac{1}{4}F_{\mu\nu\alpha A}F^{\mu\nu}_{\alpha A}\right) \\
&- \sqrt{2}\sum_{i,\alpha,A}(S^\dagger g_\alpha t_{\alpha A}\bar{\lambda}_{\alpha A}\frac{1-\gamma_5}{2}\Psi_i + h.c.) - \frac{1}{2}\sum_{\alpha,A}(\sum_i S^\dagger_i g_\alpha t_{\alpha A} S_i + \xi_{\alpha A})^2 \\
&- \sum_i \left|\frac{\partial \hat{f}}{\partial \hat{S}_i}\right|^2_{\hat{S}=S} - \frac{1}{2}\sum_{i,j}\bar{\Psi}_i\left[\left(\frac{\partial^2 \hat{f}}{\partial \hat{S}_i \partial \hat{S}_j}\right)_{\hat{S}=S}\frac{1-\gamma_5}{2}\right. \\
&\left. + \left(\frac{\partial^2 \hat{f}}{\partial \hat{S}_i \partial \hat{S}_j}\right)^\dagger_{\hat{S}=S}\frac{1+\gamma_5}{2}\right]\Psi_j
\end{aligned} \tag{3.15}$$

where, $\hat{f}$ is the superpotential. Constrained by the conservation of matter parity,

$$R = (-1)^{3B+L+2s}, \tag{3.16}$$

the general superpotential of MSSM is given by

$$\hat{f} = \mu \hat{H}_1^a \hat{H}_{2a} + \sum_{i,j=1,2,3} \left[(\mathbf{f}_u)_{ij} \epsilon_{ab} \hat{Q}_i^a \hat{H}_1^b \hat{u}_j^C + (\mathbf{f}_d)_{ij} \hat{Q}_i^a \hat{H}_{2a} \hat{D}_j^C + (\mathbf{f}_e)_{ij} \hat{L}_i^a \hat{H}_{2a} \hat{E}_j^C \right]. \tag{3.17}$$

R-parity conservation is the natural result of baryon number conservation and lepton number conservation. Otherwise the proton would decay rapidly, which conflicts with our observation. Moreover, R-parity conservation assures the stability of the lightest supersymmetric particle (LSP). The weakly interacting LSP is considered as an ideal candidate for dark matter.

Since superpartners have different masses from SM particles, SUSY must be broken by some mechanism. Therefore, we have to introduce SUSY breaking terms. If this symmetry is softly broken, the most general gauge invariant soft SUSY breaking terms are specified by

$$\begin{aligned}
\mathcal{L}_{sf} = & - \Big[\tilde{Q}_i^\dagger m_{Qij}^2 \tilde{Q}_j + \tilde{d}_{Ri}^\dagger m_{Dij}^2 \tilde{d}_{Rj} + \tilde{u}_{Ri}^\dagger m_{Uij}^2 \tilde{u}_{Rj} \\
& + \tilde{L}_i^\dagger m_{Lij}^2 \tilde{L}_j + \tilde{e}_{Ri}^\dagger m_{Eij}^2 \tilde{e}_{Rj} + m_{H_1}^2 |H_1|^2 + m_{H_2}^2 |H_2|^2 \Big] \\
& - \frac{1}{2} \left[M_1 \bar{\lambda}_0 \lambda_0 + M_2 \bar{\lambda}_A \lambda_A + M_3 \bar{\tilde{g}}_B \tilde{g}_B \right] \\
& - \frac{i}{2} \left[M_1' \bar{\lambda}_0 \gamma_5 \lambda_0 + M_2' \bar{\lambda}_A \gamma_5 \lambda_A + M_3' \bar{\tilde{g}}_B \gamma_5 \tilde{g}_B \right] \\
& + \Big[(\mathbf{a}_u)_{ij} \epsilon_{ab} \tilde{Q}_i^a H_1^b \tilde{u}_{Rj}^\dagger + (\mathbf{a}_d)_{ij} \tilde{Q}_i^a H_{2a} \tilde{d}_{Rj}^\dagger + (\mathbf{a}_e)_{ij} \tilde{L}_i^a H_{2a} \tilde{e}_{Rj}^\dagger + h.c. \Big] \\
& + \Big[(\mathbf{c}_u)_{ij} \epsilon_{ab} \tilde{Q}_i^a H_2^{*b} \tilde{u}_{Rj}^\dagger + (\mathbf{c}_d)_{ij} \tilde{Q}_i^a H_{1a}^* \tilde{d}_{Rj}^\dagger + (\mathbf{c}_e)_{ij} \tilde{L}_i^a H_{1a}^* \tilde{e}_{Rj}^\dagger + h.c. \Big] \\
& + \left[B \mu H_1^a H_{2a} + h.c. \right].
\end{aligned} \tag{3.18}$$

Therefore the tree level scalar potential is

$$\begin{aligned} V_{MSSM} =& \frac{1}{2}\sum_{\alpha,A}\left[\sum_i S_i^\dagger g_\alpha t_{\alpha A} S_i\right]^2 + \sum_i \left|\frac{\partial^2 \hat{f}}{\partial \hat{S}_i}\right|^2_{\hat{S}=S} \\ & - m_{H_1}^2 |H_1|^2 - m_{H_2}^2 |H_2|^2 - (bH_1^a H_{2a} + h.c.) \end{aligned} \tag{3.19}$$

In Eq. 3.19, we only sum the scalars over Higgs doublets, so $i = 1, 2$, $\alpha = 1, 2$ and t_A runs over the generators of $SU(2)_L \otimes U(1)_Y$. Therefore we have

$$\begin{aligned} V_{MSSM} =& (-m_1^2 + \mu^2) H_1^\dagger H_1 + (-m_2^2 + \mu^2) H_2^\dagger H_2 - B\mu (H_1^\dagger H_2 + H_2^\dagger H_1) \\ & + \frac{g^2 + g'^2}{8}[(H_1^\dagger H_1)^2 + (H_2^\dagger H_2)^2] + \frac{g^2 - g'^2}{4}[H^\dagger 1 H 1 H 2^\dagger H 2] \\ & - \frac{g^2}{2}(H_1^\dagger H_2 H_2^\dagger H_1) \end{aligned} \tag{3.20}$$

Compared with Eq. 2.13, the following results are straitforward.

$$\begin{cases} m_{11}^2 &= -m_1^2 + \mu^2 \\ m_{22}^2 &= -m_2^2 + \mu^2 \\ m_{12}^2 &= B\mu \\ \lambda_1 &= \dfrac{g^2 + g'^2}{4} \\ \lambda_2 &= \dfrac{g^2 + g'^2}{4} \\ \lambda_3 &= \dfrac{g^2 - g'^2}{4} \\ \lambda_4 &= -\dfrac{g^2}{2} \\ \lambda_5 &= 0 \end{cases} \tag{3.21}$$

And the minimal condition, Eq. 2.15 changes to

$$\begin{cases} m_{11}^2 &= B\mu \tan\beta - \dfrac{g^2+g'^2}{8} v^2 \cos 2\beta \\ m_{22}^2 &= B\mu \tan\beta + \dfrac{g^2+g'^2}{8} v^2 \cos 2\beta \end{cases} \tag{3.22}$$

With these condition, we can further reduce the number of free parameters to 2. Conventionally m_{A^0} and $\tan\beta$ are chosen as the two free parameters. Therefore the masses of Higgs bosons can be rewritten as

$$\begin{cases} m_{H^\pm}^2 &= m_{A^0}^2 + m_W^2 \\ m_{h^0,H^0}^2 &= \dfrac{1}{2}\left[(m_{A^0}^2 + m_Z^2) \mp \sqrt{(m_{A^0}^2 + m_Z^2)^2 - 4 m_{A^0}^2 m_Z^2 \cos^2\beta}\right] \end{cases} \tag{3.23}$$

Eq. 3.23 yields such inequality as $m_{h^0} \leq m_Z$ which contrasts with experimental results and pushes us to consider the higher order correction. At the one loop, the shift of the Higgs mass gets a large contribution from the quark and squark loop, therefore the light Higgs becomes heavier as shown in Eq.3.24[31],

$$\Delta m_{h^0} \approx \frac{3g^2 m_t^4}{16\pi^2 m_W^2 \sin^2\beta} \log \frac{m_{\tilde{t}_1}^2 m_{\tilde{t}_2}^2}{m_t^4}. \tag{3.24}$$

And the heavy Higgs becomes nearly degenerate with pseudoscalar[32, 33, 34]. In Fig. 3.5, we plot the one loop effect with a common mass scale, $M_{SUSY} = m_{\tilde{g}} = m_{\tilde{f}} = \mu = -A_f = 5$ TeV.

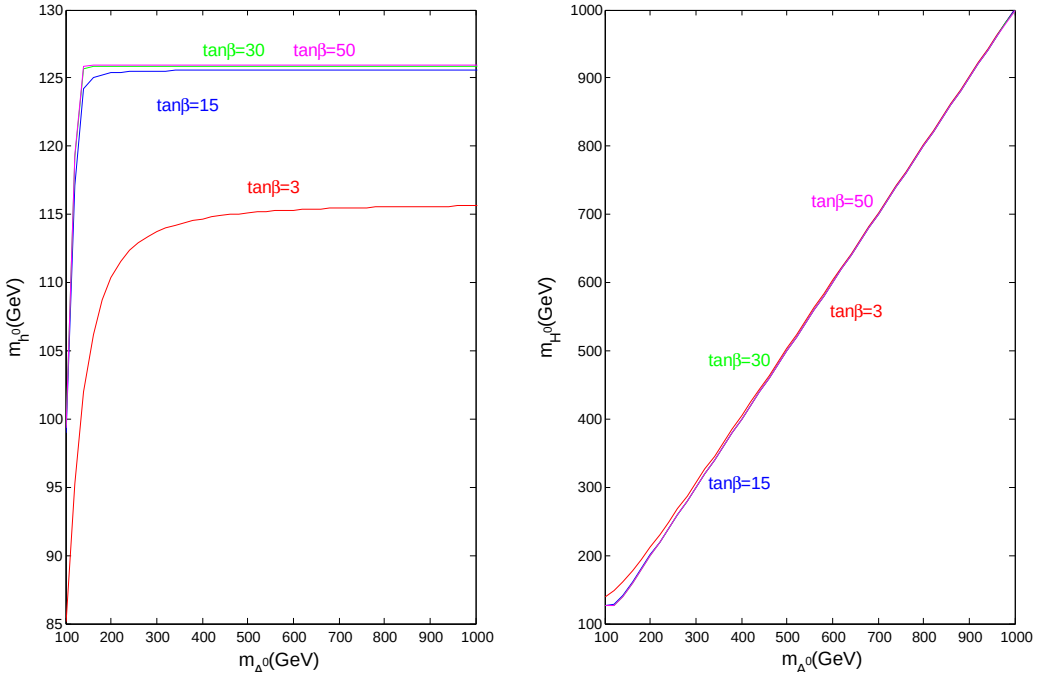

Figure 3.5: Mass of Higgs Bosons at One-Loop. The left frame refers to the one-loop correction to the mass of light Higgs where the different colors correspond to different $\tan\beta$. The right frame is for the one-loop correction to the mass of heavy Higgs.

Chapter 4

Higgs Decays to $\tau^+\tau^-$ and Mass Reconstruction

At a high energy hadron collider, Higgs bosons can be produced through many channels, e.g., gluon fusion, vector boson fusion, b-associated production and so on. Gluon fusion is the dominant process in the SM and even in the MSSM with moderate values of $\tan\beta$ [35] due to the high population of gluon and the high masses of intermediate fermions along the loop, while the production cross sections from other channels are much smaller because of kinetic reasons or because the Yukawa couplings are suppressed by the ratio of quark mass to the mass of the W boson, $Y^{SM}_{hq\bar{q}} \propto \frac{m_q}{m_W}$. However, in the decoupling limit of SUSY models, Yukawa couplings are enhanced by a large value of $\tan\beta$, especially the couplings of H^0 and A^0 with bottom flavor fermions. Therefore, b associated production would make important contributions to the concerned signal [36]. We will first consider the production of SM Higgs through such process as $pp \to gh + X$, and then the production of H^0 and A^0 via bremsstrahlung from b quarks.

Once Higgs bosons are produced, they would immediately decay to light par-

ticles. Fig 4.1 shows the dependence of branching ratios of SM Higgs on the mass of Higgs boson. In the range about $m_{h^0} = 125$ GeV, SM Higgs dominantly decays to $b\bar{b}$ pair with $Br(h^0 \to b\bar{b} \simeq 63\%)$ while $Br(h^0 \to \tau^+\tau^-) = \frac{m_\tau^2}{3m_b^2} \times Br(h^0 \to b\bar{b}) \sim 6\%$, where m_b is the running mass of b quark at energy scale of Higgs mass. However, $h^0 \to b\bar{b}$ is usually overwelmed by QCD background if without other handles. So $h^0 \to \tau^+\tau^-$ channel is more promising in search for Higgs decaying to fermions.

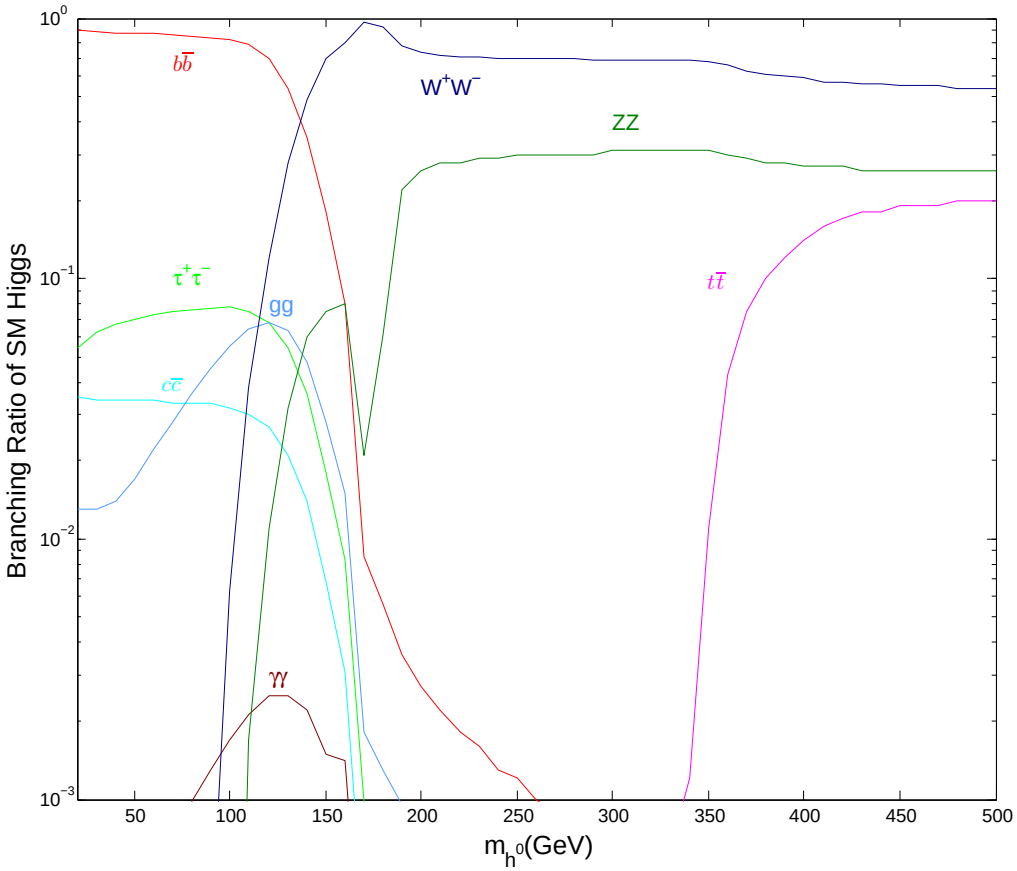

Figure 4.1: Branching Ratio of SM Higgs.

Actually τ is not the final particle either. They usually decay to lighter leptons (e/μ) or hadronic jets ($\pi/a_1/\rho$) and missing energy with certain branching ratios

which are $Br(\tau \to e\nu_e\nu_\tau) = 17.84\%$, $Br(\tau \to \mu\nu_\mu\nu_\tau) = 17.36\%$, $Br(\tau \to \pi\nu_\tau) = 11.06\%$, $Br(\tau \to \rho\nu_\tau) = 25.42\%$ and $Br(\tau \to a_1\nu_\tau) = 18.29\%$. According to the final particles, the decay modes fall into three categories: 2 leptons, 1 lepton with 1 hadronic jet and 2 jets. The first case has a cleaner background; the second case happens with highest probability; the last one is the worst case because of the huge QCD background. In this thesis, we just discuss the first two cases.

Due to the absence of tau leptons in the final state, we have to reconstruct them from the kinematics of observed particles. In the case of one lepton with one jet, the observed quantities are the transverse momentum of charged lepton (p_T^l), the transverse momentum of tau jets (p_T^h) and the missing transverse momentum ($\not{p}_T$). Since Higgs bosons are much heavier than tau lepton, the two intermediate τ's are very energetic. Then the final particles from tau decay are almost along the direction of their parent tau lepton, which is the so-called *collinear approximation* [37]. Under this approximation, we have two equations such as

$$\left(\frac{1}{x_l} - 1\right) P_T^l + \left(\frac{1}{x_h} - 1\right) P_T^h = \not{P}_T, \tag{4.1}$$

where x_l and x_h are the energy fraction carried away from the parent τ's respectively by final charged lepton and j_τ. With two unknowns in two equations, we can find x_l and x_h, and then reconstruct the momenta of two tau leptons i.e., p_{τ_1}andp_{τ_2}. In the plane of x_l x_h, the distribution of the signal is totally different from background. Take the production of double SM Higgs via gluon fusion for example, the distribution of signal events and the major background events such as $pp \to t\bar{t} \to b\bar{b}lj + \not{E}_T + X$ are shown in Fig. 4.2. So if we properly set the cuts over x_l and x_h, we can remove most of background events.

Based on the reconstructed momenta, the mass of Higgs boson is the invariant

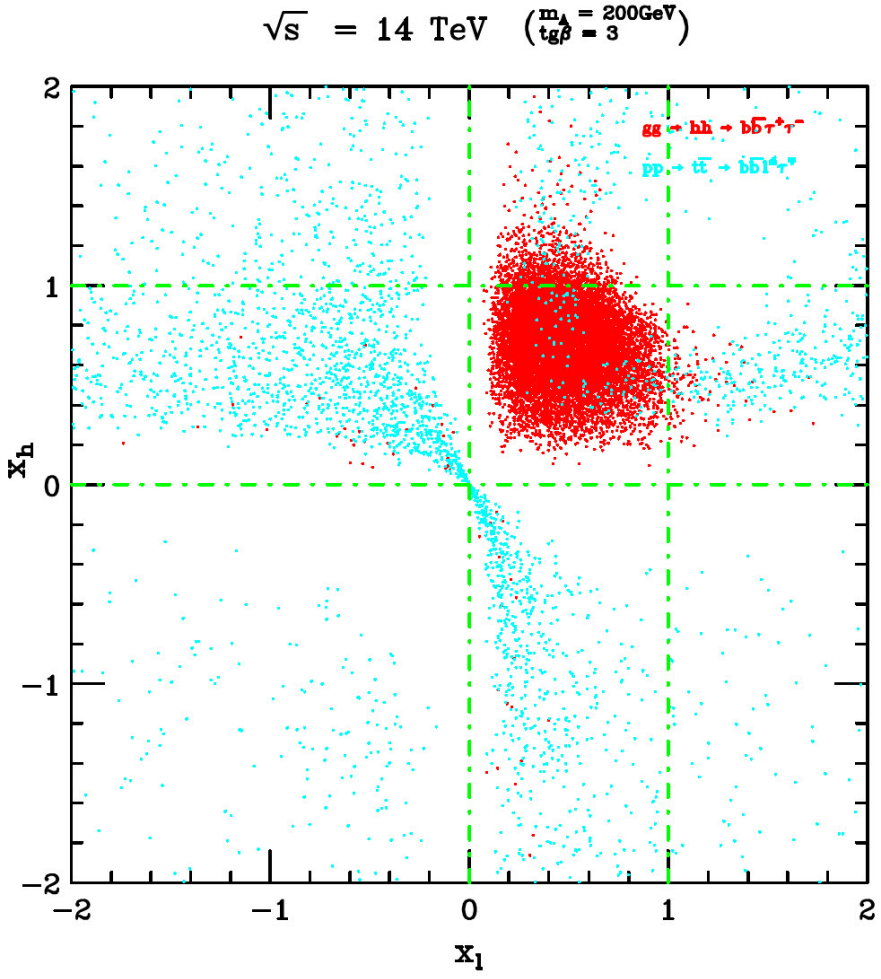

Figure 4.2: Distribution of signal and background events in the plane of x_l x_h. The red dots represent the events from gluon fusion to double pseudoscalars in MSSM while the cyan dots are for the production of $t\bar{t}$.

mass of $\tau^+\tau^-$ paris, $m_{\tau\tau} = (p_{\tau_1} + p_{\tau_2})^2$. The distribution of signal events usually peaks at the mass of expected Higgs, but the distribution of background is totally different. Fig. 4.3 shows the mass distribution of $m_{\tau\tau}$ in the processes of $gg \to hh \to b\bar{b}\tau^+\tau^-$ and $pp \to t\bar{t} \to b\bar{b}\tau^+\tau^- + \not{E}_T + X$. Events far away from the peak come from background processes very probably. By setting cuts on $m_{\tau\tau}$, we can remove most background events and then enhance the discovery potential. Actually the cuts on x_l, x_h and $m_{\tau\tau}$ are the most helpful and almost leave no space for other selection cuts to work. The details of this point will be discussed in next chapter.

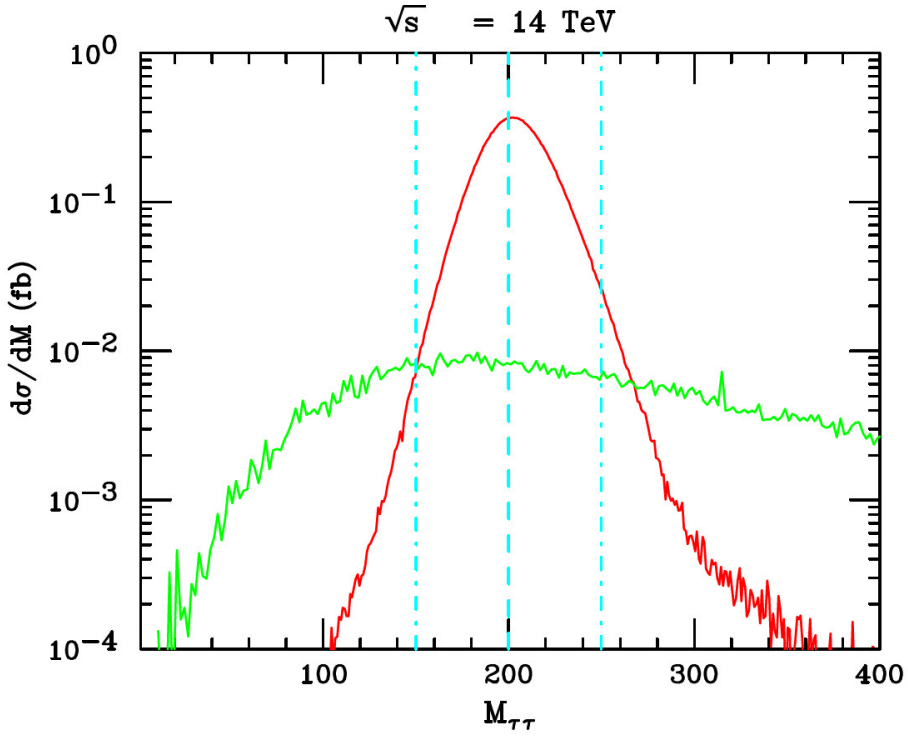

Figure 4.3: Distribution of invariant mass of reconstructed τ Pairs. The red curve stands for the mass distribution of gluon fusion with an expected pseudoscalar, e.g., $m_{A^0} = 200$ GeV. And the green curve plots the major background process, i.e., the production of top pairs.

In the computer simulation of tau decay, $e^{\pm}$, $\mu^{\pm}$ and $\pi^{\pm}$ are treated as mass-

less, so the energy fractions of these three final particles span a range from 0 to 1. However, a_1 and ρ have masses comparable to the tau mass: $m_\tau = 1.7771$ GeV, $m_{a_1} = 0.1829\ GeV$ and $m_\rho = 0.2542\ GeV$, so the energy fractions of a_1 and ρ should be greater than the ratios of their masses to tau mass and less than 1, i.e., $0.1 < x_{a_1} < 1$ and $0.14 < x_\rho < 1$. Moreover the branching ratio of τ to a_1 and ρ is much greater than the branching ratio of τ to π. Therefore it's reasonable to set x_h greater than 0.1 as shown in Fig. 4.2.

The distributions of tau decay with respect to x_l or x_h are described by different probability distribution functions in the paper [37]. For purely leptonic tau decay, the distribution function is

$$\frac{1}{\Gamma_l}\frac{d\Gamma_l}{dx_l} = \frac{1}{3}(1-x_l)[(5+5x_l-4x_l^2) + P_\tau(1+x_l-8x_l^2)], \tag{4.2}$$

where, Γ_l stands for the decay width of $\tau \to e$ or μ; P_τ denotes the polarization. For the decay $\tau \to \pi + \nu_\tau$, we have

$$\frac{1}{\Gamma_\pi}\frac{d\Gamma_\pi}{dx_h} \simeq 1 \mp P_\tau(2x_h - 1). \tag{4.3}$$

For other decay modes $\tau \to a_1$ or ρ, since these mesons are massive, the polarization states could be longitudinal or transverse. Different polarization states of final mesons corresponds to different probability distribution functions.

$$\begin{aligned}\frac{1}{\Gamma_h}\frac{d\Gamma_h^T}{dx_h} =& \frac{m_\tau^2 m_h^2}{(m_\tau^2 - m_h^2)(m_\tau^2 + 2m_h^2)} \times \left[\frac{m_\tau^2}{m_h^2}\sin^2\omega + 1 + \cos^2\omega \right. \\ & \left. + P_\tau \cos\theta \times \left(\frac{m_\tau^2}{m_h^2}\sin^2\omega - \frac{m_\tau}{m_h}\sin 2\omega \tan\theta - 1 - \cos^2\omega\right)\right]\end{aligned} \tag{4.4}$$

and

$$\frac{1}{\Gamma_h}\frac{d\Gamma_h^L}{dx_h} = \frac{m_\tau^2 m_h^2}{(m_\tau^2 - m_h^2)(m_\tau^2 + 2m_h^2)} \times \left[\frac{m_\tau^2}{m_h^2}\cos^2\omega + \sin^2\omega \right. \\ \left. + P_\tau \cos\theta \times \left(\frac{m_\tau^2}{m_h^2}\cos^2\omega + \frac{m_\tau}{m_h}\sin 2\omega \tan\theta - \sin^2\omega\right)\right], \tag{4.5}$$

where, Γ_h^T and Γ_h^L respectively represent the decay width of longitudinal and transverse mesons, and θ and ω are defined as follows.

$$\begin{cases} \cos\omega &= \dfrac{(m_\tau^2 - m_h^2) + (m_\tau^2 + m_h^2)\cos\theta}{(m_\tau^2 + m_h^2) + (m_\tau^2 - m_h^2)\cos\theta} \\ \cos\theta &= \dfrac{2x_h - 1 - m_h^2/m_\tau^2}{1 - m_h^2/m_\tau^2} \end{cases} \tag{4.6}$$

In the above equations, P_τ stands for the chirality of tau leptons. In the decay channel, $h^0 \to \tau^+\tau^-$, the polarization states of two leptons are anti-correlated due to coupling $\bar{\psi}\psi\phi$. So if we set the chirality of one τ to be $+1$, the other should be -1, and vice versa. And the two combinations of chirality states have equal probability. In the case of vector-to-fermion decay, the situation is totally different due to the different form of interaction Lagrangian, $\bar{\psi}\gamma^\mu\psi$. Now the chirality states of two fermions are in common.

Chapter 5

Higgs Bosons with Large p_T in the Standard Model

5.1 Introduction

Since the estatablishment of the SM in the 1960's, there has not been any experimental observation that decisively contradict this theory. And the reports from CMS and ATLAS separately claimed the discovery of a new scalar which seems to be the SM Higgs. So, our next major mission should be extending our research to the deeper properties of this new scalar. For example, we should take a closer look at its decay results, spin, interactions with other particles, and so on. The SM Higgs is not the only possible candidate for this scalar. It could be a compound state of other elementary particles or a scalar predicted in other models. Theoretically we have the radion, predicted in the Randall-Sundrum (RS) model [38, 39, 40, 41], and the dilaton in the lower dimensional effective theory of Kaluza-Klein theories [42, 43, 44, 45]. In this chapter we will discuss the production of the SM Higgs in such process as $pp \to j\phi + X$ at hadron colliders

and its decay in the channel of $\phi \to \tau^+\tau^- \to l^\pm j_\tau^\mp + \not{E}_T$.

5.2 Calculation Tools

When calculating the production of one SM Higgs associated with one light jet at LHC with $\sqrt{s} = 14$ TeV, we have to consider the one-loop diagrams as shown in Fig. 9.1 in the appendix. About the production of signal, there are three processes which are worthy of our concerns such as $gg \to gh^0$, $gq \to qh^0$ and $q\bar{q} \to gh^0$ with $q = u, d, c, s$. The first one is the major process of signal production and involes three box and three triangle loops at the order of α_s^3. The other two just go through triangle loops at the same order. Along the loop , the intermediate fermions are massive quarks of third generation. The masses of these quarks in Yukawa couplings have been calculated up to the one-loop QCD correction with the pole masses set to be $M_t = 173.1\ GeV$ and $M_b = 4.7\ GeV$ which are the masses of fermi propagators in the loop diagrams. As for the strong coupling, the two-loop QCD correction has been considered. The renormalization scale is set to be $\mu_R = \sqrt{p_T^2(j) + m_{h^0}^2}$. First the transition matrices of $gg \to gh^0, gq \to qh^0$ and $qq \to gh^0$ are derived by hand. And then, based on Passarino and Veltman's work [46], all tensor integrals are reduced to scalar integrals, D_0, C_0, B_0 and A_0, with the aid of FORM [47]. The decay of the Higgs boson is simulated by applying the narrow width approximation (NWA). This approximation works very well in Higgs decay because the parent particle ($m_{h^0} = 125\ GeV$) is much heavier than the daughter particles ($m_\tau = 1.7771\ GeV$). The succeeding tau decay is simulated according to the collinear approximation as explained in the last chapter.

All the background events are tackled at tree level and the transition matrix

elements are generated by Madgraph Standalone [48]. In order to include the high order correction, we just multiply our tree level resutls with K factors. The K factor is a process dependent multiplicative factor. For background calculation, the renormalization scale is the parton center of mass energy $\mu_R = \sqrt{\hat{s}}$.

Finally we simulate the pp collisions by using the parton distribution function CTEQ6L1 [49]. Here we choose different factorization scales for signal and background calculations, i.e., $\mu_F = \sqrt{p_T^2(j) + m_{h^0}^2}$ for signal but $\mu_F = \sqrt{\hat{s}}$ for background.

Throughout this thesis other SM parameters ever used are:

$$M_Z = 91.187\ GeV, \qquad \sin^2\theta_W = 0.23113, \qquad \alpha = \frac{1}{128.877}.$$

We assume that the experimental measurements satisfy the normal distribution around the theoretical values. Therefore we simulate this performance by smearing the measured momenta with Gaussian distributions as follows.

$$\begin{cases} \dfrac{\Delta E}{E} = \dfrac{0.5}{\sqrt{E}} \oplus 0.03 & \text{Hadronic Jet,} \\ \dfrac{\Delta E}{E} = \dfrac{0.25}{\sqrt{E}} \oplus 0.01 & \text{Charged Lepton.} \end{cases} \tag{5.1}$$

5.3 Analysis of Selection Cuts

To detect the final states at LHC with luminosity $\mathcal{L} = 30^{-1}\ fb$ and $\sqrt{s} = 14$ TeV, the basic acceptance cuts are:

$$\begin{cases} P_T(j) > 15\ GeV, & P_T(l) > 20\ GeV, & P_T(j_\tau) > 40\ GeV \\ \eta(j) < 2.5, & \eta(l) < 2.5, & \eta(j_\tau) < 2.5 \\ \Delta R(jj_\tau) > 0.4, & \Delta R(lj_\tau) > 0.4 & \Delta R(lj) > 0.4 \\ \not{E}_T > 40\ GeV, & m(l,\ \not{E}_T) < 30\ GeV & \Phi(l, j_\tau) < 170^\circ \end{cases} . \tag{5.2}$$

Those particles with central high P_T are required by the ATLAS and CMS triggers with high tagging effeciency. In Fig. 5.1, the p_T distributions of light jet, lepton and tau jet are plotted in red, blue and green respectively. The left frame is for the major signal process, $gg \to gh^0$. And the right frame is for the dominating background process, $pp \to j\tau^\pm\tau^\mp \to jl^\pm j_\tau^\mp$.

For light particles, the pseudorapidity η is defined as

$$\eta \equiv -\ln[\tan(\frac{\theta}{2})] \tag{5.3}$$

$$\approx -\mathrm{sgn}(p_z)\ln\left(\frac{|\vec{p}| + |p_z|}{p_T}\right) \tag{5.4}$$

which describes the angle of the outgoing particle with respect to the collision beam. Fig. 5.2 shows the η distribution of three final observable particles. The solid lines are for the signal of gluon fusion while the dot-dashed lines corresponds to the most important background process.

In order to tell particle from particle, we also need to put cuts on the angle

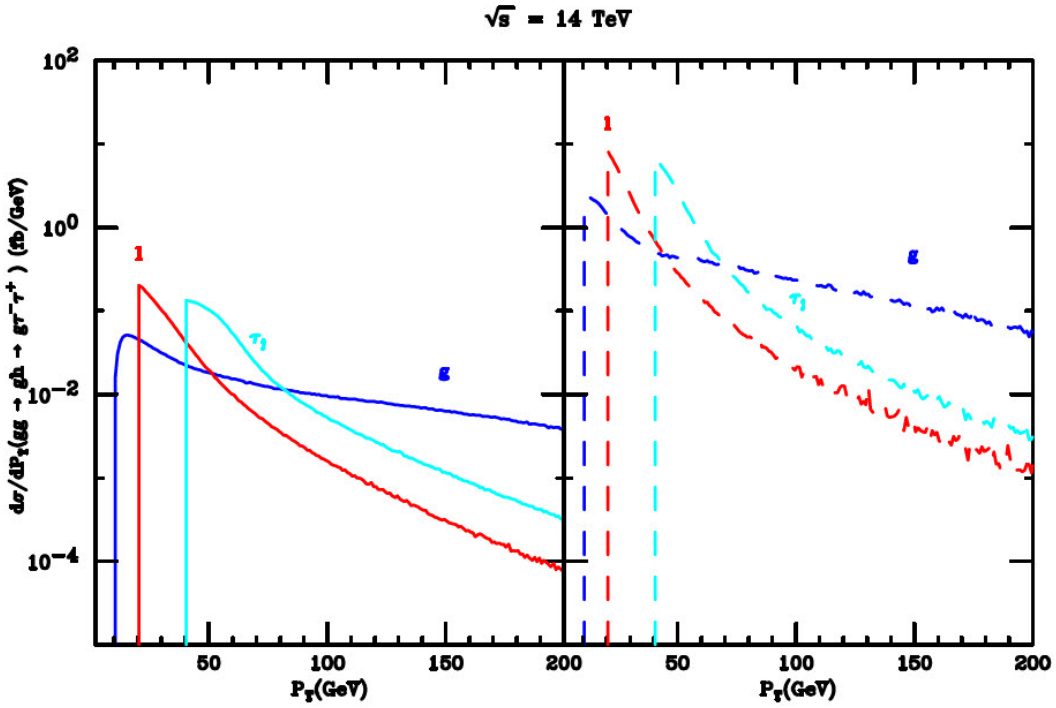

Figure 5.1: Distribution of transverse momentum. The left frame plots the distribution curves of $gg \to gh^0$ while the right frame is for the background process, i.e., $pp \to j\tau^+\tau^- + X$. The red, blue and cyan respectively for the transverse momenta of lepton, gluon and tau jet.

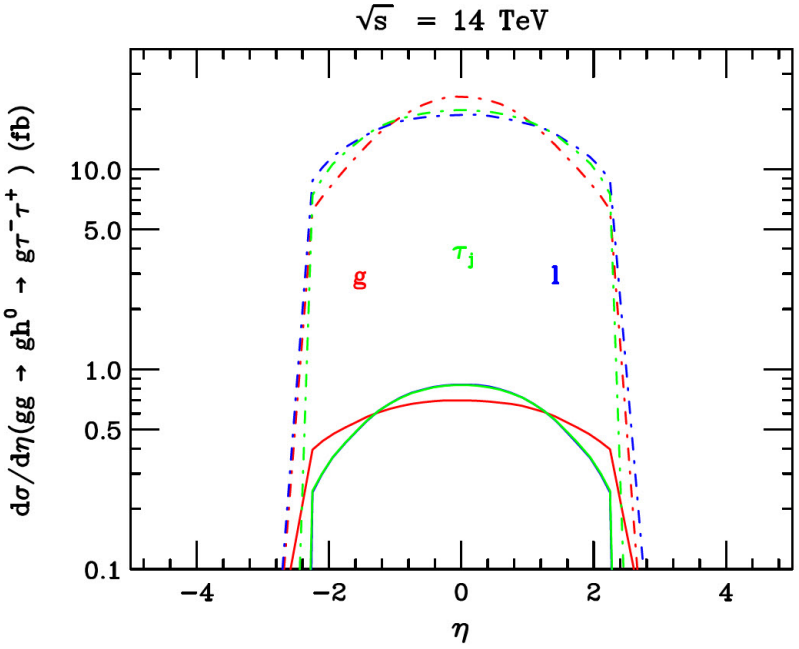

Figure 5.2: Distribution of pseudorapidity of gluon, lepton and tau jet. The solid curves are for the signal process, i.e., $gg \to gh^0$, while the dash-dotted lines are for the major background process, i.e., $pp \to j\tau^+\tau^- + X$.

seperation of final particles, ΔR which is defined as

$$\Delta R = \sqrt{(\Delta\Phi)^2 + (\Delta\eta)^2}, \tag{5.5}$$

where Φ is the angle between two particles in the transverse plane. Fig. 5.3 shows the seperations of light jet and tau jet (red), of light jet and lepton (blue), and of tau jet and lepton. From this figure it's clear that all three particles are largely seperated not only in signal events, but also in background events.

For completeness, we also draw the distribution of missing energy ($\not{E}_T$) in Fig. 5.4 and transverse angle $\phi(l, j_\tau)$ between lepton and tau jet in Fig. 5.5.

The quantity of $m(l,\ \not{E}_T)$ is the transverse mass of lepton and neutrino as defined in Barger's *Collider Physics* [50]. Transverse mass is very helpful to analyze one-to-two decay, for instance, $W^\pm \to e(\mu) + \nu$, but not so efficient in

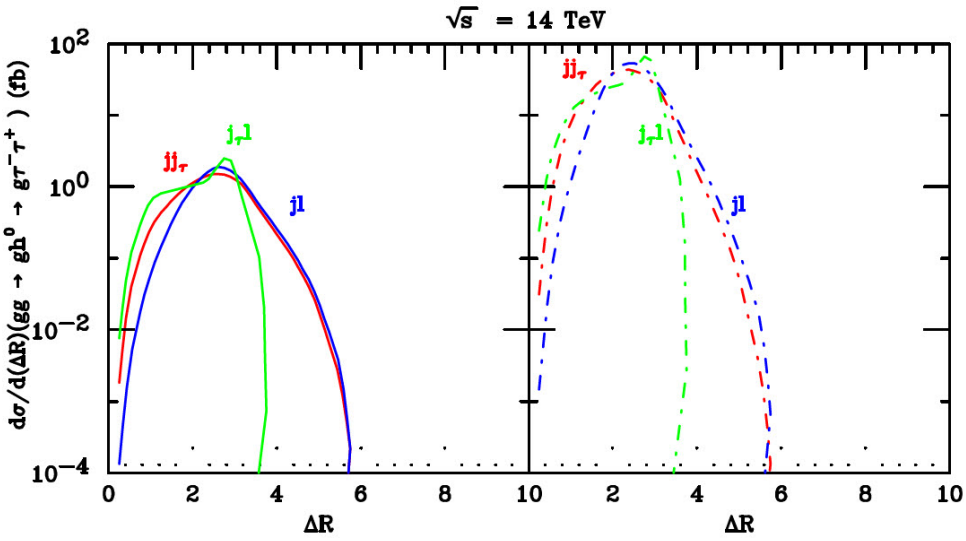

Figure 5.3: Angular separations of the three final particles. The left frame is for the signal process and the right frame is for Drell-Yan process.

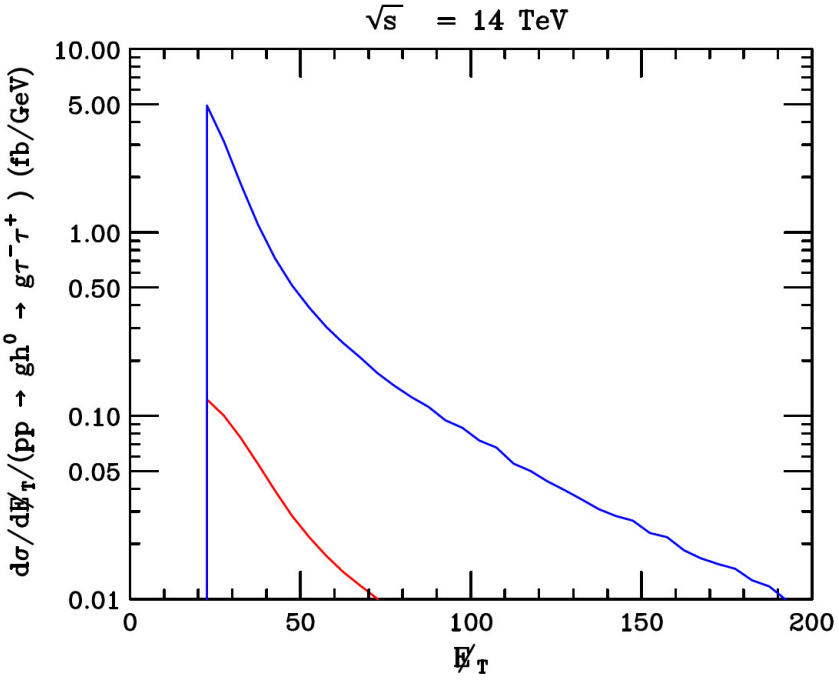

Figure 5.4: Distribution of missing transverse energy. The red line refers to the signal while the blue one to the major background.

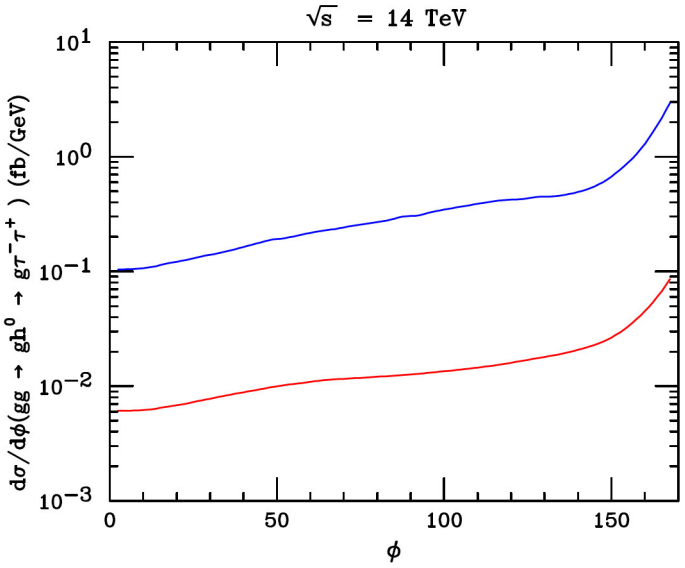

Figure 5.5: Transver angle of lepton and tau jet. Red line referes to the signal while the blue one to the major background.

this cascade decay.

In order to improve the discovery potential, we also have explored the distribution of momentum tensor. The normalized momentum tensor is defined as

$$M_{ab} = \sum_i p_{ia} p_{ib} / \sum_i p_i^2, \tag{5.6}$$

where i stands for the i^{th} particle while a and b refer to the three directions of space. Since M is a symmetric real matrix and normalized, there exist three eigenvalues, Q_1, Q_2 and Q_3. These eigenvalues are positive definite and $Q_1+Q_2+Q_3 = 1$. Usually they are labeled in the ascending order, i.e., $Q_1 \leq Q_2 \leq Q_3$. From Fig. 5.6 we can see that Q_3 is much larger than Q_1 among most events as expected in collinear approximation.

All the above discussion about different kinetic variables leads to one conclusion: no selection cut on these variables can significantly improve the situation. The reason is that the cuts over x_l, x_h and $m_{\tau\tau}$ are so stringent that all the

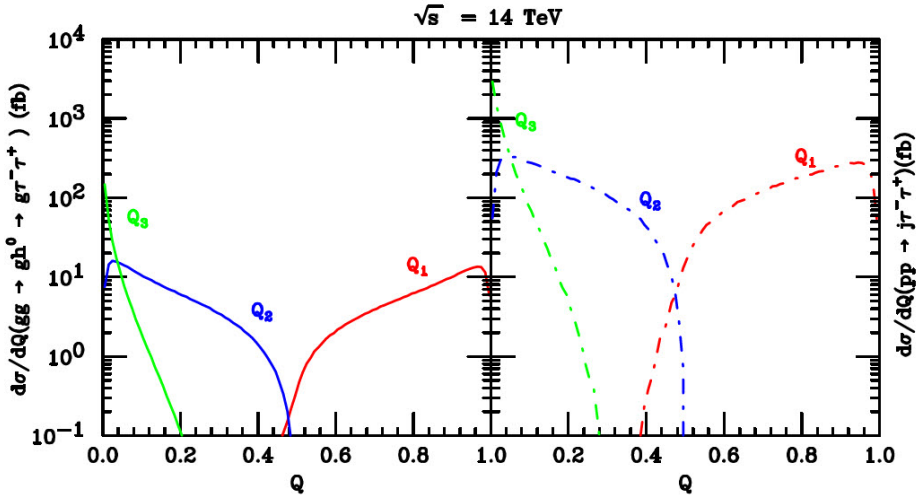

Figure 5.6: Distribution of eigenvalues of mass tensor.

selected events of signal and background follow the same distribution. With all basic cuts in Eq. 5.2 and cuts on the energy fractions, i.e., $0 \leq x_l \leq 1$ and $0 \leq x_h \leq 1$, the distribution of events over $m_{\tau\tau}$ is drawn in Fig. 5.7. And, the total cross section of $gg \to gh^0$ is $\sigma^s = 3.12\ fb$ while the dominant background in SM is $\sigma^b = 368.7\ fb$. If we further cut on $m_{\tau\tau}$, .e.g., $|m_{\tau\tau} - m_{h^0}| \leq 22.0$ GeV, the cross sections respectively drop down to $\sigma^s = 2.88\ fb$ and $\sigma^b = 70.0\ fb$. So about 92.3% of the signal passes the mass cut while more than 80% of the background events are removed. In fact this cut is more helpful when applied to other background processes. After all, $pp \to j\tau^{\pm}\tau^{\mp}$ has a Z resonance which is close to the mass of SM Higgs, 125 GeV, i.e., an irreducible process.

5.4 Analysis of Background Processes

Aimed at the production of SM Higgs associated with one light jet, we list all the relevant background processes in the descending order as follows.

(1) $pp \to j\tau^{\pm}\tau^{\mp} + X \to jl^{\pm}j_{\tau}^{\mp} + \not{E}_T + X$

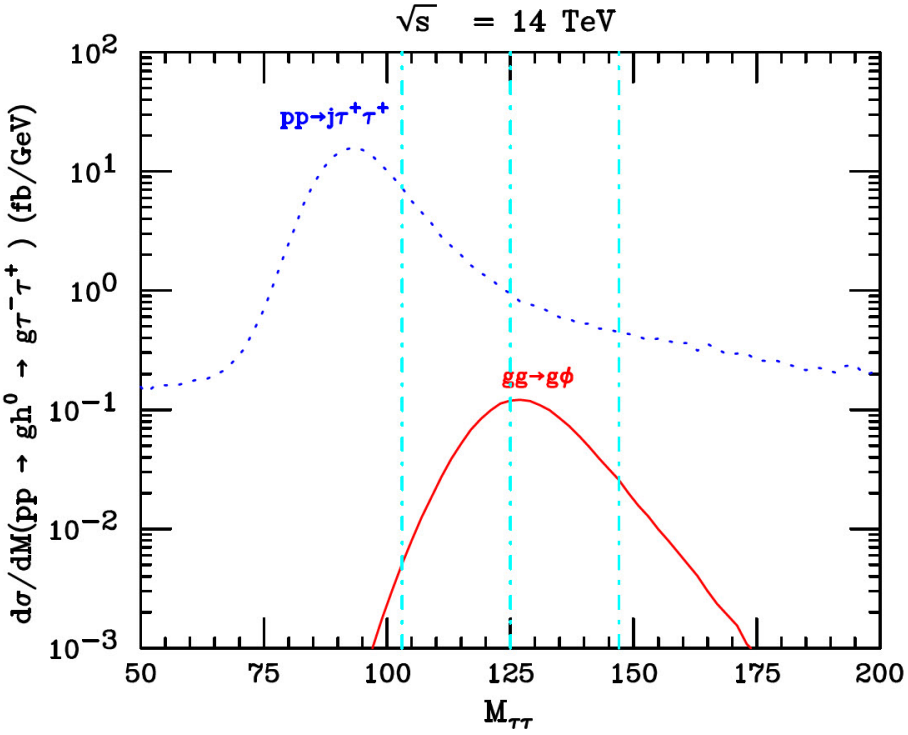

Figure 5.7: Mass distribution of signal and major background.

(2) $pp \to jW^{\pm}W^{\mp} + X \to jl^{\pm}j_2j_3 + \not{E}_T + X$

(3) $pp \to jW^{\pm}W^{\mp} + X \to j\tau^{\pm}j_2j_3 + \not{E}_T + X \to jl^{\pm}j_2j_3 + \not{E}_T + X$

(4) $pp \to jW^{\pm}W^{\mp} + X \to jl^{\pm}\tau^{\mp} + \not{E}_T + X \to jl^{\pm}j_\tau^{\mp} + \not{E}_T + X$

(5) $pp \to jW^{\pm}W^{\mp} + X \to j\tau^{\pm}\tau^{\mp} + \not{E}_T + X \to jl^{\pm}j_\tau^{\mp} + \not{E}_T + X$

(6) $pp \to jjW^{\pm} + X \to jjl^{\pm} + \not{E} + X$

(7) $pp \to jjW^{\pm} + X \to jj\tau^{\pm} + \not{E} + X \to jjl^{\pm} + \not{E} + X$

In the above expressions, l stands for e or μ and $j = g, u, d, c, s, \bar{u}, \bar{d}, \bar{c}$ or $\bar{s}$. However j_2 and j_3 come from W decay, so the possible combinations of j_2 and j_3 are $u\bar{d}$, $c\bar{s}$ and their charge conjugate states.

Among these processes, the first one is the irreducible background process and the major one as discussed in last section. The second one has 3 light jets in the final state, but we require only two pass our selection cuts and the faster

jet mimic the tau jet with a tagging efficiency equal to 1/400. The third one is almost the same as the second one except that there is one more intermediate process, i.e., $\tau^{\pm} \to e^{\pm}$ or $\mu^{\pm}$. So this process must be smaller than the last one by a factor of $0.5 \times BR(\tau \to e \text{ or } \mu)$ or so. The fourth one contributes one tau jet which would be tagged with an efficiency equal to 0.26. The difference of the fifth and the forth is the same as the difference of the third and the second. In the processes of 6 and 7, there are two light jets with the faster one mistagged as tau jet.

5.5 Results of Computer Simulation

With all the cuts and other parameters set properly, the integration over phase space gave us the results as follows.

$$\sigma(gg \to gh^0 \to g\tau^+\tau^- \to gl^{\pm}j_{\tau}^{\mp} + \not{E}_T) = 2.88\ fb \tag{5.7}$$

$$\sigma(q\bar{q} \to gh^0 \to g\tau^+\tau^- \to gl^{\pm}j_{\tau}^{\mp} + \not{E}_T) = 4.91 \times 10^{-3}\ fb \tag{5.8}$$

$$\sigma(qg \to qh^0 \to q\tau^+\tau^- \to ql^{\pm}j_{\tau}^{\mp} + \not{E}_T) = 3.71 \times 10^{-3}\ fb \tag{5.9}$$

and the calculation of background processes gave us

$$pp \to j\tau^{\pm}\tau^{\mp} + X \to jl^{\pm}j^{\mp} + \not{E}_T + X = 74.1\ fb \tag{5.10}$$

$$pp \to jjW + X \to jjl + \not{E}_T + X = 1.16\ fb \tag{5.11}$$

$$\begin{aligned} pp \to jW^{\pm}W^{\mp} + X &\to jl^{\pm}\tau^{\mp} + \not{E} + X \\ &\to jl^{\pm}j_{\tau}^{\mp} + \not{E}_T + X = 1.45 \times 10^{-1}\ fb \end{aligned} \tag{5.12}$$

$$\begin{aligned} pp \to jW^{\pm}W^{\mp} + X &\to j\tau^{\pm}\tau^{\mp} + \not{E}_T + X \\ &\to jl^{\pm}j_{\tau}^{\mp} + \not{E}_T + X = 3.38 \times 10^{-2}\ fb \end{aligned} \tag{5.13}$$

$$pp \to jW^{\pm}W^{\mp} + X \to jl^{\pm}j_2j_3 + \not{E}_T + X = 2.91 \times 10^{-2}\ fb \tag{5.14}$$

$$\begin{aligned} pp \to jW^{\pm}W^{\mp} + X &\to j\tau^{\pm}j_2j_3 + \not{E}_T + X \\ &\to jl^{\pm}j_2j_3 + \not{E}_T + X = 6.80 \times 10^{-3}\ fb \end{aligned} \tag{5.15}$$

Therefore, we have the significance of signal versus background, $N_{SS} = \frac{N_s}{\sqrt{N_b}}$, with $\mathcal{L} = 30\ fb^{-1}$ at $\sqrt{s} = 14$ GeV.

$\mathcal{L}(fb^{-1})$	30	300	3000
N_{SS}	1.80	5.75	14.4

Table 5.1: Significance of the production of SM Higgs associated with one light jet.

Chapter 6

Higgs Bosons of Minimal Supersymmertry

6.1 Introduction

This section is focused on the search for the combined Higgs signal from the process $pp \to b\phi^0 + X \to b\tau^+\tau^- + X \to bj_\tau l_\tau + \not{E}_T + X$ at LHC, where $b = b$ or $\bar{b}$ and ϕ^0 could be h^0, H^0 or A^0. And the searched Higgs mass M_{ϕ^0} spans from 100 GeV to 1000 GeV. From now on b stands for b and $\bar{b}$ in this chapter unless explicit specification is necessary. Then we have one b jet in the final states together with one neutral MSSM Higgs boson produced with one b. Furthermore, the b tagging technique is helpful to handle the fake jets. The neutral Higgs boson decays to $\tau^+\tau^-$ with a branching ratio of about 10%. Although this ratio is much smaller than $Br(\phi \to b\bar{b})$, which is about 60%, the benefit is that the charged lepton in the final state provides another method to reduce huge pure QCD background. Here we consider the largest decay mode of $\tau^+\tau^-$ pair, i.e., one to leptons and the other to τ jet with $Br(\tau \to e/\mu) = 35.2\%$ and $Br(\tau \to$

$\pi/\rho/a_1) = 54.8\%$, respectively.

6.2 Calculation Tools

Compared with the production of SM Higgs discussed in the last chapter, the MSSM Higgs bosons can be copiously produced associated with one b at the tree level if $\tan\beta$ is big enough. So the transition matrix of single Higgs production and decay to τ pair is much simpler, and can be generated by Madgraph Standalone [51] as well as all the background processes. We then simulate the pp collision by applying the parton distribution function CTEQ6L1 [49] as follows.

$$\sigma_s = \int dx_1 dx_2 \left(f_b(x_1,\mu_F) f_g(x_2,\mu_F) + f_g(x_1,\mu_F) f_b(x_2,\mu_F)\right) \sigma\left(bg \to b\phi^0 \to b\tau^+\tau^-\right) \times 2Br(\tau \to l) Br(\tau \to j_\tau) \times 2, \tag{6.1}$$

where μ_F is the factorization scale set to be $\frac{m_{\phi^0}}{4}$, and the last factor 2 represents the contribution from $\bar{b}$. Of course we can also use the narrow width approximation (NWA) when considering the decay of Higgs bosons. Then Eq. 6.1 changes to

$$\sigma_s = \int dx_1 dx_2 \left(f_b(x_1,\mu_F) f_g(x_2,\mu_F) + f_g(x_1,\mu_F) f_b(x_2,\mu_F)\right) \sigma\left(bg \to b\phi^0\right) \times Br\left(\phi^0 \to \tau^+\tau^-\right) \times 2Br(\tau \to l) Br(\tau \to j_\tau) \times 2, \tag{6.2}$$

Fig. 6.1 shows the production of pseudoscalar, A^0, associated with one b quark at LHC with $\sqrt{s} = 14$ TeV. In this case, the explored Higgs mass is $m_{A^0} = 200$ GeV and the ratio of VEV is $\tan\beta = 10$. From this figure, we can see that NWA is consistent with the full calculation except the two far ends. In fact the two ends

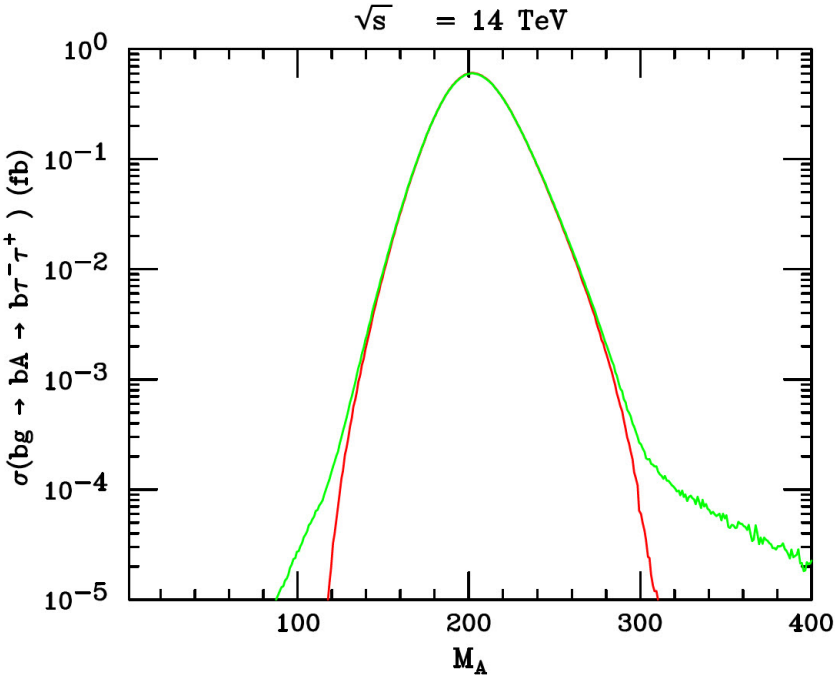

Figure 6.1: Distribution over the reconstructed mass of tau pairs. Red line stands for NWA while green line is for the full calculation.

will be cut away once a proper selection rule is chosen.

Fig. 6.2 shows the mass distribution with $m_{A^0} = 200$ GeV and $\tan\beta = 50$. Now the discrepancy between NWA and full calculation becomes bigger. It is because the couplings of pseudoscalar to certain particles increases with a bigger $\tan\beta$. Therefore the decay width becomes bigger, and then the resonance becomes flatter. So the NWA works better for parent particles with narrow width just as the name means.

This time we set the renormalization scale to be $\mu_R = \frac{m_{\phi^0}}{4}$ for both sigal and background.

One more difference is the basic cuts. The new set of cuts are listed in Tab. 6.1. Fig. 6.3 shows the transverse momentum distribution of signal and Drell-Yan processes, the major background. From the curves, we can find that

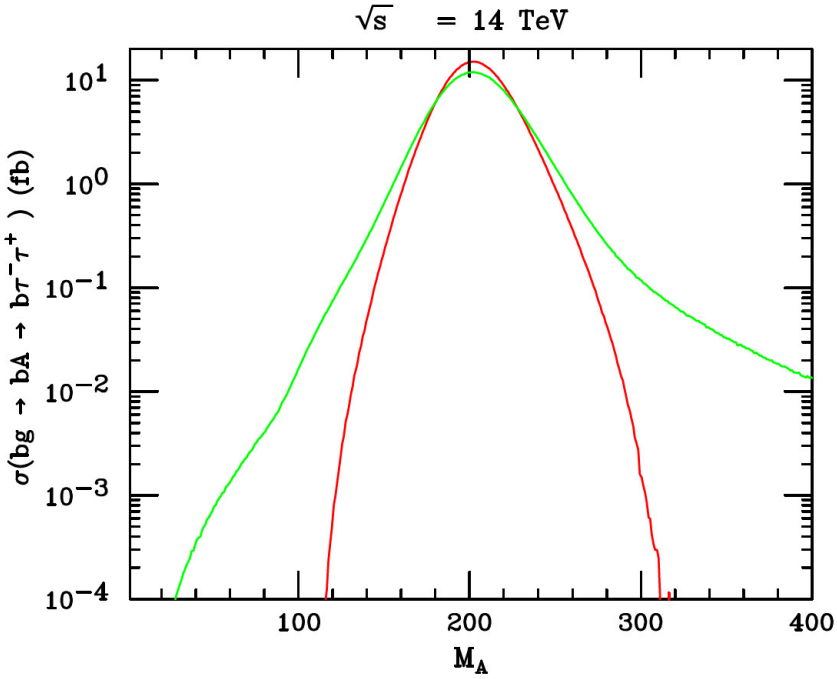

Figure 6.2: Distribution over the reconstructed mass of tau pairs. Red line stands for NWA while green line is for the full calculation.

$\sqrt{S}$(TeV)	8		14	
$\mathcal{L}(fb^{-1})$	1	10	30	300
P_T(GeV)	$P_T(b,l,j_\tau) > 15,20,40$			$P_T(b,l,j_\tau) > 30,20,40$
η	$\eta(b) < 2.5, \eta(l) < 2.5, \eta(j_\tau) < 2.5$			
ΔR	$\Delta R(lj_\tau) > 0.3$			
$\not{E}_T$(GeV)	$\not{E}_T > 20$			$\not{E}_T > 40$
$m(l,\ \not{E}_T)$(GeV)	$m(l,\ \not{E}_T) < 30$			

Table 6.1: Basic cuts for the production of MSSM Higgs bosons.

the cut over $p_T(j)$ is efficient. Although the cuts over $p_T(b)$ and $p_T(l)$ removed almost 50% of the signal, we have to pay it because the existence of a large number of fake jets makes tagging performance more important. In this paper, the tagging efficiency of a b jet is set as

$$\begin{cases} \epsilon_b = 60\% & (\mathcal{L} = 1\ fb^{-1}, 20\ fb^{-1} \text{ or } 30\ fb^{-1}), \\ \epsilon_b = 50\% & (\mathcal{L} = 300\ fb^{-1}). \end{cases} \tag{6.3}$$

At high luminosity the tagging efficiency is lower than at low luminosity due to the pile-up effect. Meanwhile the efficiency of tau jet triggering is $\epsilon_{j_\tau} = 26\%$. As to the tagging of charged leptons, we assume 100% can be correctly identified. Corresponding to these choices, the mistagging probability of fake jets as b jet or j_τ is

$$p_{g,u,d,s\to b} = 1\%, \qquad P_{c\to b} = 10\%, \qquad P_{u,d,c,s\to j_\tau} = 1/400, \qquad P_{b\to j_\tau} = 1/700.$$

The method of mass reconstruction is the same as in the case of SM Higgs production, but we require different mass cuts as follows.

$$\begin{cases} |M_{\tau\tau} - M_{\phi^0}| \leq 0.15 \times M_{\phi^0} & (\mathcal{L} = 1., 20., 30.\ fb^{-1}) \\ |M_{\tau\tau} - M_{\phi^0}| \leq 0.20 \times M_{\phi^0} & (\mathcal{L} = 300.\ fb^{-1}) \end{cases} \tag{6.4}$$

The efficiency of such cuts are limited by the performance of LHC when measuring the final state particles. The performance of detectors decreases when the luminosity increases. And it's also limited by the decay width of Higgs bosons. The larger the value of decay width is, the flatter the distribution curve spreads at the resonance of expected Higgs boson.

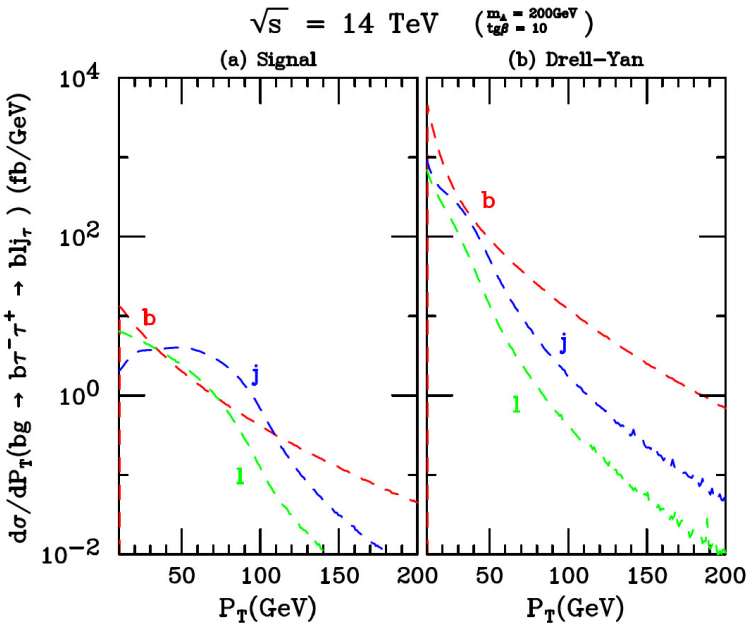

Figure 6.3: Transverse momentum distribution. j stands for the hadronic jet from τ decay.

Besides the differences discussed above, all other parameters and methods are the same as in the last chapter.

6.3 Analysis of Background Processes

The relevant background events come from Drell-Yan processes, $t\bar{t}$, tW and Wqq productions. These processes would result in both irreducible and reducible backgrounds as listed below in decreasing order of importance.

(1) Drell-Yan:

(a) $pp \to b(\bar{b})A^*(Z^*) \to b(\bar{b})\tau^+\tau^- \to b(\bar{b})lj_\tau$

(b) $pp \to q(\bar{q})A^*(Z^*) \to q(\bar{q})\tau^+\tau^- \to q(\bar{q})lj_\tau \qquad (q = u, d, c, s)$

(c) $pp \to gA^*(Z^*) \to g\tau^+\tau^- \to glj_\tau$

(2) $t\bar{t}$:

(a) $pp \to t\bar{t} \to bW^+\bar{b}W^- \to b\bar{b}l^\pm\tau^\mp \to b\bar{b}lj_\tau$

(b) $pp \to t\bar{t} \to bW^+\bar{b}W^- \to b\bar{b}\tau^+\tau^- \to b\bar{b}lj_\tau$

(c) $pp \to t\bar{t} \to bW^+\bar{b}W^- \to b\bar{b}lj_1j_2$

(d) $pp \to t\bar{t} \to bW^+\bar{b}W^- \to b\bar{b}\tau^\pm j_1j_2 \to b\bar{b}lj_1j_2$

(e) $pp \to t\bar{t} \to bW^+\bar{b}W^- \to b\bar{b}ll$

(3) tW:

(a) $pp \to t(\bar{t})W^\mp \to b(\bar{b})W^\pm W^\mp \to b(\bar{b})l^\pm\tau^\mp \to b(\bar{b})lj_\tau$

(b) $pp \to t(\bar{t})W^\mp \to b(\bar{b})W^\pm W^\mp \to b(\bar{b})\tau^\pm\tau^\mp \to b(\bar{b})lj_\tau$

(c) $pp \to t(\bar{t})W^\mp \to b(\bar{b})W^\pm W^\mp \to b(\bar{b})lj_1j_2$

(d) $pp \to t(\bar{t})W^\mp \to b(\bar{b})W^\pm W^\mp \to b(\bar{b})\tau^\pm j_1j_2 \to b(\bar{b})lj_1j_2$

(4) Wq_1q_2

(a) $pp \to Wb(\bar{b})q \to blj$

(b) $pp \to Wq_1q_2 \to lq_1q_2$

In the above list, for simplicity, we have omitted the charge signs of final particles, the missing energy, and irrelevant hadronic states X.

Among Drell-Yan processes, the light flavor quark and gluon are mistagged as b quarks. In the first 4 cases of $t\bar{t}$ production, the events with extra b jets are vetoed if both b jets pass the selection cuts. Since Case 2.c and Case 2.d have two light flavor jets in the final state, we further require that only one pass the cuts and then be mistagged as j_τ. One b quark of Case 2.e is correctly identified while the other is mistagged as j_τ. Similarly, we require that only one of the two leptons in Case 2.e pass the corresponding selection cuts. In tW production, the extra light flavor jet in Case 3.c and Case 3.d is dealt with in the same way as in Case 2.c and Case 2.d. In Wq_1q_2, the two final jets could be any possible combination of gluon, quark and anti-quark, except top. Here Case 4.a is listed separately due to the b jet in final states. Although Wq_1q_2 production involves

more than 100 Feynman diagrams, its contribution is the slightest as shown in Fig. 6.4.

To consider high level corrections, a multiplicative factor $K = 1.3$ has been included for Drell-Yan processes [52], $K = 2$ for $t\bar{t}$ [53, 54], $K = 1.5$ for tW [55], $K = 2$ for Case 4.a [56], and $K = 0.9$ for Wq_1q_2 [57].

After multiplying K factors and considering the tagging or mistagging efficiencies, we draw the mass distribution of the production of single pseudoscalar A^0, $\sigma \sim M_A$, in Fig. 6.4. This Figure shows that, although we have increased the size of mass window in the case of high luminosity $\mathcal{L} = 300 \ \ fb^{-1}$, the signal curves of this case are still lower than in the case of low luminosity $\mathcal{L} = 30 \ fb^{-1}$. This is because of the cut over $P_T(b)$ as discussed in the last section. The curve of Drell-Yan peaks in low mass ($\sim$ 100 GeV) due to the resonance around M_Z. $t\bar{t}, tW$ and Wqq dominates in the intermediate mass range, but the first two decrease with M_A faster than Wqq. So $t\bar{t}$ and tW become more important than Wqq in high mass range when we work with $\mathcal{L} = 300 \ fb^{-1}$.

6.4 Discovery Potential of MSSM Higgs at LHC

Since we are looking for the combined Higgs signal from $\phi^0 = h^0, H^0$ and A^0, we need put the contributions from h^0 and H^0 together with A^0 if $|M_{h^0}(M_{H^0}) - M_{A^0}| \leq 0.1 \times M_{A^0}$. With the assumption $M_{SUSY} = m_{\tilde{g}} = m_{\tilde{f}} = \mu = -A_f = 1$ TeV, M_{h^0} approaches its maximum value ($\sim$ 125. GeV) very fast as $\tan\beta$ increases; meanwhile, M_{H^0} and M_{A^0} are almost degenerate as shown if Fig. 3.5. So in most of parameter space $(M_{A^0}, \tan\beta)$, we just need to consider the contributions from H^0 and A^0 except the domain with low mass and low $\tan\beta$.

If $M_{SUSY} \leq 1$ TeV, the situation becomes too complex. Firstly, the rela-

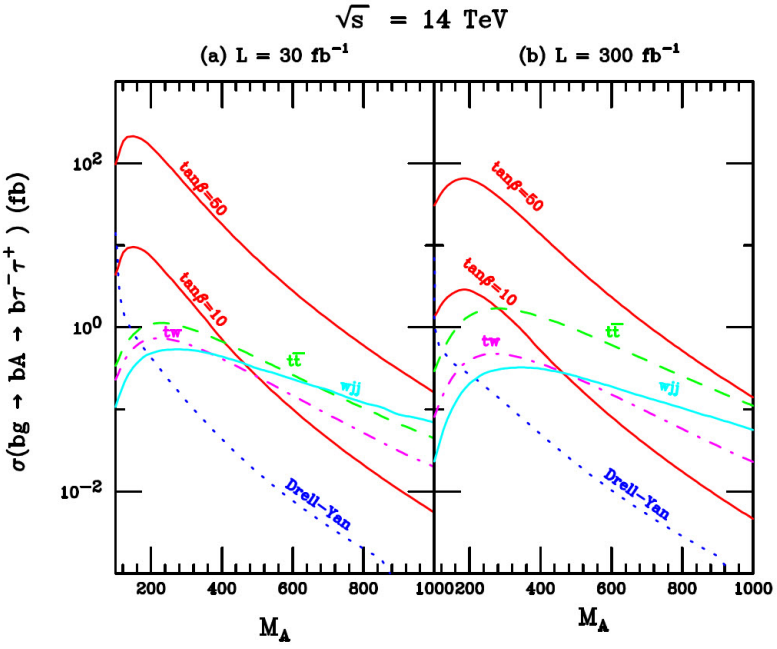

Figure 6.4: $\sigma \sim M_A$ in the production of pseudoscalar associated with b.

tionships of M_{h^0}, M_{H^0} and M_{A^0} would change because we have to consider the loop diagram of SUSY particle, especially stop, when we calculate the high level correction to these masses. Secondly, there are too many free parameters as discussed in the second chapter. Lastly, even if we choose to work with a set of specific parameters, A^0 and H^0 would decay to SUSY particles.

With all parameters set correctly, we have Table 6.2, 6.3, 6.4 and 6.5. These tables show us how the significance changes with respect to m_{A^0}, $\tan\beta$, $\sqrt{s}$ and $\mathcal{L}$.

According to the papers [58, 59], the observability of a signal could be affirmed if the cross sections of the signal and background satisfy

$$\mathcal{L}(\sigma_s + \sigma_b) - N\sqrt{\mathcal{L}(\sigma_s + \sigma_b)} > \mathcal{L}\sigma_b + N\sqrt{\mathcal{L}\sigma_b}, \tag{6.5}$$

Table 6.2: MSSM Higgs Production at $\sqrt{s} = 14$ TeV and $\mathcal{L} = 30\ fb^{-1}$

M_A(GeV)	100	200	400	800
$\sigma_s(tan\beta = 10)$	4.38	7.28	7.14×10^{-1}	2.09×10^{-2}
$\sigma_s(tan\beta = 50)$	9.75×10^{1}	1.61×10^{2}	1.81×10^{1}	6.02×10^{-1}
σ_s(Drell-Yan)	1.59×10^{1}	4.66×10^{-1}	4.60×10^{-2}	2.07×10^{-3}
$\sigma_s(b\bar{b}W^+W^-)$	2.95×10^{-1}	9.76×10^{-1}	5.40×10^{-1}	7.47×10^{-2}
$\sigma_s(bW^+W^-)$	1.89×10^{-1}	5.87×10^{-1}	3.31×10^{-1}	4.38×10^{-2}
$\sigma_s(Wjj)$	1.07×10^{-1}	4.83×10^{-1}	4.40×10^{-1}	1.21×10^{-1}
$N_{ss}(tan\beta = 10)$	6.24	24.1	3.12	0.217
$N_{ss}(tan\beta = 50)$	139	533	79.1	6.25

Table 6.3: MSSM Higgs Production at $\sqrt{s} = 14$ TeV and $\mathcal{L} = 300\ fb^{-1}$

M_A(GeV)	100	200	400	800
$\sigma_s(tan\beta = 10)$	1.34	2.83	5.21×10^{-1}	1.74×10^{-2}
$\sigma_s(tan\beta = 50)$	3.08×10^{1}	6.40×10^{1}	1.37×10^{1}	5.19×10^{-1}
σ_s(Drell-Yan)	6.99	2.64×10^{-1}	4.98×10^{-2}	2.84×10^{-3}
$\sigma_s(b\bar{b}W^+W^-)$	2.64×10^{-1}	1.32	1.24	2.20×10^{-1}
$\sigma_s(bW^+W^-)$	7.34×10^{-2}	3.76×10^{-1}	3.43×10^{-1}	5.68×10^{-2}
$\sigma_s(Wjj)$	2.31×10^{-2}	2.06×10^{-1}	3.13×10^{-1}	1.04×10^{-1}
$N_{ss}(tan\beta = 10)$	8.55	32.6	6.27	0.465
$N_{ss}(tan\beta = 50)$	197	737	165	13.9

Table 6.4: MSSM Higgs Production at $\sqrt{s} = 8$ TeV and $\mathcal{L} = 1\ fb^{-1}$

M_A(GeV)	100	200	400	800
$\sigma_s(tan\beta = 10)$	1.12	1.62	1.01×10^{-1}	1.38×10^{-3}
$\sigma_s(tan\beta = 50)$	2.49×10^{1}	3.60×10^{1}	2.57	4.01×10^{-2}
σ_s(Drell-Yan)	4.50	1.46×10^{-1}	1.29×10^{-2}	3.39×10^{-4}
$\sigma_s(b\bar{b}W^+W^-)$	4.51×10^{-2}	1.50×10^{-1}	8.52×10^{-2}	1.11×10^{-2}
$\sigma_s(bW^+W^-)$	3.95×10^{-2}	1.21×10^{-1}	5.94×10^{-2}	6.02×10^{-3}
$\sigma_s(Wjj)$	3.10×10^{-2}	1.38×10^{-1}	1.10×10^{-1}	2.27×10^{-2}
$N_{ss}(tan\beta = 10)$	3.30	12.3	1.08	0.0377
$N_{ss}(tan\beta = 50)$	73.3	273	27.4	1.10

Table 6.5: MSSM Higgs Production at $\sqrt{s} = 8$ TeV and $\mathcal{L} = 20\ fb^{-1}$

M_A(GeV)	100	200	400	800
$\sigma_s(tan\beta = 10)$	2.69×10^{-1}	5.90×10^{-1}	7.25×10^{-2}	1.14×10^{-3}
$\sigma_s(tan\beta = 50)$	6.17	1.34×10^{1}	1.91	3.45×10^{-2}
σ_s(Drell-Yan)	1.38	6.20×10^{-2}	1.05×10^{-2}	4.64×10^{-4}
$\sigma_s(b\bar{b}W^+W^-)$	4.42×10^{-2}	2.17×10^{-1}	2.00×10^{-1}	3.30×10^{-2}
$\sigma_s(bW^+W^-)$	1.30×10^{-2}	6.59×10^{-2}	5.19×10^{-2}	6.73×10^{-3}
$\sigma_s(Wjj)$	5.94×10^{-3}	5.80×10^{-2}	7.92×10^{-2}	2.04×10^{-2}
$N_{ss}(tan\beta = 10)$	3.88	16.1	2.15	0.0802
$N_{ss}(tan\beta = 50)$	89.0	366	56.6	2.43

or

$$\sigma_s > \frac{N^2}{\mathcal{L}}[1 + 2\sqrt{\mathcal{L}\sigma_b}/N], \tag{6.6}$$

where $N = 2.5$ corresponds to a 5σ signal, where σ_s is the total cross section of signal from 3 possible Higgs bosons after we require all the cuts and multiplicative factors; and σ_b is the total cross section from 4 major background processes. Therefore, we can draw a 5σ discovery contour for single MSSM Higgs at LHC as shown in Fig. 6.5.

Fig. 6.5 has two frames where the left one corresponds to the machine energy equal to 8 TeV while the right frame to 14 TeV. In both frames, the dot-dashed red curve is the result with low luminosity, i.e., 1 fb^{-1} for 8 TeV while 30 fb^{-1} for 14 TeV; the dot-dot-dashed red curve is the result with high luminosity, i.e., 10 fb^{-1} for 8 TeV while 300 fb^{-1} for 14 TeV. Above the these curves is the potential domain where the signal of MSSM Higgs bosons can be detected with the corresponding maching energy and luminosity at LHC. There are two more curves. The cyan shows the already explored region at CMS, and the green one shows the result of ATLAS. It means that the parameter space above these two cureves has been excluded. In this figure, there is a slashed blue region where the light Higgs boson has a mass about 126 GeV calculated by FeynHiggs with

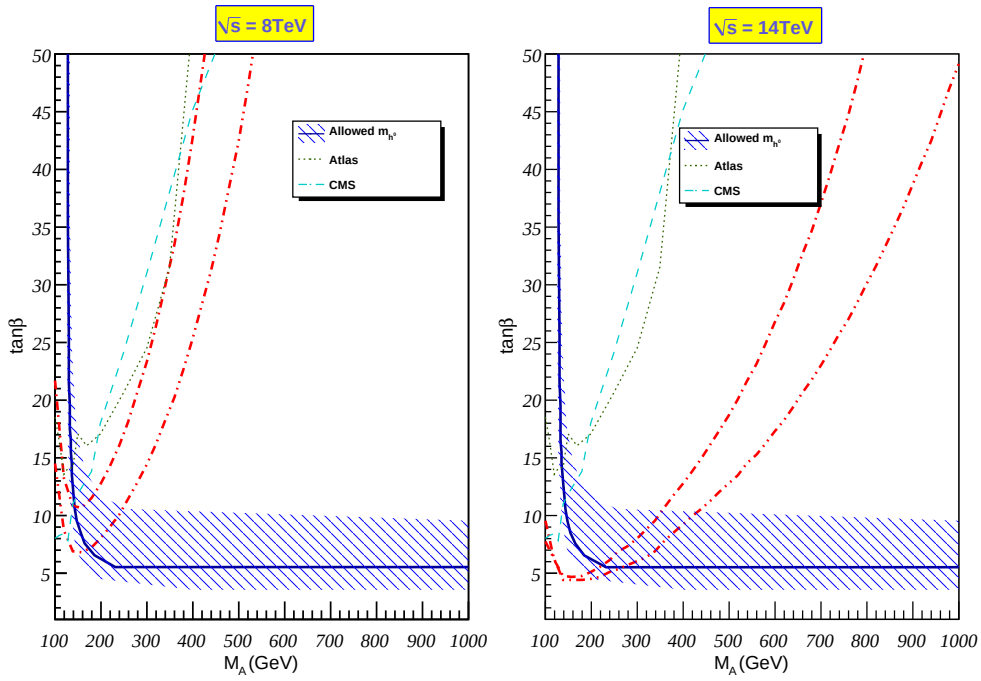

Figure 6.5: 5σ discovery contour. The back dotted curve and the cyan dashed curve respectively stand for the experimentalresults from Atlas and CMS. The blue band refers to the allowed region by the mass of light Higgs boson, $m_{h^0} = 126 \pm 3$ GeV. The red curves are the discovery contour of MSSM Higgs bosons at LHC with one referring to the low luminosity and the other to the high luminosity.

one-loop and two-loop corrections.

Even with a sizable excluded region, there still exists large space waiting for us to explore, especially the region predicted with the mass of light Higgs boson. In the near future the promising region could be $\{(\tan\beta, m_{A^0}) | 3 \leq \tan\beta \leq 10$ and 120 GeV $\leq m_A \leq 400$ GeV$\}$

Chapter 7

Supersymmetric Unified Models

7.1 Introduction

Supersymmetry (SUSY) provides an elegant solution to the fine-tunning problem through cancellations among loop diagrams. However, any SUSY model has to introduce at least one more Higgs doublet than the Standard Model (SM). In minimal SUSY model, once electroweak symmetry is broken (EWSB), three of the eight degrees of freedom in the Higgs sector are eaten and then generate the mass terms of $W^{\pm}$ and Z, while five others survive as two CP-even Higgs bosons, which are H^0 and h^0 ($M_{h^0} < M_{H^0}$), one CP-odd Higgs boson A^0, and two charged Higgs bosons $H^{\pm}$. In most of parameter space, h^0 is SM-like and expected to lie in the mass range $114.4 - 135$ GeV [60, 61, 62, 63, 64], but M_{A^0} and M_{H^0} could run through a much larger range.

Meanwhile, SUSY brings one SUSY partner for each SM particle. Owing to the absence of SUSY particles from observations [65, 66, 67, 68, 69], SUSY must be broken somehow. It was proposed that SUSY breaking could be attained by introducing extra terms [70]. Of course, there are several basic requirements

that these terms must meet, satisfying $SU(3)_C \times SU(2)_L \times U(1)_Y$ before EWSB, explicitly breaking SUSY and not causing a new quadratic divergence at loop level, i.e., *Soft SUSY Breaking Mechanism* (SSB). Therefore, soft SSB adds the mass terms of SUSY fermions and gauginos, the trilinear coupling terms between Higgs scalars and SUSY fermions, and the bilinear Higgs coupling term. One drawback of this brutal behavior is that there are 124 free parameters.

However, if heavy SUSY particles are assumed, these particles would decouple from low-energy phenomena. Therefore, there are only two free parameters involved, the mass of pseudoscalar (M_{A^0}) and the ratio of vacuum expectation values (VEVs) ($\tan\beta = \frac{v_2}{v_1}$), while other parameters are well-measured SM parameters. We will assume $M_{SUSY} = 1$ TeV in the general minimal SUSY standard model (MSSM) [71].

Another way around this difficulty is to trace back to the origin of SSB. It's commonly believed that MSSM is just one low-energy (~ 1 TeV) effective theory of some SUSY theory, which is more symmetric at a scale up to $M_X = 2 \times 10^{16}$ GeV, even Planck scale, and SUSY is spontaneously broken once some fields lying in hidden sectors develop VEVs at Λ_s ($M_{SUSY} < \Lambda_s < M_X$) and generate soft SSB terms. And then SSB is communicated to visible sectors by certain messengers, which couple to MSSM particles. Due to higher symmetry, those soft SSB terms should be related and have fewer free parameters. Based on the different breaking mechanisms, there are three most popular SUSY grand unification theories (GUTs): minimal gravity mediated SUSY breaking[72, 73, 74, 75, 76, 77, 78], minimal anomaly mediated SUSY breaking[76, 79] and minimal gauge mediated SUSY breaking[80, 81, 82, 83, 84, 85]. Even after taking several simplifications [8], MSSM still has 29 free parameters at low energy scales in addition to the SM parameters: 3 from gaugino masses (M_1, M_2, M_3), 15 from the masses of

SUSY fermions $\tilde{f} \in (\tilde{Q}_i, \tilde{u}_i^R, \tilde{d}_i^R, \tilde{L}_i, \tilde{e}_i^R)$, 2 from Higgs bosons (m_{H_u}, m_{H_d}), 3 from Yukawa couplings (y_t, y_b, y_τ), 3 from trilinear scalar couplings (A_t, A_b, A_τ), 2 from b terms (B, μ) and 1 from $\tan\beta$.

In the minimal models under consideration, gauge couplings are usually assumed unified at the GUT scale,

$$\alpha_1(M_{GUT}) = \alpha_2(M_{GUT}) = \alpha_3(M_{GUT}) = y. \tag{7.1}$$

Given the high scale parameters, the corresponding low scale values can be found through renormalization group equations (RGEs) [86, 87, 88], and vice versa. Moreover fixed point solutions to RGEs predict

$$y_t(m_t) = \frac{\sqrt{2} m_t(m_t)}{\sqrt{v_u^2 + v_d^2}\sin\beta}, \tag{7.2}$$

and analogous equations for y_b and y_τ. Therefore, we have two low scale input parameters, m_t and $\tan\beta$. Throughout this article, we set $m_t = 173.1$ GeV.

At large scale the Higgs mass squared matrix is positive definite. However, running the RGEs downwards leads to a negative eigenvalue at some scale, then electroweak symmetry is broken. The minimization condition of effective Higgs potential requires that

$$B(Q)\mu(Q) = \frac{\left(m_{H_1}^2(Q) + m_{H_2}^2(Q) + 2\mu^2(Q)\right)\sin\beta}{2}, \tag{7.3}$$

$$\mu^2(Q) = \frac{m_{H_2}^2(Q) - m_{H_1}^2(Q)\tan^2\beta}{\tan^2\beta - 1} - \frac{M_Z^2(Q)}{2}. \tag{7.4}$$

Q is the scale, where β is treated as an input parameter. Then B and μ can be found except their relative sign. So we have another input parameter $\mathrm{sgn}(\mu)$ at

low scale.

7.2 Minimal Supergravity Unified Model

SUGRA is spontaneously broken by singlet superfields in the hidden sector once they acquire VEVs. Although those fields in the hidden sector have the size of electroweak scale, they couple to MSSM particles only through gravity, so they disappear from collider phenomena with some footprints left behind, soft SSB terms. In this case, some universal boundary conditions are assumed

$$M_1(M_{GUT}) = M_2(M_{GUT}) = M_3(M_{GUT}) = m_{1/2}, \text{ (Gauginos)} \tag{7.5}$$

$$m_{\tilde{f}}(M_{GUT}) = m_{H_u}(M_{GUT}) = m_{H_d}(M_{GUT}) = m_0, \text{ (Scalars)} \tag{7.6}$$

$$A_t(M_{GUT}) = A_b(M_{GUT}) = A_\tau(M_{GUT}) = A. \text{ (Trilinear Couplings)} \tag{7.7}$$

Then the parameter space can be constructed with three high scale inputs and two low scale inputs plus one sign, i.e., $\{m_{1/2}, m_0, A, m_t, \tan\beta, \mathrm{sgn}(\mu)\}$.

For simplicity without loosing generality, we will scan a limited parameter space as follows.

$$\begin{cases} 0.\ \text{GeV} \leq m_{1/2} \leq 2000.\ \text{GeV} \\ 0.\ \text{GeV} \leq m_0 \leq 2500.\ \text{GeV} \\ A = 0.\ \text{GeV} \\ 20 \leq \tan\beta \leq 50 \\ \mathrm{sgn}(\mu) = +1 \end{cases} \tag{7.8}$$

7.3 Minimal Gauge Mediated Supersymmetry Breaking

The gauge-invariant and renormalizable superpotential for messenger superfields $(\Phi_a, \bar{\Phi}_a)$ has the general form, $\mathcal{W}_{mess} = \sum_{a=1}^{N_5} \lambda_a S \Phi_a \bar{\Phi}_a$. Here N_5 is the number of messenger superfields; λ_a is the Yukawa couplings with absolute values less than 1; S is a gauge singlet under the SM gauge group. The auxiliary component and the scalar component of S, respectively, acquire VEVs, $\langle F_s \rangle$ and $\langle s \rangle$. If $\langle F_s \rangle \neq 0$, SUSY is broken. And $\langle S \rangle$ gives mass to messenger fields. Therefore, due to gauge interaction with messengers, the gauginos get masses from the one-loop diagrams of messengers, while scalars get their masses from two-loop diagrams [89],

$$M_i(M_{mess}) \simeq \frac{\alpha_i}{4\pi} N_5 M_s \ (i = 1, 2, 3), \tag{7.9}$$

$$\begin{aligned} m_{scalar} =& \frac{2}{N_5} \left[C_3 M_3^2(M_{mess}) + C_2 M_2^2(M_{mess}) \right. \\ & \left. + \frac{3}{5} \left(\frac{Y}{2} \right)^2 M_1^2(M_{mess}) \right], \end{aligned} \tag{7.10}$$

where $M_s = \left| \frac{\langle F_s \rangle}{\langle s \rangle} \right|$ and $M_{mess} = \left| \bar{\lambda} \langle s \rangle \right|$, which is the overall scale of the messenger mass. The trilinear couplings, A's, are much smaller than the mass terms of scalars at M_{mess} , so they are set to be zero. The b term is introduced by hand and then decided by the minimization conditions of Higgs potential. If the SSB scale $\langle F_s \rangle$ doesn't coincide with the underlying breaking scale F, a dimensionless parameter $C_{grav} \geq 1$ is introduced, $F = C_{grav} \langle F_s \rangle$.

Therefore, the parameter space of mGMSB is delimited by these parameters: $\{\Lambda, M_{mess}, N_5, \tan\beta, \mathrm{sgn}(\mu), C_{grav}\}$. Λ is the effective SSB scale, Here

$\Lambda = \left|\frac{\langle F_s \rangle}{M_{mess}}\right|$. And the scanned range is

$$\begin{cases} 10.\ \text{TeV} \leq \Lambda \leq 200.\ \text{TeV} \\ 10^4.\ \text{GeV} \leq M_{mess} \leq 10^{13}\ \text{GeV} \\ 20 \leq \tan\beta \in \leq 50 \\ N_5 = 1, \text{sgn}(\mu) = +1, C_{grav} = 1 \end{cases} \tag{7.11}$$

We are interested in the points, which satisfy a set of theoretical requirements and 4 major experimental constraints. The searching for SUSY particles at LEP2 with $\sqrt{s} = 208$ GeV led to a lower boundary over chargino mass, $m_{\tilde{x}_1^\pm} \gtrsim 104$ GeV [90]. The branching ratio of B_s^0 decay to muon pair is set as $Br(B_s^0 \to \mu^+\mu^-) < 1.08 \times 10^-8$ at 95% confidence level. [91]. The newly published result about b decay is $Br(b \to s\gamma) = (3.45 \pm 0.15 \pm 0.40) \times 10^{-4}$ [92]. And the difference of the muon anomalous magnetic moment between SUSY models and SM should satisfy the limit, $\delta a_\mu = a_\mu^{exp} - a_\mu^{SM} = (25.9 \pm 8.1) \times 10^{-10}$ [93]. In addition, we require a Higgs scalar with 123 GeV $\leq m_{h^0} \leq$ 129 GeV.

7.4 Discovery Potential of Higgs Bosons of SUSY GUTs at LHC

Scanning the parameter spaces with ISAJET 7.82, we get the masses, decay widths and effective Higgs mixing angles of Higgs bosons at SUSY scale, and then plug these values into our main program with the same calculation scheme as discussed in MSSM.

7.4.1 Results of mSUGRA

Fig. 7.1 and Fig. 7.2 depict the scenarios of mSUGRA with $A = 0.\ \text{GeV}, \text{sgn}(\mu) = +1$, but the former has a center of mass energy $\sqrt{s} = 8$ GeV, while the later corresponds to $\sqrt{s} = 14$ GeV. In these figures, the solid dark domain is excluded by theoretical requirements. The solid gray domain is excluded by the cosmological requirement that the lightest neutralino should be the lightest SUSY particle. And the solid blue domain represents the exclusion reqired by chargino mass. Other experimental limits are shown in the figures with the short-dashed lines representing the experimental values and the slashed area standing for errors. And the domain above the short-dashed violet line is allowed by $Br(B_s^0 \rightarrow \mu^+\mu^-) \leq 1.08 \times 10^{-8}$. If no short-dashed violet curve is found in a figure, it means that the whole space shown in the figure is allowed by the experimental observation of B_s^0 decay. In the figures we also have long-dashed violet curves corresponding to $Br(B_s^0 \rightarrow \mu^+\mu^-) \leq 5.0 \times 10^{-9}$. The allowed region by the measurement of δa_μ is the cyan part. In the figures the mass of light Higgs is shown by the blue curve (123 GeV and green curve (126 GeV). To the right of the two curves, the expected mass of light Higgs is larger and larger. The 5σ discovery contours are drawn with red lines. The domain below these curves are promising for the Higgs signal. In the case of $\sqrt{s} = 8$ TeV, the dashed red line corresponds to $\mathcal{L} = 1\ fb^{-1}$, while the solid red line to $\mathcal{L} = 10\ fb^{-1}$. In the case of $\sqrt{s} = 14$ GeV, the dashed red line corresponds to $\mathcal{L} = 30\ fb^{-1}$, while the solid red line to $\mathcal{L} = 300\ fb^{-1}$.

Reading through the figures, we can find that, with low machine energy $\sqrt{s} = 8$ GeV, only the model with high $\tan\beta$ around 50 has a region which is allowed by all limits and could be promising to search for the Higgs signal with $\mathcal{L} = 10\ fb^{-1}$.

If the machine energy of LHC is increased to $\sqrt{s} = 14$ TeV in the future, the most desirable model to look for Higgs particles is still that with high $\tan\beta$. However, in this case, we find that even the model with intermediate value of $\tan\beta$ around 30 has a small region good to be searched with high luminosity $\mathcal{L} = 300\ fb^{-1}$.

7.4.2 Results of mGMSB

Since the gravitino is the lightest particle in this model, we can release the cosmological requirement of neutralino as dark matter. Now the theoretically excluded regions are the solid gray part. The limit from chargino mass corresponds to the solid blue domain. We can see that this requirement is screened by the theoretical limits in the model with high $\tan\beta$. The left part to the short-dashed violet line is excluded by B_s^0 decay. If no short-dashed violet line is drawn in a figure, the whole space is allowed by B_s^0 decay. Similarly, the points with $Br(B_s^0 \to \mu^+\mu^-) \leq 5.0 \times 10^{-9}$ is drawn with the long-dashed violet line. In this case, the blue curve corresponds to the points expected to have a light Higgs with $m_{h^0} = 120$ GeV. Above this curve the mass of light Higgs is bigger. So a SM-like Higgs with mass close to 125 GeV puts a very strict constraint on the parameter space of mGMSB.

Similar to mSUGRA, the most restrictive constraint is from the measurement of muon anomalous magnetic moment. If the center of mass energy is low, only in the figure of $\tan\beta = 50$, we can see the lower end of the solid red line passing through the cyan region. So the region suitable to look for the Higgs signal is small in this case. If we work with high energy $\sqrt{s} = 14$ TeV, the situation is promising. Even working with low luminosity $\mathcal{L} = 30\ fb^{-1}$, there exist a discoverable region as shown in the first frame of Fig. 7.4.

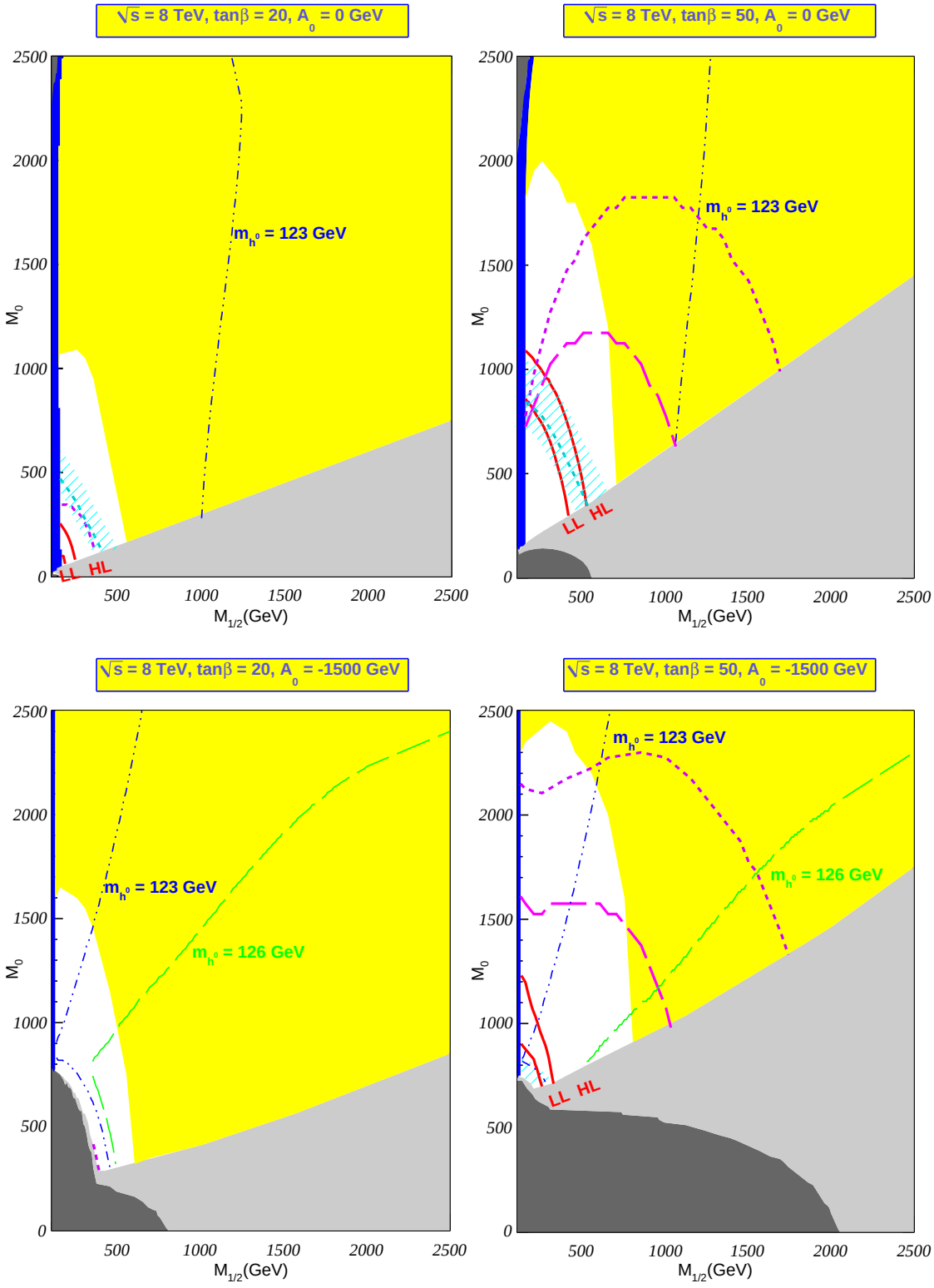

Figure 7.1: 5σ Discovery Contours of mSUGRA with $\mathrm{sgn}(\mu) = +1$ and $\sqrt{s} = 8$ TeV

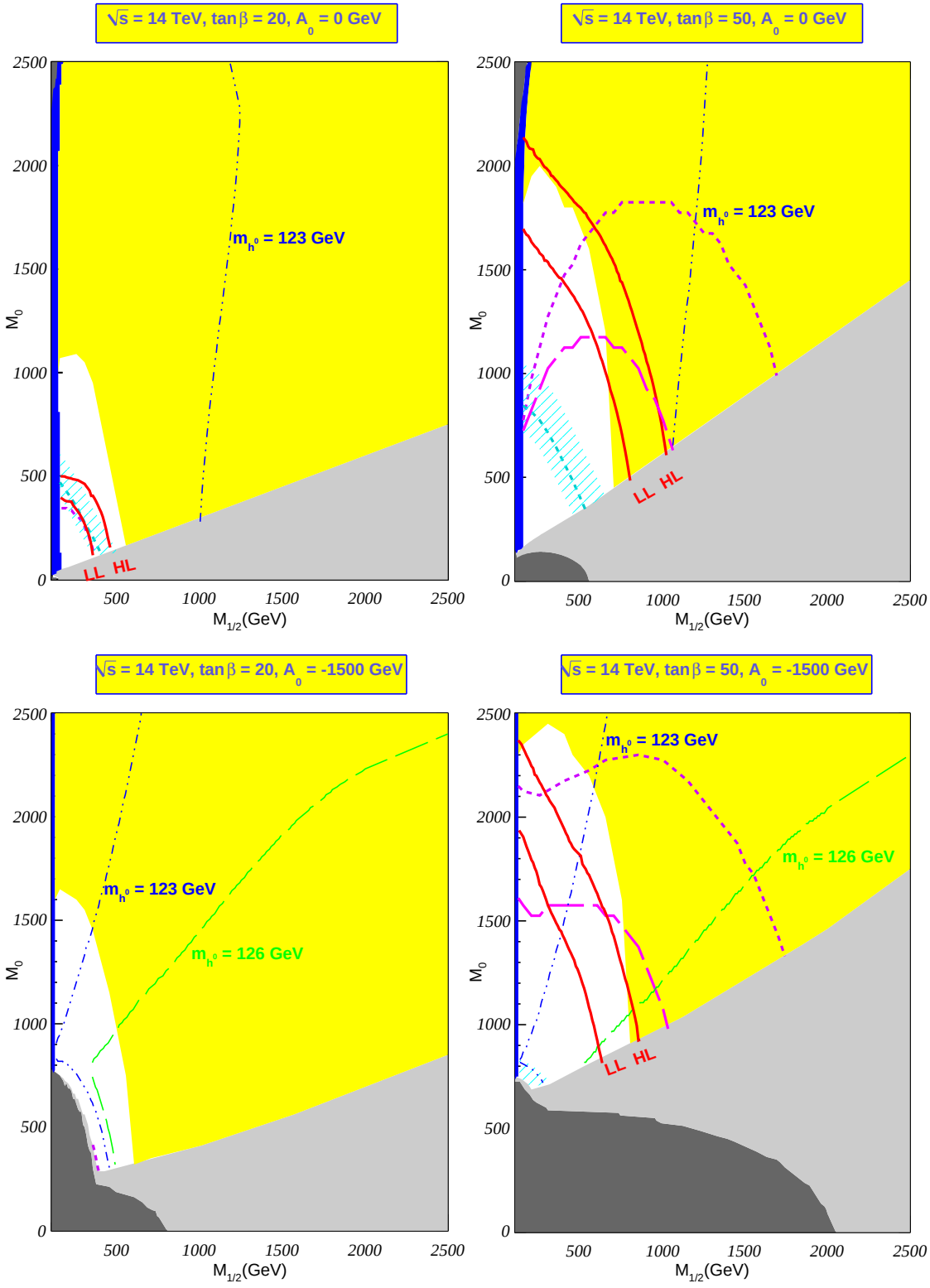

Figure 7.2: 5σ Discovery Contours of mSUGRA with $\mathrm{sgn}(\mu) = +1$ and $\sqrt{s} =$ 14 TeV

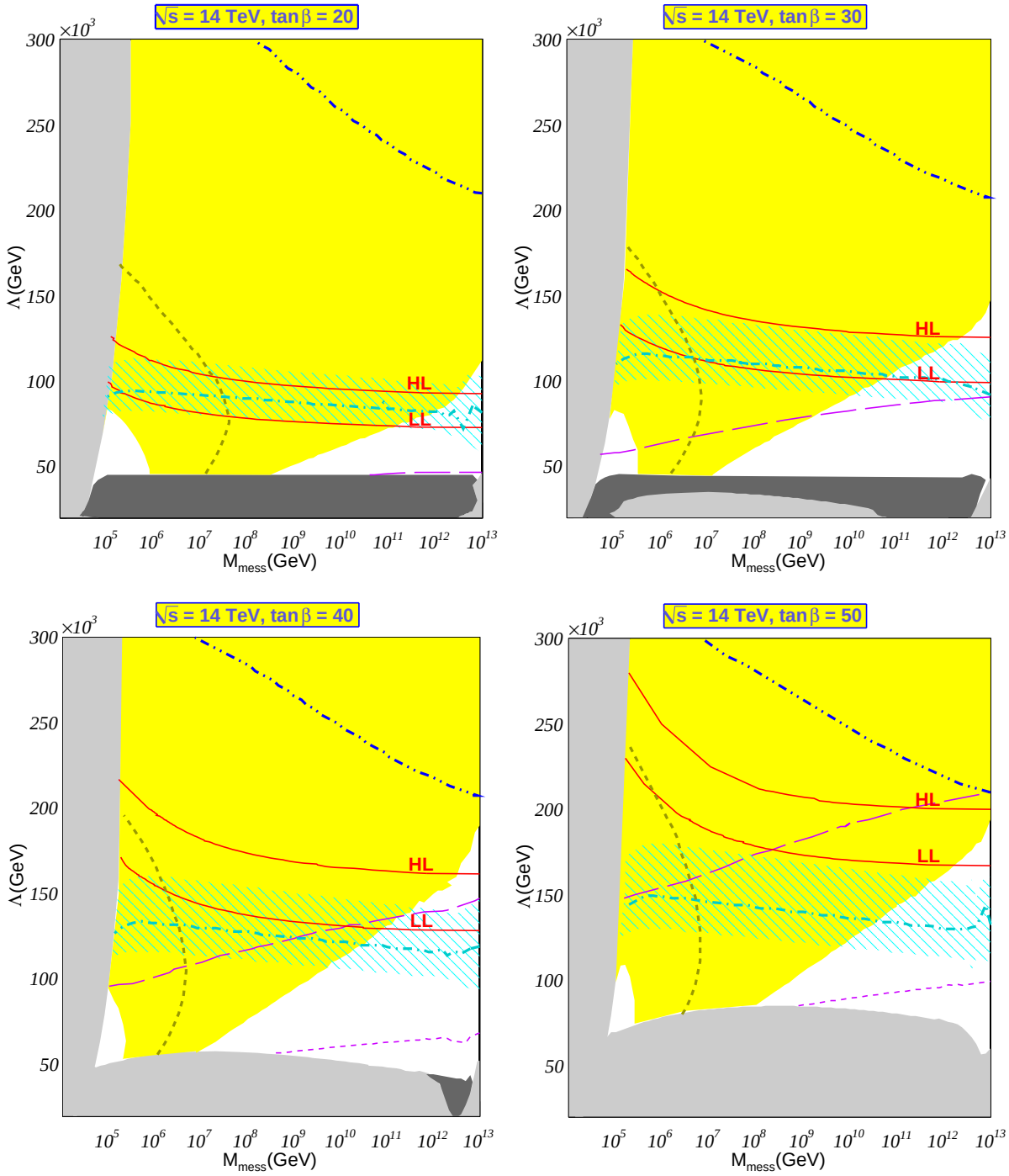

Figure 7.3: 5σ Discovery Contours of mGMSB with $N_5 = 1, \mathrm{sgn}(\mu) = +1, C_{grav} = 1$ and $\sqrt{s} = 14$ TeV

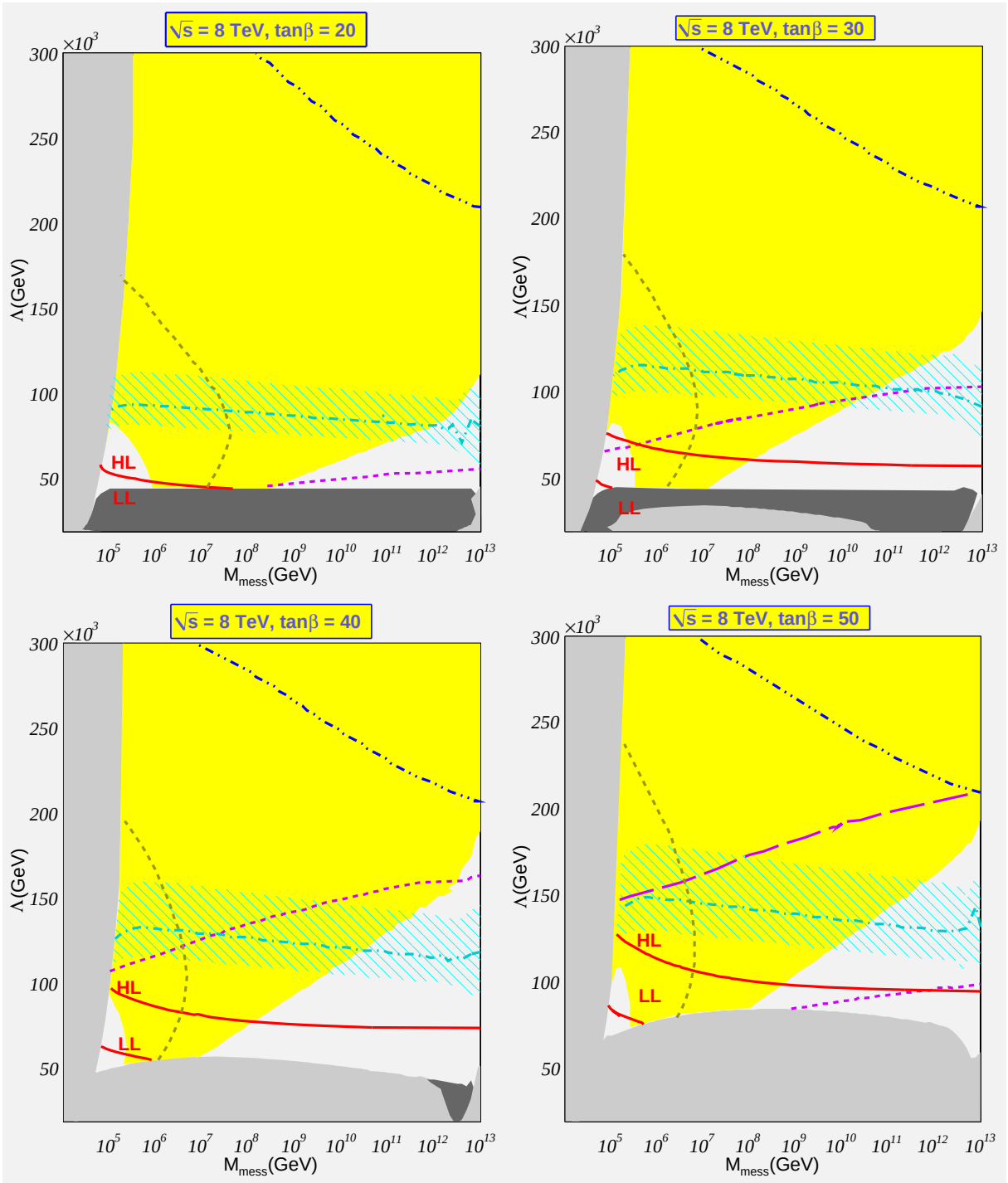

Figure 7.4: 5σ Discovery Contours of mGMSB with $N_5 = 1, \mathrm{sgn}(\mu) = +1, C_{grav} = 1$ and $\sqrt{s} = 8$ TeV

Chapter 8

Conclusions

It is very exciting that the Standard Higgs boson has recently been discovered at the Large Hadron Collider. In the near future, we need to study properties of the Higgs boson as well as Higgs couplings with gauge bosons and fermions. In addition, it is important to investigate if there are extra Higgs doublets with additional Higgs bosons. In this dissertation, we present the discovery potential of Higgs decay to tau leptons at the LHC. The discovery of $\phi \to b\bar{b}$, $\phi \to \tau^+\tau^-$, and $\phi \to \mu^+\mu^-$, will provide important information about Yukawa couplings between the Higgs bosons and the fermions.

The search for the SM Higgs through the channel of $h^0 \to \tau^\pm\tau^\mp$ may be pessimistic at $\sqrt{s} = 8$ TeV. However this channel has much cleaner background than $h^0 \to b\bar{b}$ and the technique of tau tagging is very helpful, especially for the MSSM Higgs bosons since the signal can be greatly enhanced with a large $\tan\beta$. It would be very promising to explore the parameter space with an intermediate value of $\tan\beta$ ($3 \leq \tan\beta \leq 10$) and with a pseudoscalar lighter than 500 GeV since this is the favored region of Higgs mass in the SM and it can be reached by the next run of LHC expected to start in 2015.

By investigating the phenomenology of Higgs bosons with tau leptons, we found that the cuts over x_l, x_h and $m_{\tau\tau}$ are so stringent that all the selected events of signal and background follow the same distribution.

To reduce the number of free parameters, we investigated the discovery of neutral Higgs bosons in mSUGRA and mGMSB. In mSUGRA, the mass of light Higgs is sensitive to the trillinear coupling A_0. With a negative large value of A_0, the allowed region of $m_{h^0} = 125$ GeV becomes considerable. But the excluded region is large too. At the LHC with $\sqrt{s} = 8$ TeV, we have found that there exists a large region which is consistent with the experimental measurements of $Br(B_s^0 \to \mu^+\mu^-)$, Δa_μ, m_{h^0} but $Br(b \to s\gamma)$. Moreover this region could be reached by LHC in near future. At $\sqrt{s} = 14$ GeV, the situation is the same. Although the explorable space becomes larger, the increased region is not favored by the experimental result of Δa_μ.

On the contrary to mSUGRA, mGMSB is favored by flavor problems. There are large overlapped regions by the experimental requirements of Δa_μ, $Br(b \to s\gamma)$ and $Br(B_s^0 \to \mu^+\mu^-)$, but the allowed region of light Higgs mass is very limited. Only in the region with Λ greater than 300 TeV can we find light Higgs boson with mass close to 125 GeV. However, this region is far away from regions favored by flavor problems.

Chapter 9

Appendix

9.1 Lagrangian of Higgs Sector in THDM

In the Higgs sector of THDM, the kinetic part of Lagrangian reads as

$$
\begin{aligned}
&(D^\mu H_1)^\dagger (D_\mu H_1) + (1 \to 2) \\
&= m_W^2 W^{+\mu} W_\mu^- + \frac{m_Z^2}{2} Z_\mu Z^\mu + i m_W (\partial_\mu G^- W^{+\mu} - \partial_\mu G^+ W_\mu^-) + m_Z \partial_\mu G^0 Z^\mu \\
&+ g m_W \cos(\beta-\alpha) W^{+\mu} W_\mu^- H^0 + g m_W \sin(\beta-\alpha) W^{+\mu} W_\mu^- h^0 \\
&+ \frac{g}{2}(\partial_\mu G^0 W^{+\mu} G^- + \partial_\mu G^0 W^{-\mu} G^+) - \frac{g}{2}(\partial_\mu G^- W^{+\mu} G^0 + \partial_\mu G^+ W^{-\mu} G^0) \\
&- \frac{ig}{2}\cos(\beta-\alpha)(\partial_\mu H^0 W^{+\mu} G^- - \partial_\mu H^0 W^{-\mu} G^+) \\
&- \frac{ig}{2}\sin(\beta-\alpha)(\partial_\mu h^0 W^{+\mu} G^- - \partial_\mu h^0 W^{-\mu} G^+) \\
&+ \frac{g}{2}(\partial_\mu A^0 W^{+\mu} H^- + \partial_\mu W^{-\mu} A^0 H^+) - \frac{g}{2}(\partial_\mu H^- W^{+\mu} A^0 + \partial_\mu H^+ W^{-\mu} A^0) \\
&+ \frac{ig\sin(\beta-\alpha)}{2}(\partial_\mu H^0 W^{+\mu} H^- - \partial_\mu H^0 W^{-\mu} H^+) \\
&- \frac{ig\cos(\beta-\alpha)}{2}(\partial_\mu h^0 W^{+\mu} H^- - \partial_\mu h^0 W^{-\mu} H^+)
\end{aligned}
$$

$$+\frac{ig\cos(\beta-\alpha)}{2}(\partial_\mu G^- W^{+\mu} H^0 - \partial_\mu G^+ W^{-\mu} H^0)$$
$$+\frac{ig\sin(\beta-\alpha)}{2}(\partial_\mu G^- W^{+\mu} h^0 - \partial_\mu G^+ W^{-\mu} h^0)$$
$$-\frac{ig\sin(\beta-\alpha)}{2}(\partial_\mu H^- W^{+\mu} H^0 - \partial_\mu H^+ W^{-\mu} H^0)$$
$$+\frac{ig\cos(\beta-\alpha)}{2}(\partial_\mu H^- W^{+\mu} h^0 - \partial_\mu H^+ W^{-\mu} h^0)$$
$$+gm_W\cos(\theta_w)(W^{-\mu}Z_\mu G^+ + W^{+\mu}Z_\mu G^-) + em_W(W^{-\mu}A_\mu G^+ + W^{+\mu}A_\mu G^-)$$
$$-i\frac{g^2\cos(\theta_w)}{2}(W^{-\mu}Z_\mu G^+ G^0 - W^{+\mu}Z_\mu G^- G^0)$$
$$-i\frac{g^2\cos(\theta)}{2}(W^{-\mu}Z_\mu H^+ A^0 - W^{+\mu}Z_\mu H^- A^0)$$
$$+\frac{g^2\cos(\theta_w)\cos(\beta-\alpha)}{2}(W^{-\mu}Z_\mu G^+ H^0 + W^{+\mu}Z_\mu G^- H^0)$$
$$+\frac{g^2\cos(\theta_w)\sin(\beta-\alpha)}{2}(W^{-\mu}Z_\mu G^+ h^0 + W^{+\mu}Z_\mu G^- h^0)$$
$$-\frac{g^2\cos(\theta_w)\sin(\beta-\alpha)}{2}(W^{-\mu}Z_\mu H^+ H^0 + W^{+\mu}Z_\mu H^- H^0)$$
$$+\frac{g^2\cos(\theta_w)\cos(\beta-\alpha)}{2}(W^{-\mu}Z_\mu H^+ h^0 + W^{+\mu}Z_\mu H^- h^0)$$
$$-i\frac{ge}{2}(W_\mu^- A^\mu G^+ G0 - W_\mu^+ A^\mu G^- G^0) + i\frac{ge}{2}(W_\mu^+ A^\mu H^- A^0 - W_\mu^- A^\mu H^+ A^0)$$
$$+\frac{ge\cos(\beta-\alpha)}{2}(W^{-\mu}A_\mu G^+ H^0 + W^{+\mu}A_\mu G^- H^0)$$
$$+\frac{ge\sin(\beta-\alpha)}{2}(W^{-\mu}A_\mu G^+ h^0 + W^{+\mu}A_\mu G^- h^0)$$
$$+\frac{g^2}{2}W^{-\mu}W_\mu^+ G^+ G^- + \frac{g^2}{2}W^{-\mu}W_\mu^+ H^+ H^- + \frac{g^2}{4}W^{-\mu}W_\mu^+ G^0 G^0$$
$$+\frac{g^2}{4}W^{-\mu}W_\mu^+ A^0 A^0 + \frac{g^2}{4}W^{-\mu}W_\mu^+ H^0 H^0 + \frac{g^2}{4}W^{-\mu}W_\mu^+ h^0 h^0$$
$$-\frac{ge\sin(\beta-\alpha)}{2}(W_\mu^+ A^\mu H^- H^0 + W_\mu^- A^\mu H^+ H^0)$$
$$+\frac{ge\cos(\beta-\alpha)}{2}(W_\mu^+ A^\mu H^- h^0 + W_\mu^- A^\mu H^+ h^0)$$
$$+\frac{ge\cos(2\theta_w)}{\cos(\theta_w)}Z_\mu A^\mu G^+ G^- + \frac{ge\cos(2\theta_w)}{\cos(\theta_w)}Z_\mu A^\mu H^+ H^-$$

$$
\begin{aligned}
&+ i\frac{g\cos(2\theta_w)}{2\cos(\theta_w)}(\partial_\mu G^- Z^\mu G^+ - \partial_\mu G^+ Z^\mu G^-) \\
&+ i\frac{g\cos(2\theta_w)}{2\cos(\theta_w)}(\partial_\mu H^- Z^\mu H^+ - \partial_\mu H^+ Z^\mu H^-) \\
&- \frac{g\cos(\beta-\alpha)}{2\cos(\theta_w)}\partial_\mu H^0 Z^\mu G^0 - \frac{g\sin(\beta-\alpha)}{2\cos(\theta_w)}\partial_\mu h^0 Z^\mu G^0 \\
&+ \frac{g\sin(\beta-\alpha)}{2\cos(\theta_w)}\partial_\mu H^0 Z^\mu A^0 - \frac{g\cos(\beta-\alpha)}{2\cos(\theta_w)}\partial_\mu h^0 Z^\mu A^0 \\
&+ \frac{g\cos(\beta-\alpha)}{2\cos(\theta_w)}\partial_\mu G^0 Z^\mu H^0 - \frac{g\sin(\beta-\alpha)}{2\cos(\theta_w)}\partial_\mu A^0 Z^\mu H^0 \\
&+ \frac{g\sin(\beta-\alpha)}{2\cos(\theta_w)}\partial_\mu G^0 Z^\mu h^0 + \frac{g\cos(\beta-\alpha)}{2\cos(\theta_w)}\partial_\mu A^0 Z^\mu h^0 \\
&+ \frac{gm_Z\cos(\beta-\alpha)}{2\cos(\theta_w)} Z_\mu Z^\mu H^0 + \frac{gm_Z\sin(\beta-\alpha)}{2\cos(\theta_w)} Z_\mu Z^\mu h^0 \\
&+ \left(\frac{g\cos(2\theta_w)}{2\cos(\theta_w)}\right)^2 Z_\mu Z^\mu G^+ G^- + \left(\frac{g\cos(2\theta_w)}{2\cos(\theta_w)}\right)^2 Z_\mu Z^\mu H^+ H^- \\
&+ \left(\frac{g}{2\sqrt{2}\cos(\theta_w)}\right)^2 Z_\mu Z^\mu G^0 G^0 + \left(\frac{g}{2\sqrt{2}\cos(\theta_w)}\right)^2 Z_\mu Z^\mu A^0 A^0 \\
&+ \left(\frac{g}{2\sqrt{2}\cos(\theta_w)}\right)^2 Z_\mu Z^\mu H^0 H^0 + \left(\frac{g}{2\sqrt{2}\cos(\theta_w)}\right)^2 Z_\mu Z^\mu h^0 h^0 \\
&+ ie(\partial_\mu G^- A^\mu G^+ - \partial_\mu G^+ A^\mu G^-) + ie(\partial_\mu H^- A^\mu H^+ - \partial_\mu H^+ A^\mu H^-) \\
&+ e^2 A_\mu A^\mu G^+ G^- + e^2 A_\mu A^\mu H^+ H^- \\
&+ \partial_\mu G^+ \partial^\mu G^- + \partial_\mu H^+ \partial^\mu H^- \\
&+ \frac{1}{2}\partial_\mu G^0 \partial^\mu G^0 + \frac{1}{2}\partial_\mu A^0 \partial^\mu A^0 + \frac{1}{2}\partial_\mu H^0 \partial^\mu H^0 + \frac{1}{2}\partial_\mu h^0 \partial^\mu h^0
\end{aligned} \tag{9.1}
$$

9.2 Gauge Invariance

The process of $gg \to g\phi$ basically involves one box and one triangle as shown in Fig. 9.1, where all momentum are incoming, a's are the color indices, and μ's are Lorentz indices. The transition amplitude matrices of the two loops can be

written as

$$M_{\square} = (-ig_s)^3 \left(\frac{-igm}{2m_W}\right) \int \frac{d^4l}{(2\pi)^4} \mathrm{Tr}\left[\frac{i}{\not l + \not k_1 + \not k_2 + \not k_3 - m}\gamma^{\mu_3} \frac{i}{\not l + \not k_1 + \not k_2 - m}\gamma^{\mu_2} \frac{i}{\not l + \not k_1 - m}\gamma^{\mu_1} \frac{i}{\not l - m}\right] \frac{d^{a_3a_2a_1} + if^{a_3a_2a_1}}{4} \times \epsilon_{\mu_1}\epsilon_{\mu_2}\epsilon^*_{\mu_3} \quad (9.2)$$

and

$$M_{\triangle} = (-ig_s)^2 \left(\frac{-igm}{2m_W}\right)(-g_s)\frac{f^{a_2a_3a_1}}{2}(g^{\mu_2\mu_3}(k_2-k_3)^{\alpha} + g^{\mu_3\alpha}(k_2+2k_3)^{\mu 2} + g^{\alpha\mu_2}(-2k_2-k_3)^{\mu_3})\frac{-ig_{\alpha\beta}}{(k_2+k_3)^2}\int \frac{d^4l}{(2\pi)^4}\mathrm{Tr}\left[\frac{i}{\not l + \not k_1 + \not k_2 + \not k_3 - m}\gamma^{\beta} \frac{i}{\not l + \not k_1 - m}\gamma^{\mu_1}\frac{i}{\not l - m}\right] \times \epsilon_{\mu_1}\epsilon_{\mu_2}\epsilon^*_{\mu_3}. \quad (9.3)$$

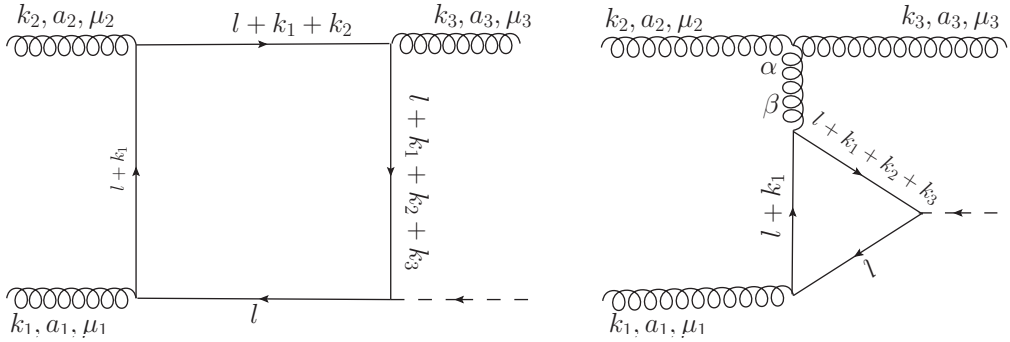

Figure 9.1: production of gluon and Higgs by gluon fusion.

If we cross the gluon lines and change the direction of the internal momentum l, we have 12 diagrams in total, see 9.2.

To save space, we will ignore all the common factors, even the integration and

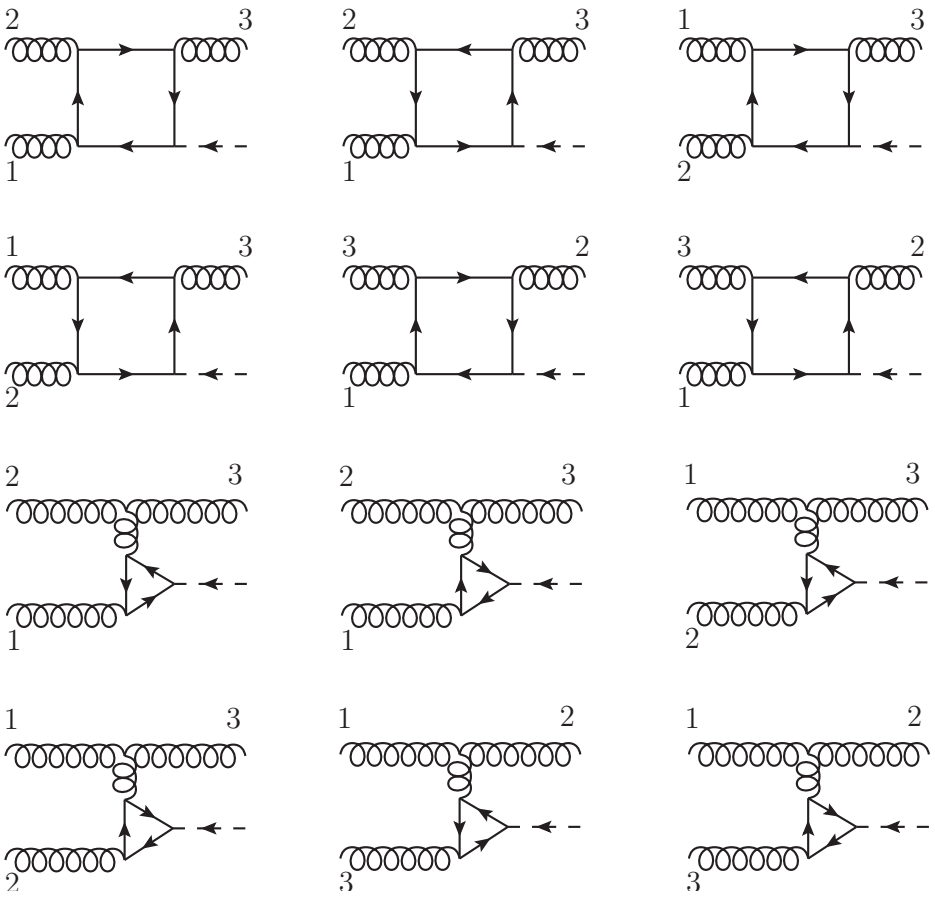

Figure 9.2: total diagrams of $gg \to gh$

trace symbols. Therefore the 12 diagrams can reexpressed as follows.

$$
\begin{aligned}
M^1_{\square} &= [D^{-1}_{123}\ \not{\epsilon}^*_3 D^{-1}_{12} - D^{-1}_{23}\ \not{\epsilon}^*_3 D^{-1}_2]\ \not{\epsilon}_2 D^{-1}_0 \frac{d^{123} - if^{123}}{4} \\
M^2_{\square} &= [D^{-1}_{23} - D^{-1}_{123}]\ \not{\epsilon}_2 D^{-1}_3\ \not{\epsilon}^*_3 D^{-1}_0 \frac{d^{123} + if^{123}}{4} \\
M^3_{\square} &= D^{-1}_{123}\ \not{\epsilon}^*_3 [D^{-1}_2 - D^{-1}_{12}]\ \not{\epsilon}_2 D^{-1}_0 \frac{d^{123} + if^{123}}{4} \\
M^4_{\square} &= D^{-1}_{123}\ \not{\epsilon}_2 [D^{-1}_3 - D^{-1}_{13}]\ \not{\epsilon}^*_3 D^{-1}_0 \frac{d^{123} - if^{123}}{4} \\
M^5_{\square} &= [D^{-1}_{123}\ \not{\epsilon}_2 D^{-1}_{13} - D^{-1}_{23}\ \not{\epsilon}_2 D^{-1}_3]\ \not{\epsilon}^*_3 D^{-1}_0 \frac{d^{123} + if^{123}}{4} \\
M^6_{\square} &= [D^{-1}_{23} - D^{-1}_{123}]\ \not{\epsilon}^*_3 D^{-1}_2\ \not{\epsilon}_2 D^{-1}_0 \frac{d^{123} - if^{123}}{4} \\
M^1_{\triangle} &= \frac{if^{123}(\epsilon_2 \cdot \epsilon^*_3(k_2 - k_3)_\beta + 2\epsilon^*_{3\beta}\epsilon_2 \cdot k_3 - 2\epsilon_{2\beta} k_2 \cdot k_3)}{2(k_2 + k_3)^2} \times [D^{-1}_{123} - D^{-1}_{23}]\gamma^\beta D^{-1}_0 \\
M^2_{\triangle} &= \frac{if^{123}(\epsilon_2 \cdot \epsilon^*_3(k_2 - k_3)_\beta + 2\epsilon^*_{3\beta}\epsilon_2 \cdot k_3 - 2\epsilon_{2\beta} k_2 \cdot k_3)}{2(k_2 + k_3)^2} \times [D^{-1}_{23} - D^{-1}_{123}]\gamma^\beta D^{-1}_0 \\
M^3_{\triangle} &= \frac{if^{123}}{2} \left\{ \frac{k_1 \cdot \epsilon^*_3 [D^{-1}_2 - D^{-1}_{123}]\ \not{\epsilon}_2 D^{-1}_0}{(k_1 + k_3)^2} - D^{-1}_{123}\ \not{\epsilon}^*_3 D^{-1}_2\ \not{\epsilon}_2 D^{-1}_0 \right\} \\
M^4_{\triangle} &= \frac{if^{123}}{2} \left\{ \frac{k_1 \cdot \epsilon^*_3 [D^{-1}_{123} - D^{-1}_2]\ \not{\epsilon}_2 D^{-1}_0}{(k_1 + k_3)^2} - D^{-1}_{123}\ \not{\epsilon}_2 D^{-1}_{13}\ \not{\epsilon}^*_3 D^{-1}_0 \right\} \\
M^5_{\triangle} &= \frac{if^{123}}{2} D^{-1}_{123}\ \not{\epsilon}_2 D^{-1}_3\ \not{\epsilon}^*_3 D^{-1}_0 \\
M^6_{\triangle} &= \frac{if^{123}}{2} D^{-1}_{123}\ \not{\epsilon}^*_3 D^{-1}_{12}\ \not{\epsilon}_2 D^{-1}_0
\end{aligned}
\tag{9.4}
$$

The Ward identity means that the value of transition amplitude becomes 0 when the polarization vector of any external vetor boson is replaced with its momentum. So, not losing generality, we have done such replacement as $\epsilon_1 \to k_1$ in Eq. 9.4, where $D_{rst} = \not{l} + \not{k}_r + \not{k}_s + \not{k}_t - m$. When deriving Eq. 9.4 we also have applied $D^{-1}_{1rs}\ \not{k}_1 D^{-1}_{rs} = D^{-1}_{rs} - D^{-1}_{1rs}$ and $D^{-1}_{rst} D^{-1}_{rs} D^{-1}_r = D^{-1}_{st} D^{-1}_s D^{-1}_0$. The latter comes from the fact that the shift of interal momentum doesn't change the

integration. Therefore the summation of box diagrams reduces to

$$M_{\Box} = D_{123}^{-1} \left(\not{\epsilon}_3^* D_2^{-1} \not{\epsilon}_2 + \not{\epsilon}_2 D_{13}^{-1} \not{\epsilon}_3^* - \not{\epsilon}_3^* D_{12}^{-1} \not{\epsilon}_2 - \not{\epsilon}_2 D_3^{-1} \not{\epsilon}_3^* \right) D_0^{-1} \frac{if^{123}}{2} \quad (9.5)$$

And the triangle diagrams sum up to

$$M_{\triangle} = D_{123}^{-1} \left(\not{\epsilon}_3^* D_{12}^{-1} \not{\epsilon}_2 + \not{\epsilon}_2 D_3^{-1} \not{\epsilon}_3^* - \not{\epsilon}_3^* D_2^{-1} \not{\epsilon}_2 - \not{\epsilon}_2 D_{13}^{-1} \not{\epsilon}_3^* \right) D_0^{-1} \frac{if^{123}}{2} \quad (9.6)$$

In conclusion, we have the Ward identity.

$$\begin{aligned} k_1^{\mu} M_{\mu} &= M_{\Box} + M_{\triangle} \\ &= 0 \end{aligned} \quad (9.7)$$

9.3 General Procedure of Computer Simulation of Parton Collisions

9.3.1 Cross Section

The cross section of elastic collision is defined as

$$\sigma = \frac{dN_{int}}{j \times dt \times N_{tar}}, \quad (9.8)$$

where the symbols each stand for

- $\star$ N_{int}: number of interactions
- $\star$ N_{tar}: number of target particle
- $\star$ j: incident flux.

And the incident flux is defined as

$$j = \frac{dN_{inc}}{A \times dt}. \tag{9.9}$$

We can see $[\sigma] = L^2$. So the cross section, σ, can be thought of as the effective cross scectional area of the target particles for the interation to occur, but in general this has nothing to do with the pysical size of the traget.

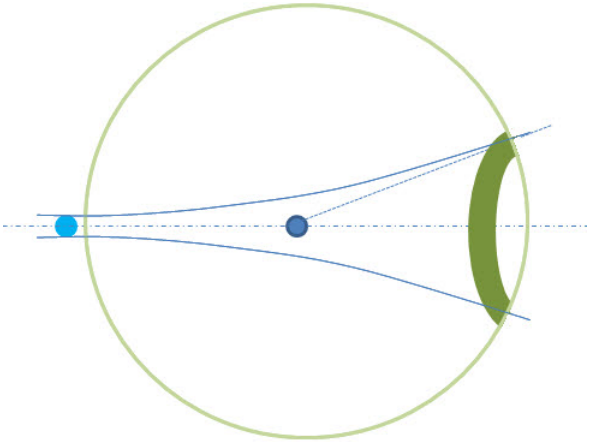

Figure 9.3: cross section

Experimentally we can collect the particles scattered to (θ, ϕ) directions, therefore we have

$$\sigma = \int \frac{d\sigma}{d\Omega} d\Omega \tag{9.10}$$

For simplicity, let's consider a single particle of type a with velocity, v_a, transversing a region of area A containing n_b particles of type b per unit volume, as shown in Fig. 2.

In time δt a particle of type a transverses a region containing $n_b(v_a + v_b)A\delta t$

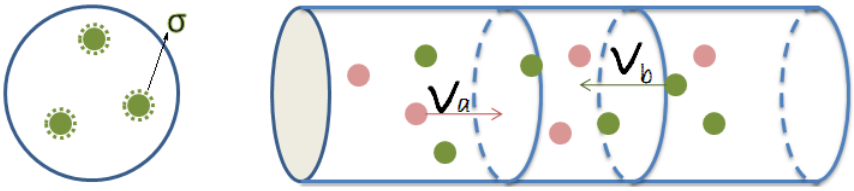

Figure 9.4: cross section

particles of type b. During this period the interaction probability of one a-type particle can be expressed as

$$P = \frac{n_b(v_a + v_b)A\delta t\sigma}{A} = n_b v \delta t \sigma \qquad [v = v_a + v_b]. \tag{9.11}$$

So the rate of interaction per a-type particle is

$$R = \frac{\delta P}{\delta t} = n_b v \sigma. \tag{9.12}$$

If this experiment happens in a enclosed space of volume V, then the total reaction rate equals to the summation over each a-type particle.

$$R = (n_b v\sigma) \cdot (n_a V), \tag{9.13}$$

$$= j_a N_b \sigma, \tag{9.14}$$

where, $j_a = n_a v$ and $N_b = n_v V$.

For any collision process with n final particles as shown in Fig. 1, the interaction rate is given by Fermi's Golden Rule

$$\Gamma_{fi} = (2\pi)^4 \int |T_{fi}|^2 \delta^4(p_1 + p_2 - k_1 - k_2 - \cdots - k_n) \frac{d^3\vec{k}_1}{(2\pi)^3} \cdots \frac{d^3\vec{k}_n}{(2\pi)^3}, \tag{9.15}$$

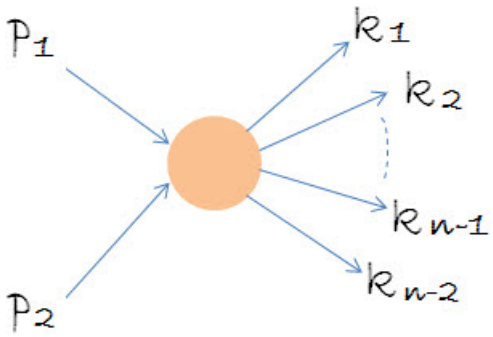

Figure 9.5: two-to-n

where T_{fi} is the transition matrix for one a-type particle and one b-type particle per unit volume. According to Eq. 9.15, Γ_{fi} can also be expressed as

$$\Gamma_{fi} = (v_a + v_b)\sigma. \tag{9.16}$$

Eq. 9.15 and Eq. 9.16 lead to

$$\begin{aligned} \sigma &= \frac{\Gamma_{fi}}{(v_a + v_b)} && (9.17) \\ &= \frac{(2\pi)^4}{v_a + v_b} \int |T_{fi}|^2 \delta^4(p_1 + p_2 - k_1 - k_2 \cdots - k_n) \frac{d^3\vec{k}_1}{(2\pi)^3} \cdots \frac{d^3\vec{k}_n}{(2\pi)^3}. && (9.18) \end{aligned}$$

In this expression, all the terms are not Lorentz invariant except the delta function. Now let's redefine the wave function normalized to $2E$ particles and introduce Lorentz invariant matrix element as follows,

$$\begin{cases} \phi &= (2E)^{\frac{1}{2}}\phi, \\ M_{fi} &= (2E_a 2E_b 2E_1 \cdots 2E_n)^{\frac{1}{2}} T_{fi}. \end{cases} \tag{9.19}$$

Then we get the Lorentz invariant form,

$$\sigma = \frac{(2\pi)^4}{F}\int |M_{fi}|^2\delta^4(p_1+p_2-k_1-k_2-\cdots-k_n)\frac{d^3\vec{k}_1}{(2\pi)^3 2E_1}\cdots\frac{d^3\vec{k}_n}{(2\pi)^3 2E_n}, \quad (9.20)$$

where $F = 2E_a 2E_b(v_a+v_b) = 4[(p_a\cdot p_b)^2 - m_a^2 m_b^2]^{1/2}$.

9.3.2 Phase Space Factor

The phase space factor is Lorentz invariant, so we can explicitly write it in any referrence frame without changing its value. For convenience, we write it in the CM frame of initial particle, i.e., $\vec{p}_\alpha = 0$.

$$\begin{aligned}
d\phi_2(p_\alpha; k_1, k_2) &= (2\pi)^4\delta^4(p_\alpha - k_1 - k_2)\frac{d^3k_1}{(2\pi)^3 2E_1}\frac{d^3k_2}{(2\pi)^3 2E_2} \\
&= (2\pi)^{-2}\delta(\sqrt{s} - \sqrt{p^2+m_1^2} - \sqrt{p^2+m_2^2})\frac{d^3p}{2\sqrt{p^2+m_1^2}}\frac{1}{2\sqrt{p^2+m_2^2}} \\
&= (2\pi)^{-2}\delta(\sqrt{s} - \sqrt{p^2+m_1^2} - \sqrt{p^2+m_2^2})\frac{p^2 dp d\Omega}{2\sqrt{p^2+m_1^2}}\frac{1}{2\sqrt{p^2+m_2^2}} \\
&= (2\pi)^{-2}\frac{1}{\left|-\frac{|p_0|}{\sqrt{p_0^2+m_1^2}} - \frac{|p_0|}{\sqrt{p_0^2+m_2^2}}\right|}\frac{p_0^2 d\Omega}{2\sqrt{p_0^2+m_1^2}}\frac{1}{2\sqrt{p_0^2+m_2^2}} \\
&= (2\pi)^{-2}\frac{\sqrt{(p_0^2+m_1^2)(p_0^2+m_2^2)}}{|p_0|(\sqrt{p_0^2+m_1^2}+\sqrt{p_0^2+m_2^2})}\frac{p_0^2 d\Omega}{2\sqrt{p_0^2+m_1^2}}\frac{1}{2\sqrt{p_0^2+m_2^2}} \\
&= (2\pi)^{-2}\frac{|p_0| d\Omega}{4\sqrt{s}},
\end{aligned}$$

where

$$s = (p_\alpha)^2$$

and

$$|p_0| = \sqrt{\frac{s^2+m_1^4+m_2^4-2sm_1^2-2sm_2^2-2m_1^2m_2^2}{4s}}.$$

A more concise expression can be written as

$$d\phi_2(p_\alpha; k_1, k_2) = (2\pi)^{-2}\frac{\lambda(s, m_1^2, m_2^2)}{8s}d\Omega, \tag{9.21}$$

where

$$\lambda(s, m_1^2, m_2^2) = \sqrt{s^2 + m_1^4 + m_2^4 - 2sm_1^2 - 2sm_2^2 - 2m_1^2m_2^2}.$$

In principle, the phase space factor is Lorentz invariant, but when we code our porgrams we should express it in the CM frame of m_1 and m_2 because the λ function is meaningful only in this frame and we also see that the solid angle is not Lorentz invariant.

9.3.3 Phase Space Reduction

For the process $a + b \to 1 + 2 + \cdots + n$, the n-dimensional phase space factor can be expressed as

$$d\phi_n(p_\alpha; k_1, k_2, \cdots, k_n) = (2\pi)^{-1}d\phi_{n-1}(p_\alpha; k_{12}, k_3, \cdots, k_n) \times d\phi_{12}(k_{12}, k_1, k_2)dM_{12}^2, \tag{9.22}$$

where

- $\star\ p_\alpha = p_1 + p_2$,
- $\star\ k_{12} = k_1 + k_2$,
- $\star\ k_{12}^2 = (k_1 + k_2)^2 = M_{12}^2$,
- $\star\ d\phi_n(p_\alpha; k_1, k_2, \cdots, k_n) \equiv (2\pi)^4\delta^4(\sum_{i=1}^{n} k_i - p_\alpha)\prod_{i=1}^{n}\frac{d^3k_i}{(2\pi)^3(2E_i)}$.

proof:

Let's rewrite the n-dimensional phase space factor as

$$\begin{aligned} d\phi_n &= (2\pi)^4\delta^4(p_\alpha - k_{12} - k_3 - \cdots - k_n)\prod_{i=1}^{n}\frac{d^3k_i}{(2\pi)^3 2E_i} \times \delta^4(k_{12} - k_1 - k_2)d^4k_{12} \\ &= (2\pi)^4\delta^4(p_\alpha - k_{12} - k_3 - \cdots - k_n)\prod_{i=3}^{n}\frac{d^3k_i}{(2\pi)^3 2E_i} d^4k_{12} \times (2\pi)^{-4} d\phi_2(k_{12}; k_1, k_2) \end{aligned}$$

Due to

$$\delta(F(x))dx = \sum_i \frac{1}{|F'(x_i)|_{F(x_i)=0}}\delta(x - x_i)dx, \tag{9.23}$$

We have

$$\begin{aligned} \delta\left(E^2 - |\vec{p}|^2 - m^2\right)dE &= \frac{1}{2\sqrt{|\vec{p}|^2 + m^2}}\left(\delta\left(E - \sqrt{|\vec{p}|^2 + m^2}\right)\right. \\ &\quad \left. + \delta\left(E + \sqrt{|\vec{p}|^2 + m^2}\right)\right)dE. \end{aligned} \tag{9.24}$$

Introducing a step function in the LHS of Eq.18 leads to

$$\delta\left(E^2 - |\vec{p}|^2 - m^2\right)\theta(E)dE = \frac{1}{2\sqrt{|\vec{p}|^2 + m^2}}\delta\left(E - \sqrt{|\vec{p}|^2 + m^2}\right)dE. \tag{9.25}$$

Multiply d^3p in both sides, we get

$$\frac{d^3p}{2\sqrt{|\vec{p}|^2 + m^2}} = d^3pdE\delta\left(E^2 - |\vec{p}|^2 - m^2\right)\theta(E) \tag{9.26}$$

And then integrateing over m^2 yield

$$\frac{d^3pdm^2}{2\sqrt{|\vec{p}|^2 + m^2}} = d^4p, \tag{9.27}$$

which means the integration over 4-vector can be mathematically achieved by integrating over 3-vector and the invariant mass squared under the ordinary

condition $p^0 = \sqrt{|\vec{p}|^2 + m^2}$. In fact, we can get Eq.(21) naivly from variable substitution.

Therefore we can substitute d^4k_{12} with $d^3k_{12}dM_{12}^2$, and then get

$$\begin{aligned} d\phi_n &= (2\pi)^{-1} \times (2\pi)^4 \delta(p_\alpha - k_{12} - k_3 - \cdots - k_n) \\ &\quad \times \prod_{i=3}^{n} \frac{d^3k_i}{(2\pi)^3 2E_i} \frac{d^3k_{12}dM_{12}^2}{(2\pi)^3 2E_{12}} d\phi_2(k_{12}; k_1, k_2) \\ &= (2\pi)^{-1} d\phi_{n-1}(p_\alpha; k_{12}, k_3, \cdots, k_n) d\phi_2(k_{12}; k_1, k_2) dM_{12}^2 \end{aligned} \tag{9.28}$$

Especially for a two-to-four process, we have

$$\begin{aligned} d\phi_4(p_\alpha; k_1, k_2, k_3, k_4) &= (2\pi)^{-2} d\phi_2(p_\alpha; k_{12}, k_{34}) d\phi_2(k_{12}; k_1, k_2) \\ &\quad \times d\phi_2(k_{34}, k_3, k_4) dM_{12}^2 dM_{34}^2 \\ &= (2\pi)^{-2} \left((2\pi)^{-2} \frac{\lambda(s, M_{12}^2, M_{34}^2) d\Omega_1}{8s} \right) \\ &\quad \times \left((2\pi)^{-2} \frac{\lambda(M_{12}^2, m_1^2, m_2^2) d\Omega_2}{8M_{12}^2} \right) \\ &\quad \times \left((2\pi)^{-2} \frac{\lambda(M_{34}^2, M_3^2, M_4^2) d\Omega_3}{8M_{34}^2} \right) dM_{12}^2 dM_{34}^2 \end{aligned} \tag{9.29}$$

Be aware that $d\Omega_1, d\Omega_2$ and $d\Omega_3$ are expressed in different frames, as discussed in the end of Subsection 2.

As to the two-to-six process, the phase space factor can be rewriten as

$$\begin{aligned}
d\phi_6(p_\alpha; k_1, k_2, k_3, k_4, k_5, k_6) &= (2\pi)^{-2} d\phi_4(p_\alpha; k_1, q_{23}, k_4, q_{56}) \\
&\quad \times d\phi_2(q_{23}; k_2, k_3) d\phi_2(q_{56}; k_5, k_6) dM_{23}^2 dM_{56}^2 \\
&= (2\pi)^{-4} d\phi_2(p_\alpha; q_{123}, q_{456}) d\phi_2(q_{123}; k_1, q_{23}) \\
&\quad \times d\phi_2(q_{456}; k_4, q_{56}) d\phi_2(q_{23}; k_2, k_3) d\phi_2(q_{56}; k_5, k_6) \\
&\quad \times dM_{23}^2 dM_{56}^2 dM_{123}^2 dM_{456}^2 \\
&= (2\pi)^{-4} \left((2\pi)^{-2} \frac{\lambda(s, M_{123}^2, M_{456}^2) d\Omega_1}{8s} \right) \\
&\quad \times \left((2\pi)^{-2} \frac{\lambda(M_{123}^2, m_1^2, M_{23}^2) d\Omega_2}{8M_{123}^2} \right) \\
&\quad \times \left((2\pi)^{-2} \frac{\lambda(M_{456}^2, m_4^2, M_{56}^2) d\Omega_3}{8M_{456}^2} \right) \\
&\quad \times \left((2\pi)^{-2} \frac{\lambda(M_{23}^2, m_2^2, m_3^2) d\Omega_4}{8M_{23}^2} \right) \\
&\quad \times \left((2\pi)^{-2} \frac{\lambda(M_{56}^2, m_5^2, m_6^2) d\Omega_5}{8M_{56}^2} \right) \\
&\quad \times dM_{23}^2 dM_{56}^2 dM_{123}^2 dM_{456}^2 \qquad (9.30)
\end{aligned}$$

While coding this part, we have

$$\sqrt{\hat{s}} = \left(\sqrt{s} - (m_1 + \cdots + m_6) \right) W(1) + (m_1 + \cdots + m_6), \qquad (9.31)$$

and

$$\begin{aligned}
M_{123} &\geq m_1 + m_2 + m_3, \qquad (9.32) \\
M_{456} &\geq m_4 + m_5 + m_6, \qquad (9.33) \\
M_{23} &\geq m_2 + m_3, \qquad (9.34) \\
M_{56} &\geq m_5 + m_6. \qquad (9.35)
\end{aligned}$$

During any process, the observed energy always changes if boosted to a different frame. Among these different values, the CM energy is the smallest. No matter whichever frame we choose, the energy always increases. Therefore, as long as the given CM energy is greater than the total rest mass of final particles, this process is kinematically possible. As to the 3D momentum, there principally exist innumerable sets of solutions. At first we can arbitrarily assign each final particle a 3D momentum $\vec{P}_i$ only required to be consistent with $\sum_{i=1}^{n} \vec{P}_i = 0$. Due to the arbitrariness, the total energy maybe violates the energy conservation law, $\sum_{i=1}^{n} \sqrt{m_i^2 + |\vec{P}_i|^2} = \sqrt{\hat{s}}$, the CM energy E_{CM}. But we can introduce a multiplier, k, which changes each particle's momentum to be $k\vec{P}_i$. In this trick, we still hold the momentum conservation law, $k\sum_{i=1}^{n} \vec{P}_i = 0$. Meanwhile, the energy changes to $\sum_{i=1}^{n} \sqrt{m_i^2 + k^2|\vec{P}_i|^2}$. Now we scale the multiplier up or down in the domain $[0, +\infty)$. Due to the fact, $\sqrt{\hat{s}} \geq \sum_{i=1}^{n} m_i$, it is 100% sure that we can find a k which satisies $\sum_{i=1}^{n} \sqrt{m_i^2 + k^2|\vec{P}_i|^2} = \sqrt{\hat{s}}$.

Therefore, Eq. 9.31 assure the possibility of the concerned process. As to M_{123} and M_{456}, we can write down such codes as

$$\begin{aligned} M_{123}^2 &= \left\{ \left[\sqrt{\hat{s}} - (m_4 + m_5 + m_6) \right]^2 - (m_1 + m_2 + m_3)^2 \right\} \\ &\quad \times W(2) + (m_1 + m_2 + m_3)^2, \qquad (9.36) \\ M_{456}^2 &= \left[(\sqrt{\hat{s}} - M_{123})^2 - (m_4 + m_5 + m_6)^2 \right] \\ &\quad \times W(3) + (m_4 + m_5 + m_6)^2. \qquad (9.37) \end{aligned}$$

Similarly, M_{23}^2 and M_{56}^2 can be coded as

$$M_{23}^2 = \left[(M_{123} - m_1)^2 - (m_2 + m_3)^2\right] W(4) + (m_2 + m_3)^2, \quad (9.38)$$

$$M_{56}^2 = \left[(M_{456} - m_4)^2 - (m_5 + m_6)^2\right] W(5) + (m_5 + m_6)^2. \quad (9.39)$$

Bibliography

[1] John David Jackson. *Classical Electrodynamics The Third Edition.* John Wiley & Sons, Inc., 1998.

[2] C. N. Yang and R. L. Mills. Conservation of Isotopic Spin and Isotopic Gauge Invariance. *Physical Review*, 96, oct 1954.

[3] Peter W. Higgs. Broken Symmetries and the Masses of Gauge Bosons. *Phys. Rev. Lett.*, 13:508–509, Oct 1964.

[4] G. S. Guralnik, C. R. Hagen, and T. W. B. Kibble. Global Conservation Laws and Massless Particles. *Phys. Rev. Lett.*, 13:585–587, Nov 1964.

[5] F. Englert and R. Brout. Broken symmetry and the mass of gauge vector mesons. *Phys. Rev. Lett.*, 13:321–323, Aug 1964.

[6] Steven Weinberg. A Model of Leptons. *Phys. Rev. Lett.*, 19:1264–1266, Nov 1967.

[7] Makoto Kobayashi and Toshihide Maskawa. CP Violation in the Renormalizable Theory of Weak Interaction. *Prog.Theor.Phys.*, 49:652–657, 1973.

[8] Howard Baer and Xerxes Tata. *Weak Scale Supersymmetry.* Cambridge University Press, 2006.

[9] John F. Gunion, Howard E. Haber, Gordon L. Kane, and Sally Dawson. THE HIGGS HUNTER'S GUIDE. *Front.Phys.*, 80:1–448, 2000.

[10] Howard E. Haber. Introductory low-energy supersymmetry. 1993.

[11] Stephen P. Martin. A Supersymmetry primer. 1997.

[12] T. D. Lee. A Theory of Spontaneous T Violation. *Phys. Rev. D*, 8:1226–1239, Aug 1973.

[13] John F. Gunion and Howard E. Haber. Conditions for CP violation in the general two-Higgs-doublet model. *Phys. Rev. D*, 72:095002, Nov 2005.

[14] Ilya F. Ginzburg and Maria Krawczyk. Symmetries of two Higgs doublet model and CP violation. *Phys. Rev. D*, 72:115013, Dec 2005.

[15] A. D. Sakharov. SPECIAL ISSUE: Violation of CP in variance, C asymmetry, and baryon asymmetry of the universe. *Soviet Physics Uspekhi*, 34:392–393, may 1991.

[16] C. Jarlskog. Commutator of the Quark Mass Matrices in the Standard Electroweak Model and a Measure of Maximal CP Nonconservation. *Phys. Rev. Lett.*, 55:1039–1042, Sep 1985.

[17] H.E. Haber, G.L. Kane, and T. Sterling. The fermion mass scale and possible effects of Higgs bosons on experimental observables. *Nuclear Physics B*, 161(2V3):493 – 532, 1979.

[18] Sheldon L. Glashow and Steven Weinberg. Natural conservation laws for neutral currents. *Phys. Rev. D*, 15:1958–1965, Apr 1977.

[19] John F. Donoghue and Ling-Fong Li. Properties of charged Higgs bosons. *Phys. Rev. D*, 19:945–955, Feb 1979.

[20] T. P. Cheng and Marc Sher. Mass-matrix ansatz and flavor nonconservation in models with multiple Higgs doublets. *Phys. Rev. D*, 35:3484–3491, Jun 1987.

[21] Benjamin W. Lee, C. Quigg, and H. B. Thacker. Strength of Weak Interactions at Very High Energies and the Higgs Boson Mass. *Phys. Rev. Lett.*, 38:883–885, Apr 1977.

[22] G. Altarelli and G. Isidori. Lower limit on the Higgs mass in the standard model: An update. *Physics Letters B*, 337(1V2):141 – 144, 1994.

[23] Thomas Hambye and Kurt Riesselmann. SM Higgs mass bounds from theory. 1997.

[24] S. Chatrchyan et al. Observation of a new boson at a mass of 125 GeV with the CMS experiment at the LHC. *Physics Letters B*, 716(1):30 – 61, 2012.

[25] G. Aad et al. Observation of a new particle in the search for the Standard Model Higgs boson with the ATLAS detector at the LHC. *Physics Letters B*, 716(1):1 – 29, 2012.

[26] John N. Bahcall. Solar Neutrinos. I. Theoretical. *Phys. Rev. Lett.*, 12:300–302, Mar 1964.

[27] Ahmad et al. Measurement of the Rate of $\nu_e + d \rightarrow p + p + e^-$ Interactions Produced by ^8B Solar Neutrinos at the Sudbury Neutrino Observatory. *Phys. Rev. Lett.*, 87:071301, Jul 2001.

[28] M. Bishai, M. Diwan, S. Kettell, J. Stewart, R. Tschirhart, et al. Precision Neutrino Oscillation Measurements using Simultaneous High-Power, Low-Energy Project-X Beams. 2013.

[29] J. Beringer et al. Review of Particle Physics. *Phys. Rev. D*, 86:010001, Jul 2012.

[30] U Dore and D Orestano. Experimental results on neutrino oscillations. *Reports on Progress in Physics*, 71(10):106201, 2008.

[31] Micheal S. Berger. Radiative Corrections to Higgs Boson Mass Sum Rules in the Minimal Supersymmetric Extension to the Standard Model. *Phys.Rev.*, D41:225, 1990.

[32] Yasuhiro Okada, Masahiro Yamaguchi, and Tsutomu Yanagida. Upper bound of the lightest higgs boson mass in the minimal supersymmetric standard model. *Progress of Theoretical Physics*, 85(1):1–5, 1991.

[33] Howard E. Haber and Ralf Hempfling. Can the mass of the lightest higgs boson of the minimal supersymmetric model be larger than m_z? *Phys. Rev. Lett.*, 66:1815–1818, Apr 1991.

[34] Howard E. Haber and Ralf Hempfling. Renormalization-group-improved higgs sector of the minimal supersymmetric model. *Phys. Rev. D*, 48:4280–4309, Nov 1993.

[35] S. Dawson. The standard model intermediate mass Higgs boson. 1997.

[36] Jun-jie Cao, Guang-ping Gao, Robert J. Oakes, and Jin Min Yang. Higgs-boson production associated with a bottom quark at hadron colliders with supersymmetric QCD corrections. *Phys. Rev.*, D68:075012, 2003.

[37] Kaoru Hagiwara, Alan D. Martin, and D. Zeppenfeld. Tau Polarization Measurements at LEP and SLC. *Phys. Lett.*, B235:198–202, 1990.

[38] Lisa Randall and Raman Sundrum. Large mass hierarchy from a small extra dimension. *Phys. Rev. Lett.*, 83:3370–3373, Oct 1999.

[39] Vernon Barger, Muneyuki Ishida, and Wai-Yee Keung. Dilaton at the LHC. *Phys.Rev.*, D85:015024, 2012.

[40] Vernon Barger, Muneyuki Ishida, and Wai-Yee Keung. Differentiating the Higgs boson from the dilaton and the radion at hadron colliders. *Phys.Rev.Lett.*, 108:101802, 2012.

[41] Yoshiko Ohno and Gi-Chol Cho. Production and decay of a heavy radion in Rundall-Sundrum model at the LHC. *EPJ Web Conf.*, 49:18003, 2013.

[42] W. A. Bardeen, C. N. Leung, and S. T. Love. Dilaton and chiral-symmetry breaking. *Phys. Rev. Lett.*, 56:1230–1233, Mar 1986.

[43] M.G. Ryskin and A.G. Shuvaev. Higgs Boson as a Dilaton. *Phys.Atom.Nucl.*, 73:965–970, 2010.

[44] Tomohiro Abe, Ryuichiro Kitano, Yasufumi Konishi, Kin-ya Oda, Joe Sato, et al. Minimal Dilaton Model. *Phys.Rev.*, D86:115016, 2012.

[45] Brando Bellazzini, Csaba Csaki, Jay Hubisz, Javi Serra, and John Terning. A Higgslike Dilaton. *Eur.Phys.J.*, C73:2333, 2013.

[46] G. Passarino and M.J.G. Veltman. One Loop Corrections for e+ e- Annihilation Into mu+ mu- in the Weinberg Model. *Nucl.Phys.*, B160:151, 1979.

[47] J. Kuipers, T. Ueda, J.A.M. Vermaseren, and J. Vollinga. FORM version 4.0. *Comput.Phys.Commun.*, 184:1453–1467, 2013.

[48] Johan Alwall, Michel Herquet, Fabio Maltoni, Olivier Mattelaer, and Tim Stelzer. MadGraph 5 : Going Beyond. *JHEP*, 1106:128, 2011.

[49] J. Pumplin et al. New generation of parton distributions with uncertainties from global QCD analysis. *JHEP*, 07:012, 2002.

[50] Vernon D. Barger and Roger J.N. Phillips. *Collider Physics Updated Edition.* Westview Press, 1996.

[51] Fabio Maltoni and Tim Stelzer. MadEvent: Automatic event generation with MadGraph. *JHEP*, 02:027, 2003.

[52] John M. Campbell, R. Keith Ellis, F. Maltoni, and S. Willenbrock. Associated production of a Z Boson and a single heavy quark jet. *Phys. Rev.*, D69:074021, 2004.

[53] Roberto Bonciani, Stefano Catani, Michelangelo L. Mangano, and Paolo Nason. NLL resummation of the heavy-quark hadroproduction cross- section. *Nucl. Phys.*, B529:424–450, 1998.

[54] P. Nason, S. Dawson, and R. Keith Ellis. The Total Cross-Section for the Production of Heavy Quarks in Hadronic Collisions. *Nucl. Phys.*, B303:607, 1988.

[55] S. Zhu. Next-to-leading order QCD corrections to b g → t W- at the CERN Large Hadron Collider. *Phys. Lett.*, B524:283–288, 2002.

[56] J. Campbell, R. K. Ellis, F. Maltoni, and S. Willenbrock. Production of a w boson and two jets with one b-quark tag. *Phys. Rev. D*, 75:054015, Mar 2007.

[57] John M. Campbell, R. Keith Ellis, and David L. Rainwater. Next-to-leading order QCD predictions for W + 2jet and Z + 2jet production at the CERN LHC. *Phys. Rev.*, D68:094021, 2003.

[58] Howard Baer, Mike Bisset, Duane Dicus, Chung Kao, and Xerxes Tata. The Search for Higgs bosons of minimal supersymmetry: Impact of supersymmetric decay modes. *Phys. Rev.*, D47:1062–1079, 1993.

[59] N. Brown. Degenerate Higgs and Z boson at LEP-200. *Z. Phys.*, C49:657–662, 1991.

[60] R. Barate et al. Search for the standard model Higgs boson at LEP. *Phys. Lett.*, B565:61–75, 2003.

[61] Howard E. Haber, Ralf Hempfling, and Andre H. Hoang. Approximating the radiatively corrected Higgs mass in the minimal supersymmetric model. *Z. Phys.*, C75:539–554, 1997.

[62] S. Heinemeyer, W. Hollik, and G. Weiglein. Higher-order results in the Higgs sector of the MSSM. 1999.

[63] Jose Ramon Espinosa and Ren-Jie Zhang. Complete two-loop dominant corrections to the mass of the lightest CP-even Higgs boson in the minimal supersymmetric standard model. *Nucl. Phys.*, B586:3–38, 2000.

[64] Howard Baer, Vernon Barger, Peisi Huang, and Azar Mustafayev. Implications of a high mass light mssm higgs scalar for supersymmetry searches at the lhc. *Phys. Rev. D*, 84:091701, Nov 2011.

[65] Joao Barreiro Guimaraes da Costa et al. Search for squarks and gluinos using final states with jets and missing transverse momentum with the ATLAS detector in $\sqrt{s} = 7$ TeV proton-proton collisions. *Phys. Lett.*, B701:186–203, 2011.

[66] Georges Aad et al. Search for supersymmetry in pp collisions at $\sqrt{s} = 7$TeV in final states with missing transverse momentum and b-jets. *Phys. Lett.*, B701:398–416, 2011.

[67] Altan Cakir. Searches for Supersymmetry with the CMS Experiment. 2011.

[68] M. Gataullin, S. Rosier, L. Xia, and H. Yang. Searches for Gauge-Mediated SUSY Breaking Topologies with the L3 Detector at LEP. *AIP Conf. Proc.*, 903:217–220, 2007.

[69] Gabriella Pasztor. Search for gauginos and gauge mediated SUSY breaking scenarios at LEP. *PoS*, HEP2005:346, 2006.

[70] Savas Dimopoulos and Howard Georgi. Softly Broken Supersymmetry and SU(5). *Nucl. Phys.*, B193:150, 1981.

[71] Chung Kao, Duane A. Dicus, Rahul Malhotra, and Yili Wang. Discovering the Higgs Bosons of Minimal Supersymmetry with Tau Leptons and a Bottom Quark. *Phys. Rev.*, D77:095002, 2008.

[72] R. M. Godbole, Monoranjan Guchait, and D. P. Roy. Using Tau Polarization to probe the Stau Co-annihilation Region of mSUGRA Model at LHC. *Phys. Rev.*, D79:095015, 2009.

[73] Abdelhak Djouadi, Manuel Drees, and Jean-Loic Kneur. Updated constraints on the minimal supergravity model. *JHEP*, 03:033, 2006.

[74] Jonathan L. Feng, Arvind Rajaraman, and Bryan T. Smith. Minimal supergravity with m(0)**2 ¡ 0. *Phys. Rev.*, D74:015013, 2006.

[75] C. Kao. Discovering Higgs bosons of minimal supergravity with muons. 2003. Prepared for International Conference on 20 Years of SUGRA and Search for SUSY and Unification (SUGRA 20), Boston, Massachusetts, 17-20 Mar 2003.

[76] A. Dedes, S. Heinemeyer, S. Su, and G. Weiglein. The lightest Higgs boson of mSUGRA, mGMSB and mAMSB at present and future colliders: Observability and precision analyses. *Nucl. Phys.*, B674:271–305, 2003.

[77] Frank E. Paige. SUSY signatures at LHC. *Czech. J. Phys.*, 55:B185–B196, 2005.

[78] Vernon D. Barger and Chung Kao. Detecting the Higgs bosons of minimal supergravity with muon pairs. *Phys. Lett.*, B424:69–75, 1998.

[79] Howard Baer, Radovan Dermisek, Shibi Rajagopalan, and Heaya Summy. Neutralino, axion and axino cold dark matter in minimal, hypercharged and gaugino AMSB. *JCAP*, 1007:014, 2010.

[80] Yevgeny Kats, Patrick Meade, Matthew Reece, and David Shih. The Status of GMSB After 1/fb at the LHC. 2011.

[81] Dorthe Ludwig and for the ATLAS collaboration. Expected Performance of the ATLAS Detector in GMSB Models with Tau Final States. *PoS*, HCP2009:073, 2009.

[82] R. N. Mohapatra, Nobuchika Okada, and Hai-Bo Yu. ν-GMSB with Type III Seesaw and Phenomenology. *Phys. Rev.*, D78:075011, 2008.

[83] Kazuhiro Tobe, James D. Wells, and Tsutomu Yanagida. Neutrino induced lepton flavor violation in gauge-mediated supersymmetry breaking. *Phys. Rev.*, D69:035010, 2004.

[84] Savas Dimopoulos, Michael Dine, Stuart Raby, and Scott D. Thomas. Experimental Signatures of Low Energy Gauge Mediated Supersymmetry Breaking. *Phys. Rev. Lett.*, 76:3494–3497, 1996.

[85] Riccardo Rattazzi and Uri Sarid. Large tan(beta) in gauge-mediated SUSY-breaking models. *Nucl. Phys.*, B501:297–331, 1997.

[86] Vernon D. Barger, M. S. Berger, and P. Ohmann. Yukawa coupling evolution in SUSY GUTs. 1993.

[87] Vernon D. Barger, M. S. Berger, and P. Ohmann. The Supersymmetric particle spectrum. *Phys. Rev.*, D49:4908–4930, 1994.

[88] Vernon D. Barger, M. S. Berger, P. Ohmann, and R. J. N. Phillips. RGE results for supersymmetric GUTs. 1993.

[89] Rohini M. Godbole Manuel Drees and Probir Roy. *Weak Scale Supersymmetry*. World Scientific, 2004.

[90] A. Djouadi, Manuel Drees, and J. L. Kneur. Constraints on the minimal supergravity model and prospects for SUSY particle production at future linear e+ e- colliders. *JHEP*, 08:055, 2001.

[91] Search for the rare decay $b_s^0 \to \mu^+\mu^-$ at the lhc with the cms and lhcb experiments. Aug 2011. LHCb-ANA-2011-039.

[92] Wenfeng Wang. $b \to s\gamma$ and $b \to d\gamma$ (B factories). 2011.

[93] Gi-Chol Cho, Kaoru Hagiwara, Yu Matsumoto, and Daisuke Nomura. The MSSM confronts the precision electroweak data and the muon g-2. *JHEP*, 11:068, 2011.